# ACTIVE THERMAL PROTECTION FOR INDUCTION MOTORS FED BY MOTOR CONTROL DEVICES

A Dissertation
Presented to
The Academic Faculty

by

Pinjia Zhang

In Partial Fulfillment
Of the Requirements for the Degree
Doctor of Philosophy in the
School of Electrical and Computer Engineering

Georgia Institute of Technology
May 2010

# ACTIVE THERMAL PROTECTION FOR INDUCTION MOTORS FED BY MOTOR CONTROL DEVICES

Approved by:


Dr. Thomas G. Habetler, Advisor
School of ECE
Georgia Institute of Technology

Dr. David G. Taylor
School of ECE
Georgia Institute of Technology

Dr. Ronald G. Harley
School of ECE
Georgia Institute of Technology

Dr. J. Rhett Mayor
School of ME
Georgia Institute of Technology

Dr. Deepak M. Divan
School of ECE
Georgia Institute of Technology


Date Approved: Mar 9th, 2010

*To my dear parents*

*Mr. Huaguang Zhang*
*Mrs. Liqin Zhao*

*And my dear wife*

*Mrs. Jing Dai*

# ACKNOWLEDGEMENTS

A doctoral dissertation is usually considered to be a personal accomplishment. However, it would not have been possible for me to finish this work without the inspiration, encouragement and support from many people.

First of all, I would like to express my most sincere gratitude to Dr. Thomas G. Habetler. He has been a wise and trusted advisor throughout the entire process. His trust of my abilities has given me invaluable opportunities to improve my research and communication skills, which helped me tremendously in my study and future career. I am deeply grateful for his guidance.

I am grateful to Dr. Ronald G. Harley and Dr. Deepak M. Divan for their knowledge and experience in my interactions with them, and especially for their suggestions and guidance on my research work. I would like to thank Dr. David G. Taylor and Dr. J. Rhett Mayor for being my dissertation committee members and for their support in completion of this work.

I would like to acknowledge the Eaton Corporation for providing the support for this work. I would like to especially thank Dr. Bin Lu for his continuous support and encouragement. I would also like to thank Peter J. Theisen, Steven A. Dimino, Charles J. Luebke and Peter J. Marshall at the Eaton Innovation Center for their valuable inputs and constant support.

Also a thank you goes to Dr. Sang-bin Lee. His work on the induction motor thermal protection has been the basis for this work and has inspired me in my research. Another thank you goes to Dr. Jose Aller for his valuable support and suggestions.

It is very fortunate for me to have the opportunity to work with the exceptional fellow graduate students in the electric power group at the Georgia Institute of Technology. Among them, I wish to especially thank Yi Du, Yao Duan, Yi Yang, Siwei Cheng, Jiaqi Liang and Stefan Grubic for the invaluable collaborations and discussions. I would also like to thank Anish Prasai, Jyoti Sastry, Frank Kreikebaum, Dr. Youngkook Lee, Aristidis Zachas, Andrew Paquette, Debrup Das, Diogenes Molina, Dustin Howard, Jorge Hernandez, Rohit Moghe, Sangtaek Han, Dr. Long Wu, Dr. Wei Zhou, Dr. Wei Qiao, and Dr. Zhi Gao for their friendship and support.

There are numerous names of faculty, family and friends that I should mention here, who have helped me during my four year at Georgia Tech. I want to express my gratitude to all of the people I know.

Most of all, I owe the greatest debt of gratitude to my family. My parents have always been the source of encouragement and support throughout my life. My dear wife, Jing Dai, has shared every single step in this long journey with me. Without their great love, encouragement, and understanding, everything would not have been possible.

# TABLE OF CONTENTS

Page

# LIST OF TABLES

Page

# LIST OF FIGURES

Page

# SUMMARY

Induction motors are widely used in industrial processes. The malfunction of a motor may not only lead to high repair costs, but also cause immense financial losses due to unexpected process downtime. Approximately 30-35% of motor failures are related to stator winding insulation [1-3]. Since thermal overload is one of the major root causes of stator winding insulation failure, an accurate and reliable monitoring of the stator winding temperature is crucial to increase the mean time to catastrophic motor breakdown, and to reduce the extraordinary financial losses due to unexpected process downtime. Because of the fast development and increased use of motor control devices, such as variable-frequency motor drives and reduced-voltage motor starters, the development of an improved thermal protection method that is applicable in combination with the motor control devices is highly desirable.

The objective of this research is to develop a non-intrusive, sensorless thermal protection scheme for induction motors fed by motor control devices under both in-service and de-energization conditions, using only motor terminal quantities, i.e. currents and voltages.

A comprehensive literature survey is presented to summarize the state of the art of stator winding temperature estimation techniques for in-service induction motors. These techniques are compared in terms of accuracy, implementation complexity, and practical feasibility. A novel thermal model reduction study is presented to further discuss the feasibility of the traditional type of thermal protection approaches. Based on the study of the existing techniques, the scope of this research is defined as: non-intrusive stator

winding temperature estimation method for induction motors fed by motor control devices.

To provide a reliable thermal protection for induction motors fed by motor control devices, a dc signal-injection method is proposed for in-service induction motors fed by soft-starter and variable-frequency drives. The stator winding temperature can be monitored based on the estimated stator winding resistance using the dc model of induction motors. In addition, a cooling capability monitoring technique is proposed to monitor the cooling capability of induction motors and to warn the user for proactive inspection and maintenance in the case of cooling capability deterioration. The proposed cooling capability monitoring technique, combined with the proposed stator winding temperature monitoring technique, can provide a complete thermal protection for in-service induction motors fed by motor control devices. The feasibility of the proposed thermal protection scheme consisting of the stator winding temperature monitoring and the motor cooling capability monitoring is validated by experimental results.

In addition, the active stator temperature estimation concept is extended to the application on de-energized induction motors. DC signals can be injected into induction motors without inducing any output torque for de-energized motors using soft-starters, based on which the stator winding temperature can be estimated. Via stator temperature estimation, the required thermal recovery time for intermittently operated motors can be minimized, which can largely improve the usage of the overall motor system.

Aside from online thermal protection during a motor's normal operation, the thermal protection of de-energized motors is also essential to prolong a motor's lifetime. Moisture condensation is one of the major causes to motor degradation especially in

high-humidity environments. To prevent moisture condensation, a non-intrusive motor heating technique is proposed by injecting currents into the motor stator winding using soft-starters. A motor's temperature can be kept above the ambient temperature due to the heat dissipation, so that the moisture condensation can be avoided.

To sum up, active stator winding temperature estimation techniques for induction motors under both operating and de-energization conditions are proposed in this dissertation for both thermal protection and optimizing the operation of a motor system. The importance of these proposed techniques lies in their non-intrusive nature: only the existing hardware in a motor control device is required for implementation; a motor's normal operation is not interrupted.

The conclusions, the recommendations for future research, as well as the major contributions of this research are presented at the end.

# CHAPTER 1 Introduction and Objective of Research

## 1.1 Background

Induction motors are extensively used in modern industry for converting electrical energy to mechanical energy. They consume more than 60% of the produced electrical energy and are typically essential components in industrial processes. As a result, the malfunction of induction motor may not only lead to the repair or replacement of the motor, but also cause extraordinary financial losses due to unexpected process downtime. For this reason, reliable motor protection is crucial in industrial processes for increasing the mean time to catastrophic motor breakdown and reducing the extraordinary financial losses due to unexpected process downtime.

Condition monitoring for proactive monitoring and reliable protection of induction motors has experienced a fast growth in recent years. Thermal protection is one of the most important features of the motor condition monitoring system. The thermal overload of a motor can lead to deterioration of the key components of the motor, including stator winding insulation, bearing, motor conductors, core, etc, and therefore is one of major underlying root causes of motor failures. As the most vulnerable part to thermal overload, the stator winding insulation normally reaches its thermal limit before any other motor component. Therefore, stator thermal protection is critical for extending the motor lifetime and preventing destructive motor failures.

Thus, thermal protection of the stator winding is the main scope of this research.

## 1.2 Stator Winding Insulation Failure

Motor winding insulation failure is one of the most common failures for induction motors. About 35-40% of induction motor failures are related to winding insulation failure [1-3].

The insulation failure is often the result of long-term thermal aging [4]. The electrical performance of the insulation material is largely degraded irreversibly due to chemical reactions when operated above the thermal limit. Such thermal overload often accelerates the deterioration of the insulation, and eventually reduces the motor's lifetime. As a rule of thumb, it is estimated that motor's life is reduced by 50% for every 10°C increase above the stator winding temperature limit. The typical thermal limits of the stator winding for different insulation classes are listed in Table 1.1 [5].

Table 1.1: Temperature limits for different insulation classes.

| Insulation Class | Ambient Temperature (ºC) | Rated Temperature Rise (ºC) | Hot Spot Temperature (ºC) |
|---|---|---|---|
| A | 40 | 60 | 105 |
| B | 40 | 80 | 130 |
| F | 40 | 105 | 155 |
| H | 40 | 125 | 180 |

The conditions under which the thermal limit of the motor can be exceeded are listed in Table 1.2 [6]:

Two examples of stator winding damage due to thermal overload are shown in Figure 1.1. Figure 1.1-(a) shows the stator winding damage due to unbalanced supply voltage; while Figure 1.1-(b) shows the stator winding damage due to overload.

Table 1.2: Thermal overload conditions.

| | |
|---|---|
| transient thermal overload | • overloading under transient;<br>• frequent starting;<br>• motor stall;<br>• short circuit, ground fault; |
| running thermal overload | • overload;<br>• unbalanced supply voltage; |
| abnormal cooling capabilities | • high ambient temperature;<br>• reduced motor cooling ability. |

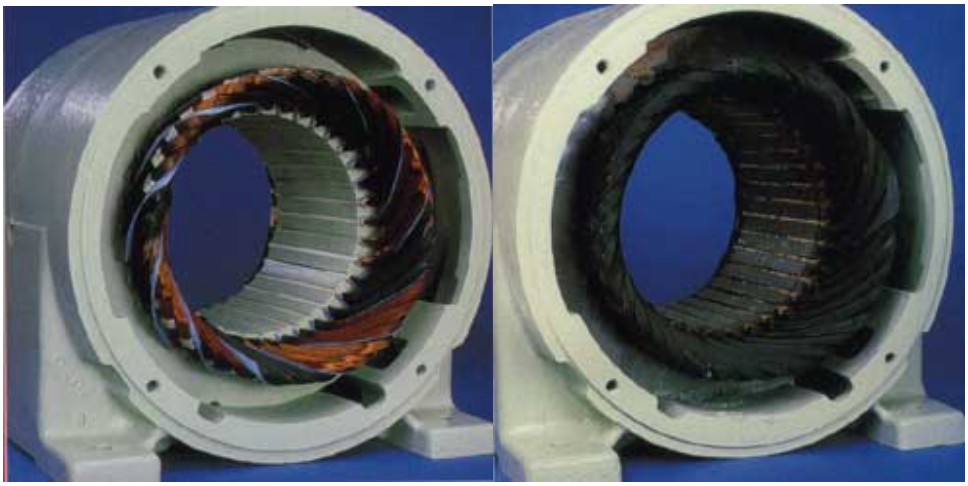

(a) unbalanced supply voltage (b) overload

Figure 1.1: Stator winding damage due to thermal overload.

### 1.3 Thermal Protection for Induction Motors

To proactively protect the motor from stator winding insulation failure and extend the motor's lifetime, the stator winding temperature must be continuously monitored

during operation. Numerous techniques have been developed for the thermal protection of induction motors. Generally, these techniques can be classified into three categories:

1. direct temperature measurement;
2. thermal model-based stator winding temperature estimation;
3. parameter-based stator winding temperature estimation.

The direct temperature measurement of the stator winding is typically performed using embedded thermal sensors, such as thermocouples, resistance thermal detectors (RTDs), infrared thermal sensors, etc. The embedded thermal sensors are not considered cost-efficient, especially for small- to medium- size motors, due to the high cost of their installation. Therefore, the practical application of these embedded thermal sensors is limited.

Thermal model-based stator winding temperature estimation techniques are broadly used in the thermal overload relays for thermal protection. These techniques first calculate the losses in a motor, and then estimate the stator winding temperature based on a motor's thermal model. However, the main drawback of these thermal model-based approaches is that the thermal parameters are not constant and measurements must be made for each motor under different operating conditions. In addition, as the thermal parameters are fixed after identification, these methods can not adapt to the change in the cooling capability of the motor.

Parameter-based stator winding temperature estimation techniques are proposed to estimate the stator winding temperature from the stator resistance, given that the variations of temperature are proportional to the variations of resistance for stator

winding coils. Since the stator resistance estimation techniques based on the motor's equivalent circuit are not accurate enough for accurate temperature estimation, dc signal injection-based methods are proposed to estimate the stator winding resistance using the motor's dc model [7-9]. However, the application of these dc signal injection-based methods is limited due to their high intrusiveness because an extra dc injection circuit needs to be installed in series with one of the motor loads. The major advantages of the parameter-based methods are:

1. they can adapt to the change in the cooling capability of the motor;
2. only the motor terminal quantities are required;
3. the motor's normal operation is not interrupted.

Aside from the stator temperature monitoring, the detection of abnormal cooling capability is also an important aspect of thermal protection of induction motors. An impaired cooling capability increases the temperature of the motor under the same operating condition, and therefore accelerates the deterioration of the insulation. In the case of impaired cooling capability, it is important to detect the problem as early as possible, so that the motor can be inspected and repaired proactively to avoid unscheduled process downtime due to catastrophic failure and extend the motor life.

With the fast development of motor control devices, such as solid-state motor starters, and variable-frequency motor drives, the thermal protection of the induction motor fed by motor control devices requires special attention for the thermal protection of these motors.

## 1.4 Problem Statement

As stated in the previous sections, the thermal protection for induction motors fed by motor control devices is of great importance for the reliable protection of induction motors, increasing the mean time to catastrophic motor breakdown, and reducing the extraordinary financial losses due to unexpected process downtime.

The objective of this research is to develop a non-intrusive, sensorless thermal protection scheme for induction motors fed by motor control devices under both in-service and de-energized operating conditions, using only motor terminal quantities.

## 1.5 Dissertation Outline

Chapter 2 presents a comprehensive survey of the previous work on stator winding temperature estimation for in-service induction motors. Chapter 3 summarizes the previous work on monitoring the cooling capabilities of the induction motor. A further study on the thermal model-based stator winding temperature estimation techniques is presented in Chapter 4. The proposed signal injection-based online stator winding temperature estimation techniques for soft-starter-connected and variable-frequency drive-fed induction motors are presented in Chapter 5 and Chapter 6, respectively. A study on the magnetic effects of dc signal injection of operating induction motors is shown in Chapter 7. Chapter 8 proposes a cooling capability monitoring scheme for in-service motors based on the estimated stator temperature via dc signal injection. In addition, a stator temperature estimation technique for de-energized induction motors is presented in Chapter 9 for improving the usage of intermittently operated motor systems. The non-intrusive motor heating technique using soft-starters for preventing moisture condensation is shown in Chapter 10. Experimental studies are conducted for the

validation of the proposed approaches. The conclusions, contributions and the recommendation for future work are summarized in Chapter 11.

# CHAPTER 2 Previous Work on Stator Temperature Estimation

## 2.1 Overview

Thermal overload is one of the major underlying root causes of motor failures. Therefore, the accurate monitoring of the stator winding temperature is critical to proactively protect the motor [10].

Due to the high cost of embedded thermal sensors and their installation, many stator winding temperature estimation techniques have been developed over the years. They can be generally classified into two categories:

1. thermal model-based stator temperature estimation;
2. parameter-based stator temperature estimation.

In this chapter, these two types of techniques are summarized and compared in terms of accuracy, implementation complexity and practical feasibility.

## 2.2 Thermal Model-based Stator Temperature Estimation

### 2.2.1 Induction Motor Losses

The temperature rise of induction motors is caused by the accumulation of losses in different components of the motor, including stator winding, stator core, rotor cage, rotor core, friction, etc. IEEE Std 112 defines five types of losses in induction motors [11], as (2.1).

$$W_{Losses} = P_{input} - P_{output} = W_s + W_r + W_{core} + W_{fw} + W_{LL}, \quad (2.1)$$

where $P_{\text{input}}$ and $P_{\text{output}}$ are the input and output powers of the motor, respectively, and $W_{\text{Losses}}$ is the total loss in the motor.

Stator copper loss $W_s$ is the copper loss in the stator windings. It equals $3I_s^2R_s$ for a three-phase motor, where $I_s$ is the rms phase current; and $R_s$ is the average per-phase stator resistance. Rotor copper loss $W_r$ is the loss in the rotor windings. Core loss $W_{core}$ is caused by the magnetizing hysteresis and eddy currents in the iron. It varies approximately with the frequency and the square of the input voltage. For fixed input voltage, it remains approximately constant from no load to full load. Windage and friction loss $W_{fw}$ is the mechanical rotational loss resulting from the friction and windage. Stray-load loss $W_{LL}$ is the loss in a motor not accounted for by the sum of $W_s$ , $W_r$ , $W_{core}$ , and $W_{fw}$ . The typical power flow in induction motors is shown in Figure 2.1[12].

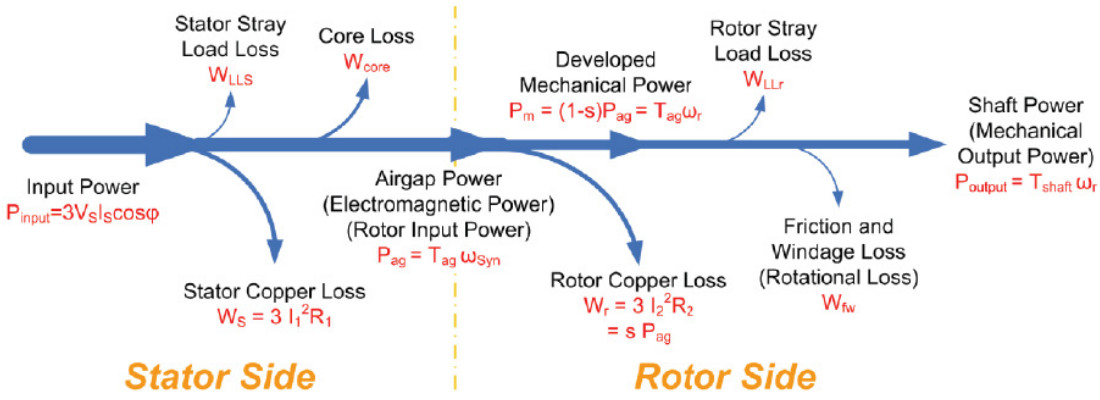


Figure 2.1: Typical power flow in induction motors [12].

Accurate stator temperature estimation via thermal models requires an accurate estimation of the losses in an induction motor, and accurate identification of thermal parameters.

For mains-fed or soft-starter-connected induction motors, the stator and rotor copper losses can be estimated using current measurements; however, the estimation of core loss, windage and friction loss and stray loss is difficult, and requires complex offline testing.

For variable-frequency drive-fed induction motors, the core loss, the windage loss and the friction loss vary largely due to the change of the frequency and magnitude of the input voltages, and the variations of the rotor speed. Therefore, the estimation of losses for these motors is even more difficult.

### 2.2.2 First-order Thermal Model

#### 2.2.2.1 Thermal limit curve

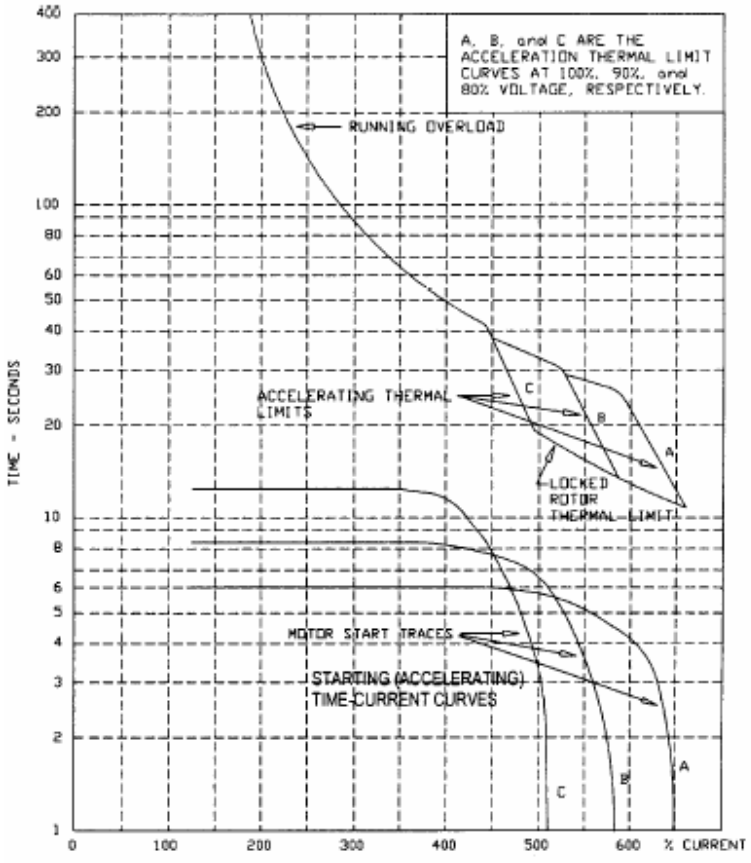


Figure 2.2: Typical thermal limit curve of induction motors [13].

To protect induction motor from thermal overload, delay-time fuses and microprocessor-based thermal relays are broadly used for their simplicity. These devices

are designed based on thermal limit curves, which defines the safe operating time for different magnitudes of input currents under locked rotor condition, acceleration, and running overload condition [13]. To protect the motor, these devices trip the motor once the thermal limit is reached. The typical thermal limit curve is shown in Figure 2.2. These thermal limit curves are fundamentally equivalent to thermal protection which is based on the first-order thermal model.

2.2.2.2 First order thermal model

The first-order thermal models normally require the estimation of only the stator copper loss, not the other losses, and therefore are broadly used due to their implementation simplicity. However, because of their negligence of the stator temperature rise caused by the other losses, the first-order thermal models lack accuracy.

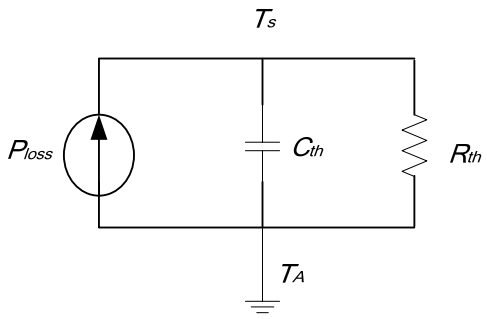


Figure 2.3: First-order thermal model of induction motor.

The first-order thermal model is represented by a uniform thermal body with a single thermal capacitor and a single thermal resistor, as shown in Figure 2.3. $T_s$ and $T_A$ represent the stator winding temperature and the ambient temperature, respectively; $C_{th}$ represents the equivalent thermal capacitance, which models the intrinsic thermal characteristic of the stator winding; $R_{th}$ represents the equivalent thermal resistance,

which models the cooling capability from the stator winding to the ambient; $P_{loss}$ represents the heat dissipation in the stator winding, which is mainly the copper loss, given by,

$$P_{loss} = 3I_{rms}^2 R_s , \tag{2.2}$$

where $I_{rms}$ represents the rms value of the phase current.

Using the first-order thermal model, the stator temperature can be calculated as,

$$T_s(t) = P_{loss} \cdot R_{th}(1 - e^{-\frac{t}{\tau}}) + T_{s0} e^{-\frac{t}{\tau}} + T_A , \tag{2.3}$$

where $T_{s0}$ is the initial stator winding temperature; and $\tau$ is the thermal time constant ($R_{th} \cdot C_{th}$).

Given $R_{th}$, $T_A$, and the thermal limit, $T_{max}$, the time needed to trip the motor is

$$t = \tau \ln[\frac{I^2 R_s \cdot R_{th}}{I^2 R_s \cdot R_{th} - (T_{max} - T_A)}], \tag{2.4}$$

and

$$T_{max} - T_A = I_{max}^2 R_s \cdot R_{th} . \tag{2.5}$$

Therefore

$$t = \tau \ln[\frac{I^2 R_s \cdot R_{th}}{I^2 R_s \cdot R_{th} - I_{max}^2 R_s \cdot R_{th}}] = \tau \ln(\frac{I^2}{I^2 - I_{max}^2}) . \tag{2.6}$$

2.2.2.3 Thermal parameter identification based on motor's nameplate information

Since the time to trip is only related to the product of $R_{th}$ and $C_{th}$, and $I_{max}$, the calculation of the trip time requires the identification of thermal parameters.

With the service factor defined as $SF = \frac{I_{\max}}{I_{rated}}$, the time to trip is then given by,

$$t = \tau \ln(\frac{I_{pu}^{\ 2}}{I_{pu}^{\ 2} - SF^2}). \quad (2.7)$$

where $I_{pu} = \frac{I}{I_{rated}}$.

The trip class ($TC$) of induction motors is defined as the maximum time of safe overload operation when the input current is six times the rated current. Therefore, given the trip class and the service factor of induction motor, the thermal time constant can be roughly estimated as,

$$\tau = TC / \ln(\frac{6^2}{6^2 - SF^2}). \quad (2.8)$$

Accordingly, the trip time can be calculated as,

$$t = \tau \ln(\frac{I_{pu}^{\ 2}}{I_{pu}^{\ 2} - SF^2}) = TC \bullet \ln(\frac{I_{pu}^{\ 2}}{I_{pu}^{\ 2} - SF^2}) / \ln(\frac{6^2}{6^2 - SF^2}). \quad (2.9)$$

Equation (2.9) is equivalent to the thermal limit curve as shown in Figure 2.2. The thermal limit curve method is equivalent to estimate the stator temperature using equation (2.3), and trip the motor when the thermal limit is reached.

Equation (2.9) is equivalent to the thermal limit curve as shown in Figure 2.2. The thermal limit curve method is equivalent to estimating the stator temperature using equation (2.3), and tripping the motor when the thermal limit is reached.

The first-order thermal model of induction motors is broadly used due to its implementation simplicity: only the motor current needs to be measured; thermal parameters can be estimated using the nameplate information of the motor [14]. However, as these approaches neglect the temperature rise caused by the other losses and the change of the motor's thermal behavior under different operating conditions, these

thermal models are generally inaccurate and conservative, and therefore trip the motor long before the actual thermal limit is reached.

### 2.2.3 High-order Thermal Networks

To improve the stator temperature estimation accuracy by considering the effect of different losses on stator temperature, high-order thermal models are proposed.

#### 2.2.3.1 Second-order thermal models

References [15-17] propose second-order thermal models to estimate the stator temperature. The stator and the rotor are modeled separately so that the effects of the rotor losses and the rotor temperature rise on the stator temperature rise can be considered. An example of a second-order thermal model is shown in Figure 2.4. To estimate the stator and rotor temperature, the stator and rotor losses must be estimated, and the thermal parameters have to be identified.

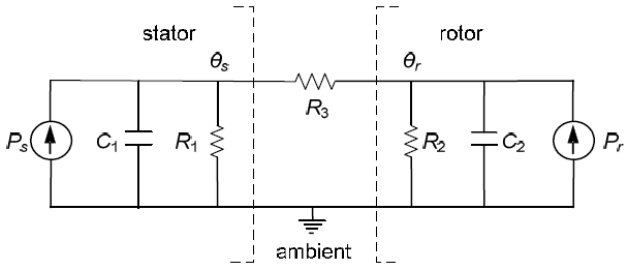


Figure 2.4: Second-order thermal model of induction motor [15].

It is proposed in [15, 18-19] to first estimate the rotor temperature from the rotor resistance using the motor's electrical model, and then estimate the stator temperature. It is roughly estimated that 60% percent of the rotor losses pass through the air-gap to the stator [20]. However, these approaches still require the identification of the thermal

parameters, which is difficult, since the identification needs to be accomplished for every motor under each cooling condition.

2.2.3.2 Higher-order thermal networks

Since the second-order thermal models can only model the stator and rotor of the motor, higher-order thermal models are proposed to model the thermal behavior of different motor components [20-24]. An example of a five-component thermal network is shown in Figure 2.5. The five nodes represent 1) stator core, 2) stator slot section, 3) stator end-winding, 4) rotor squirrel cage and 5) rotor core. The thermal parameters can be identified using embedded thermal sensors. Although these higher-order thermal networks are a more accurate representation of the motor's thermal behavior, their practical applications are limited due to the difficulty in loss estimation and thermal parameter identification.

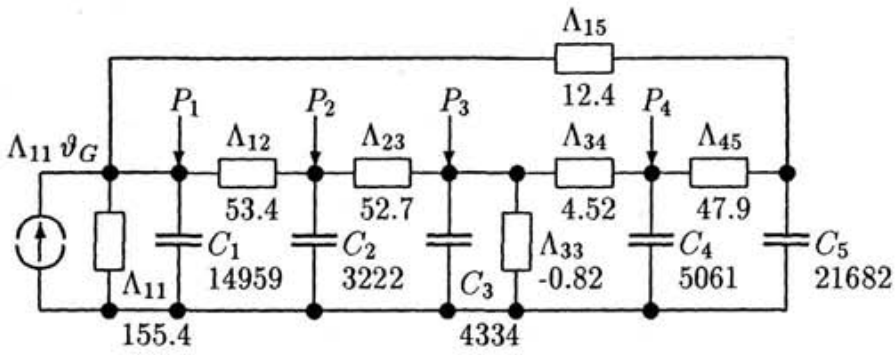


Figure 2.5: Five-component thermal model of induction motor [24].

Reference [25] proposes to calculate the thermal parameters based on the dimensions of the motor. However, the identification of thermal parameters associated with convection is difficult, which limits the accuracy of thermal parameter identification

using this approach. Besides, the accurate measurements of the dimensions of the motor components are required, which may not be available.

#### 2.2.3.3 Summary

Generally, the practical applications of these higher-order thermal models are limited due to the difficulty in the motor loss estimation and the thermal parameter identification. In addition, since these approaches cannot adapt to a change in the motor's cooling capability, thermal parameter identification is required under each operating condition using embedded sensors. However, this is often impractical, especially for small- to medium-size induction motors due to economic reasons.

## 2.3 Parameter-based Stator Temperature Estimation

### 2.3.1 Introduction

Parameter-based stator temperature estimation approaches estimate the stator temperature from a stator resistance estimation, since the variations of the temperature is proportional to the variations of resistance for stator windings [26]:

$$\hat{T}_s = T_{s0} + \frac{(\hat{R}_s - R_{s0})}{\sigma R_{s0}}, \tag{2.10}$$

where $T_{s0}$ and $R_{s0}$ represents $T_s$ and $R_s$ at room temperature; $\hat{T}_s$ and $\hat{R}_s$ are the estimated $T_s$ and $R_s$, respectively; and $\sigma$ is the temperature coefficient of resistivity.

Therefore, the stator temperature can be simply monitored based on the estimation of stator resistance, and the stator temperature estimation accuracy is highly dependent on the accuracy of stator resistance estimation.

The stator resistance estimation techniques can be generally classified into two categories:

1. motor model-based stator resistance estimation;
2. signal injection-based stator resistance estimation.

### 2.3.2 Motor Model-based Stator Resistance Estimation

#### 2.3.2.1 Electrical model of induction motor

The motor model-based stator resistance estimation approaches are typically based on the motor's electrical model.

Neglecting the zero sequence components in the stator voltages and currents, the stator voltage and current space vectors in the d-q stationary reference frame, $\bar{v}_{dqs}$ and $\bar{i}_{dqs}$ , can be derived as,

$$\bar{v}_{dqs} = \begin{bmatrix} \sqrt{\frac{2}{3}}\left[ v_{ab}\cos\left(\theta_{da} - \frac{2\pi}{3}\right) - v_{ca}\cos\left(\theta_{da} - \frac{4\pi}{3}\right)\right] \\ \sqrt{\frac{2}{3}}\left[ v_{ab}\sin\left(\theta_{da} - \frac{2\pi}{3}\right) - v_{ca}\sin\left(\theta_{da} - \frac{4\pi}{3}\right)\right] \end{bmatrix}, \tag{2.11}$$

$$\bar{i}_{dqs} = \begin{bmatrix} \sqrt{\frac{2}{3}}\left[ i_a\cos\theta_{da} + i_b\cos\left(\theta_{da} - \frac{2\pi}{3}\right) - \left(i_a + i_b\right)\cos\left(\theta_{da} - \frac{4\pi}{3}\right)\right] \\ -\sqrt{\frac{2}{3}}\left[ i_a\sin\theta_{da} + i_b\sin\left(\theta_{da} - \frac{2\pi}{3}\right) - \left(i_a + i_b\right)\sin\left(\theta_{da} - \frac{4\pi}{3}\right)\right] \end{bmatrix}, \tag{2.12}$$

where $\theta_{da}$ is defined as the angle between the d-axis of the d-q transform and the a-axis of the stator winding.

The electrical model of induction motors in d-q reference frame is presented as,

$$\begin{bmatrix} V_{qs} \\ V_{ds} \\ V_{qr} \\ V_{dr} \end{bmatrix} = \begin{bmatrix} R_s + pL_s & \omega_s L_s & pL_m & \omega_s L_m \\ -\omega_s L_s & R_s + pL_s & -\omega_s L_m & pL_m \\ pL_m & s\omega_s L_m & R_r + pL_r & s\omega_s L_r \\ -s\omega_s L_m & pL_m & -s\omega_s L_r & R_r + pL_r \end{bmatrix} \begin{bmatrix} i_{qs} \\ i_{ds} \\ i_{qr} \\ i_{dr} \end{bmatrix}, \quad (2.13)$$

where $\omega_s$ is the synchronous speed; $L_m$, $L_s$, $L_r$ are the mutual inductance, stator inductance and rotor inductance; $R_s$ and $R_r$ are the stator and rotor resistance, respectively.

2.3.2.2 Motor model-based stator resistance estimation

The proposed stator resistance estimation techniques are mainly used for improving the field-oriented control performance at low speed or improving the sensorless speed estimation accuracy [27-37]. In [38], the stator resistance is estimated based on the error between measured stator current and the current command. In [30], the stator-flux linkage, $\lambda_{qds}$, is estimated from the rotor-flux-linkage estimate that is obtained from the rotor equations when the motor is operated at low speed. The value of $R_s$ is then estimated from $\lambda_{qds}$ using the stator-flux equation. It is proposed in [39] to calculate $R_s$ using the estimate of the rotor resistance, $R_r$ , by assuming $R_s/R_r$ is constant.

Reference [40] proposes a mutual model reference adaptive system (MRAS) approach for estimating $R_s$ and $R_r$, which is shown in Figure 2.6.

In [41], a cascade $R_s$ and $R_r$ estimation scheme in the steady state is proposed. The overall structure of the estimator is shown in Figure 2.7.

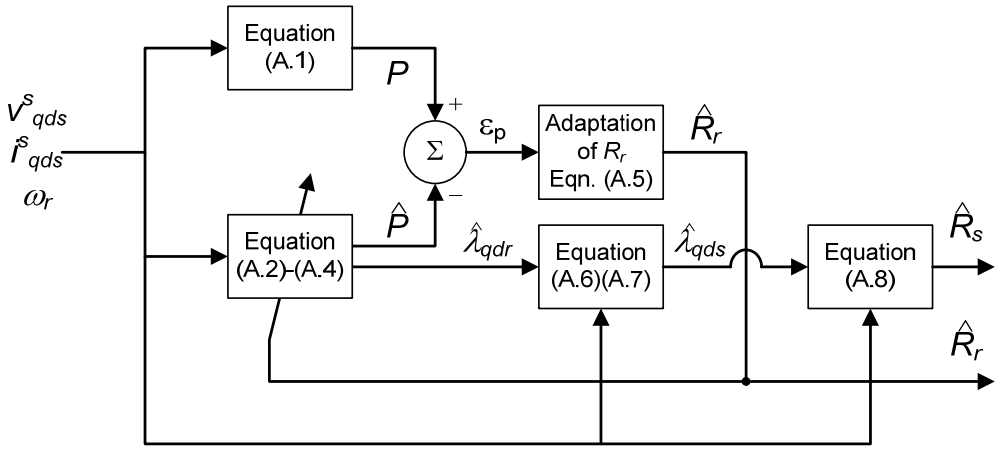


Figure 2.6: Structure of the MRAS $R_s$ and $R_r$ estimator [40].

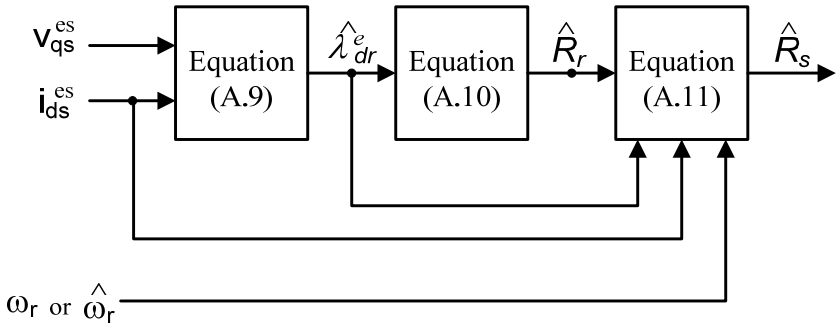


Figure 2.7: Structure of the cascade $R_s$ and $R_r$ estimator.

2.3.2.3 Sensitivity analysis

For the motor model-based stator resistance estimation approaches, the other motor parameters, such as $R_r$, $L_m$, $L_s$, $L_r$, etc, need to be known before the estimation of the stator resistance. However, these parameters are affected by the operating point of the induction motor and change due to saturation, temperature, speed etc.

In [41] it is shown that the stator resistance estimation is highly sensitive to variations of the motor parameters, especially under high speed conditions. Therefore, the practical application of these approaches for thermal protection purposes is limited,

since high stator resistance estimation accuracy for the reliable thermal protection of induction motors is required.

### 2.3.3 Signal Injection-based Stator Resistance Estimation

As the motor model-based stator resistance estimation approaches are too sensitive to the variations of motor parameters, the dc model of induction motors is also used to estimate the stator resistance.

It is first proposed in [7] to inject a dc signal by installing power diodes between one of the motor leads, as shown in Figure 2.8. The dc signal is injected due to the difference in the voltage drop when the stator current is flowing in different directions. However, the injected dc signal induces a torque oscillation, which is undesirable. Since there is no control mechanism for the operation of the diodes the magnitude of the injected dc signal cannot be controlled and therefore, the magnitude of the torque oscillation cannot be adjusted.

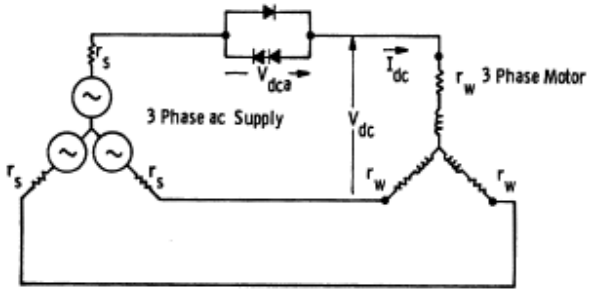


Figure 2.8: DC signal injection using power diodes.

As the dc signal injection circuit cannot control the actually injected dc voltage, it is proposed in [8-9] to inject dc signals using a MOSFET and a resistance. The dc signal injection circuit is shown in Figure 2.9. By controlling the switching of the MOSFET, the equivalent resistance of the dc signal injection circuit varies when the current flows in

different directions, as shown in Figure 2.10. The actually injected dc voltage can be controlled by adjusting the resistance in the signal injection circuit. The dc signal is only injected for 0.25 second every 30 seconds to limit the effects of the torque oscillation.

The dc injection approaches estimate the resistance relatively accurate since it is not affected by the variations of motor parameters, but the practical applications of these dc signal injection-based stator resistance estimation methods are limited by their high intrusive nature: an extra circuit needs to be installed between one of the motor leads.

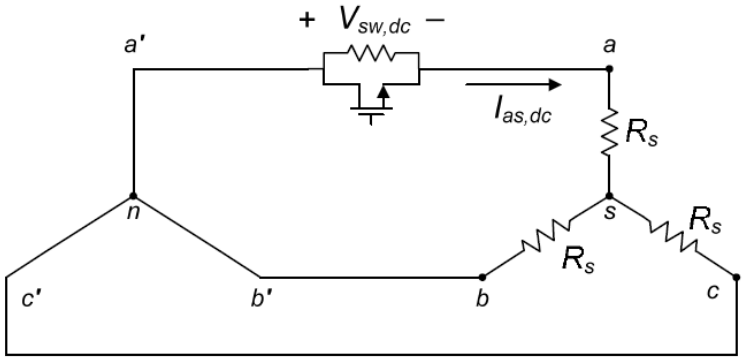


Figure 2.9: DC model during dc signal injection using MOSFET.

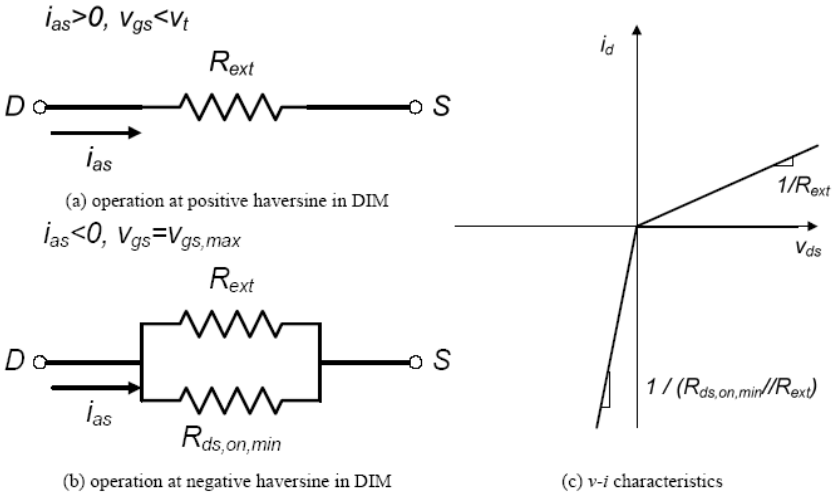


Figure 2.10: DC signal injection circuit using MOSFET.

## 2.4 Chapter Summary

In this chapter, the previous works on the stator temperature estimation approaches are reviewed. These methods are compared in terms of accuracy, implementation complexity, and practical feasibility.

The stator temperature estimation techniques can be generally classified into two categories:

1. thermal model-based stator temperature estimation;
2. parameter-based stator temperature estimation.

The thermal model-based stator temperature estimation methods estimate the stator temperature based on the motor's thermal model. However, these methods suffer from the difficulty of thermal parameter identification and the motor loss estimation. In addition, these methods cannot adapt to the variations of the motor's cooling capability.

The parameter-based stator temperature estimation techniques estimate the stator temperature from the estimated stator resistance. The motor model-based stator resistance approaches are generally too sensitive to the variations of motor parameters, and therefore can not provide enough accuracy for the reliable thermal protection of induction motors. As a result, dc signal injection-based methods are proposed to estimate the stator resistance from the motor's dc model. However, these dc signal injection-based methods suffer from their high intrusive nature: an extra circuit needs to be installed between at one of the motor leads.

For induction motors fed by motor control devices, the difficulty of thermal parameter identification and the motor loss estimation for thermal model-based

approaches still exists. Furthermore, the motor model-based stator resistance estimation approaches are not accurate enough for thermal protection purposes. The variations of the motor parameters can be expected to be even larger for variable-frequency drive-fed motors than for mains-fed motors, due to the variations of input frequency, input voltage magnitude, and rotor speed. Therefore, dc signal injection-based approaches are considered to be the perfect candidate for the thermal protection of induction motors fed by motor control devices. The dc signal injection can be achieved by changing the operation of motor control devices. Thus, no additional hardware is required and the high intrusiveness of the existing dc signal injection-based methods can be avoided.

# CHAPTER 3 Previous Work on Cooling Capability Monitoring

## 3.1 Overview

Monitoring the stator winding temperature is crucial to protect the motor from thermal overload. In case of a thermal overload the motor must be tripped immediately to avoid catastrophic motor failures. However, the monitoring of the stator winding temperature alone is not sufficient for the thermal protection of induction motors, since it does not identify the cause of the temperature rise.

As shown in Table 1.2, thermal overload can be caused by various reasons, such as overload, unbalanced input voltage, impaired cooling capabilities, etc. The impaired cooling capability increases the motor temperature rise, and accelerates the deterioration of induction motor components. Thus, in the case of impaired cooling capabilities, it is important to detect the problem as early as possible, so that the motor can be inspected and repaired to proactively avoid catastrophic process downtime and extend the motor life. The impaired cooling capability can occur when the motor's ability to radiate heat is obstructed due to the follow reasons [8]:

- broken cooling fan;
- motor frame dust build-up;
- obstruction of coolant flow in duct/vent;
- winding dirt build-up;
- clogged/covered motor fins/casing.

The early detection of impaired cooling capability can avoid the motor temperature rise due to impaired cooling, and therefore prolong motor's life.

### 3.2 Detecting Impaired Cooling Capability of Induction Motors

A parameter tuning technique is proposed in [16] to track the stator and rotor resistance of the induction motor. The error between the estimated rotor speed from terminal measurements and the estimated rotor speed from the rotor slot harmonics, is used to tune the rotor resistance. The rotor thermal parameters are then calculated based on the estimated rotor resistance. The change of the rotor's thermal parameters indicates the impaired cooling capability or a motor failure. However, the requirement of thermal/electrical model parameters limits its practical use.

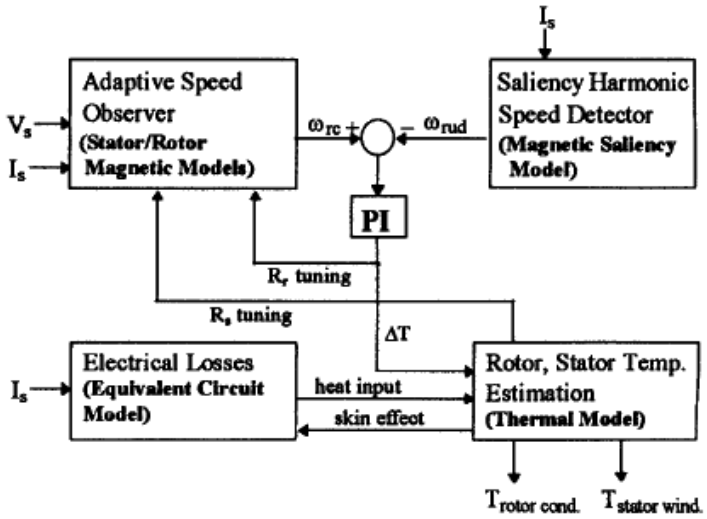


Figure 3.1: Stator and rotor resistance tuning scheme [16].

In [42] it is proposed to use the error between the stator temperature estimated by the electrical model, and the one estimated from motor's thermal model to detect an impaired cooling condition. One thermocouple is installed on the surface of the motor, as a part of the thermal model. A Kalman filtering technique is used to estimate parameters based on given models. However, besides its requirement of electrical/thermal parameters, the

requirement of thermocouple limits its practical use, since it is not feasible especially for small- to medium- size motors for economic reasons.

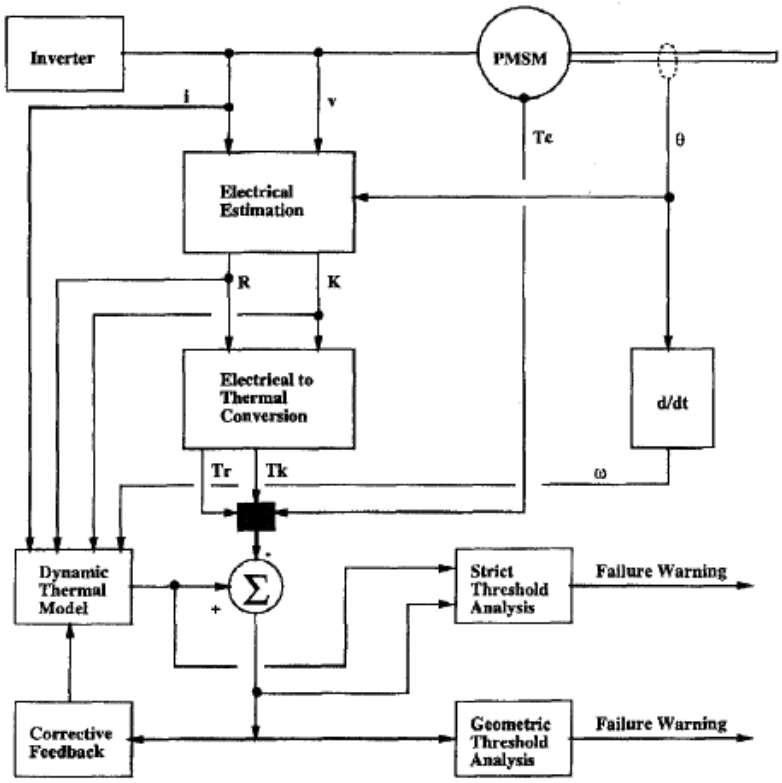


Figure 3.2: Thermal condition monitoring system [42].

In [8], it is proposed to compare the stator resistance estimated using the motor's thermal model, and the one estimated using dc signal injection for monitoring the cooling capability. The thermal parameters are estimated using the estimated stator resistance via dc signal injection under healthy condition. The thermal model using the estimated thermal parameters is then used to estimate the stator temperature/resistance. The error between the estimated stator resistance using the thermal model and the one using dc signal injection is then used as the fault indicator. However, all the thermal parameters

have to be estimated under each load condition from cold start, which may not be feasible for practical applications.

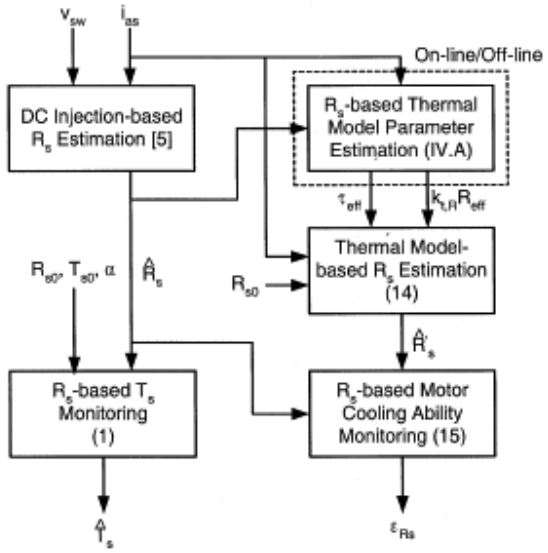


Figure 3.3: Scheme of cooling capability monitoring [8].

## 3.3 Chapter Summary

Although monitoring the cooling capability of induction motors is critical for the reliable thermal protection of induction motors, very few approaches are currently available.

The fundamental of the proposed methods lies in the comparison between the estimated stator resistance using the motor's electrical model, and the one using motor's thermal model. However, these approaches all suffer from the requirement of electrical/thermal parameters. The difficulty in the identification of thermal parameters still limits their practical applications.

# CHAPTER 4 A Transfer Function-based Thermal Model Reduction Study

## 4.1 Overview

Thermal model-based stator winding temperature estimation is one of the most popular approaches used in thermal overload relays. To fully understand and evaluate the feasibility of these techniques with different requirements on implementation complexity and computational efforts, a transfer-function-based thermal model reduction study is presented in this chapter.

The thermal behaviors of a mains-fed induction machine are analyzed, based on a novel simplified thermal model for mains-fed induction machine. This novel thermal model for induction machine has two major advantages: low implementation complexity and high accuracy. Experimental testing is conducted for the validation of the proposed thermal model.

Although the proposed thermal model is accurate and simple for implementation, its major disadvantages are that complex processes are required for the identification of the thermal parameters; it can not adapt to the change of a motor's cooling capability.

## 4.2 A Novel Simplified Thermal Model of Induction Machines

### 4.2.1 Thermal Behavior of Mains-fed Induction Machine for Thermal Model Reduction

The increase of stator winding temperature is an accumulated effect of all different loss mechanisms in the induction machine during operation, such as stator/rotor copper loss, core loss, friction loss, etc. The power flow and losses in induction machines are

illustrated in Figure 2.1. Since these losses are induced in different locations of the induction machine, their impact on the stator winding temperature are different due to the different heat transfer capability from different motor components to the stator. Due to the complex thermal behavior of induction machines, simplified thermal models, as illustrated in Figure 2.3, are typically inaccurate to monitor the stator winding temperature for thermal protection purposes.

The thermal behavior of induction machines can be generally represented in a transfer function form [43], as,

$$\theta_s(s) = \sum Z_i(s) \bullet P_{loss}(s), \tag{4.1}$$

where $P_{loss}$ is motor losses in different components of induction machines; $Z_i$ is the transfer function representing the heat transfer capability from each motor component to the stator; $\theta_s$ represents the $T_s$ rise above ambient temperature.

Since the thermal responses of different losses to the stator temperature vary greatly, the overall thermal behavior of induction machines varies largely under different operating conditions. For instance, for a shorter operating duration, the thermal effects of losses with faster response dominate the stator temperature rise, whereas, for a longer operating duration, the thermal effects of losses with slower response dominate the stator temperature rise. Under different load conditions, the response of the stator winding temperature also varies largely due to the fact that the distribution of motor losses changes due to the change of load condition. For instance, for a higher load condition, the thermal effects of the copper losses increase, and therefore, the stator temperature has a stronger dependence on the thermal transient of copper losses.

As a result, although widely used in current thermal overload relays, the first-order thermal model, as illustrated in Figure 2.3, is not capable of providing accurate modeling of the machine's thermal behavior, since only one time constant is used under all different operating conditions with all the aforementioned thermal effects neglected. Even when second-order thermal models are applied as illustrated in Figure 2.4, the effects of many other motor losses, such as core loss, friction loss, etc, are still neglected.

Therefore, it is highly desirable to develop an accurate yet simple thermal model for the real-time implementation in thermal protective relays for the reliable thermal protection of mains-fed induction machines.

### 4.2.2 Motor Losses in Mains-fed Induction Machines for Stator Temperature Estimation

Since the thermal behavior of induction machines is the accumulation of thermal effects of different motor losses, it is essential to understand the change of different motor losses under different operating conditions. For mains-fed induction machines, since both the magnitude and the frequency of the input voltage do not vary, the actual rotor speed only varies slightly under different load conditions, since the slip is typically very small even under full load conditions. Therefore, the change of friction and windage losses is small under different load conditions. The iron core losses, which are roughly a function of the magnitude and frequency of the input voltage [44], also vary slightly. The copper losses, which are functions of the stator and rotor current, may change largely under different load conditions, due to the change of current magnitudes. Therefore, the motor losses can be generally classified into two categories: copper losses, which change largely with operating condition; and the other losses, which only vary slightly with the

change of operating conditions. The segregation of these two types of losses is denoted as $Loss_1$ and $Loss_2$.

As discussed above, with $Loss_2$ only varying slightly under different operating conditions, it is essential to obtain accurate estimation of the copper losses, $Loss_1$, for the estimation of stator temperature. Using a motor's equivalent circuit, the copper losses can be accurately monitored online, since both the stator current and rotor current can be calculated. However, these calculations require the knowledge of key motor parameters, such as mutual inductance, stator/rotor leakage inductance, etc. Therefore, for simplicity in real-time implementation, with the magnetizing current neglected, the copper losses can be roughly represented as,

$$Loss_1 = 3(R_s + R_r)I_s^2, \tag{4.2}$$

where $R_s$ and $R_r$ are the stator and rotor resistance, respectively, and $I_s$ is the rms value of the phase current. Although (4.2) is far from accurate especially under low-load conditions, such approximation is still feasible for obtaining an accurate estimation of the stator temperature for thermal overload protection purposes. Since the purposes of the thermal overload protection is to prevent the motor from thermal overload, which typically happens under overload conditions when a machine's cooling capability is not impaired, the accuracy of stator temperature estimation under high-load conditions are more important than that under low-load conditions. Therefore, although inherently inaccurate, (4.2) does not largely affect the accuracy in the estimation of the copper losses and thus stator temperature for thermal protection purposes, especially under high load conditions.

### 4.2.3 A Novel Simplified Thermal Model of Mains-fed Induction Machine

Based on the classification of motor losses, the thermal behavior of induction machines can be simplified as,

$$\theta_s(s) = Z_1(s) \cdot Loss_1(s) + Z_2(s) \cdot Loss_2(s), \tag{4.3}$$

where $Z_1$ and $Z_2$ represent the thermal responses of $Loss_1$ and $Loss_2$, respectively. For simplicity, transfer functions $Z_1$ and $Z_2$ can be approximated using 1st order transfer functions with a single time constant, as,

$$Z_1(s) = \frac{\alpha_1}{s + 1/\tau_1}; Z_2(s) = \frac{\alpha_2}{s + 1/\tau_2}, \tag{4.4}$$

where $\alpha_1$ and $\alpha_2$ are the gains; $\tau_1$ and $\tau_2$ are the time constants.

Considering that $Loss_2$ is almost constant under normal operating conditions, using (4.4), the stator temperature rise caused by different motor losses can be shown as,

$$\begin{aligned} \theta_s(s) &= \frac{\alpha_1}{s + 1/\tau_1} \cdot Loss_1 + \frac{\alpha_2}{s + 1/\tau_2} \cdot Loss_2 \\ &= \frac{k_1 {I_s}^2}{s + 1/\tau_1} + \frac{k_2}{s + 1/\tau_2} \end{aligned}, \tag{4.5}$$

where $k_1$ and $k_2$ are constants. In time domain, the $T_s$ rise can be represented as,

$$T_s(t) = k_1 {I_s}^2 (1 - e^{-t/\tau_1}) + k_2 (1 - e^{-t/\tau_2}), \tag{4.6}$$

when the machine is started from room temperature.

Therefore, the rise of $T_s$ can be considered as the combined contributions from two parts: the temperature rise due to copper losses, which vary for different load conditions; and the temperature rise due to other losses, which can be considered constant for different load conditions. It should be noted that based on the above analysis, since $Loss_2$ does not vary greatly under different operating conditions, for long time varying

load operations, the temperature rise caused by $Loss_2$ can be considered constant and independent of any load change after a certain amount of operating time. Therefore, the stator winding temperature can be modeled using only three parameters,

$$T_s(t) = k_1 I_s^{\,2}(1 - e^{-t/\tau_1}) + k_2 . \qquad (4.7)$$

In other words, the thermal transient of machines after cold startup is the combined effects of both $Loss_1$ and $Loss_2$; while after hot startup, the thermal transient is mainly attributed to the change of copper losses, $Loss_1$. This explains the difference of thermal transient after cold and hot startup [43].

Based on (4.6) and (4.7), the stator temperature can be accurately monitored with much fewer thermal parameters required yet higher accuracy, since the effects of different motor losses are considered.

The main advantages of this novel simplified thermal model lie in its feasibility in real-time implementation: low computation effort is required; only stator current needs to be monitored.

## 4.3 Experimental Validation

### 4.3.1 Experimental Setup

The proposed thermal model is tested on a 7.5-hp ODP induction motor, whose ratings and parameters are shown in Table 4.1. The motor phase currents are measured using Hall-effect sensors. The data are then acquired and stored using a *NI/LabView* data acquisition system with 16-bit A/D conversion at 5 kHz sampling frequency. The motor is instrumented with 9 K-type thermocouples at different locations in the stator winding (3 in each phase) to record its average winding temperature for validation purposes.

Another K-type thermocouple is installed to measure the ambient temperature. The accuracy of the thermocouple data logger is claimed to have an error within 1.1°C. The overall experimental setup is shown in Figure 4.1.

Table 4.1: Nameplate Information of Induction Motor

| Induction Motor for Experimental Testing | | | |
|---|---|---|---|
| HP | 7.5 | Brand | Leeson |
| CAT. NO. | G140417 | RPM | 1760 |
| Volts | 230/460 | NEMA | B |
| Nom. Pf | 0.72 | Nom. Eff. | 0.885 |
| F.L. AMPS | 20.0/10.0 | ENCL. | ODP |

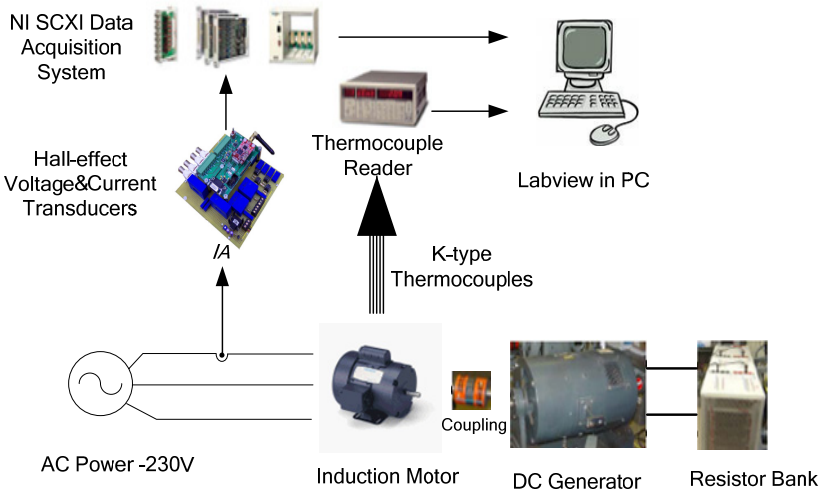


Figure 4.1: Experimental Setup.

### 4.3.2 Parameter Identification for the Proposed Thermal Model

Based on the analysis presented in Section 4.2.3, the stator temperature rise caused by $Loss_2$ can be considered constant after a certain amount of operating time. Therefore, to estimate the thermal parameters in (4.6) and validate the analysis presented in Section 4.2.3, the motor is first operated from cold start under 25% of the rated load for 1.5 hours,

when it is assumed that thermal equilibrium is reached; then the motor is operated under a varying load condition: 50%→75%→100%→125% of the rated load. The measured average stator winding temperature is shown in Figure 4.2.

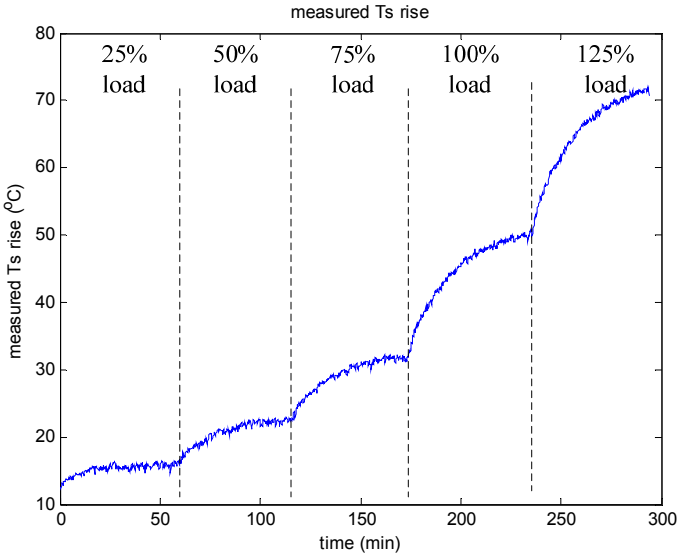


Figure 4.2: Measured $T_s$ rise under varying load condition.

The thermal time constant for each load condition is then identified using least-square nonlinear curve fitting to the following function:

$$T_s(t) = T_s(\infty)(1 - e^{-t/\tau}) + T_{s0}\,, \tag{4.8}$$

where τ represents the thermal time constant; and $T_s(\infty)$ represents the $T_s$ after the motor reaches thermal balance. It can be observed in Figure 4.3 that the thermal time constants under 50%, 75%, 100%, and 125% load conditions are roughly the same, while the time constant under 25% load condition differs largely from the ones under the other load conditions. This is because the $T_s$ rise under 25% load condition is the combined results of $Loss_1$ and $Loss_2$; while under 50%-125% load, the $T_s$ rise caused by $Loss_2$ has reached steady state, and therefore these thermal transients are mainly caused by $Loss_1$. This

observation confirms the analysis in Section 4.2.3. Assuming that the thermal transients under 50-125% load conditions are purely caused by the copper losses, $Loss_1$, the thermal time constant, $\tau_1$, can be estimated as the thermal time constants under 50%-125% load conditions.

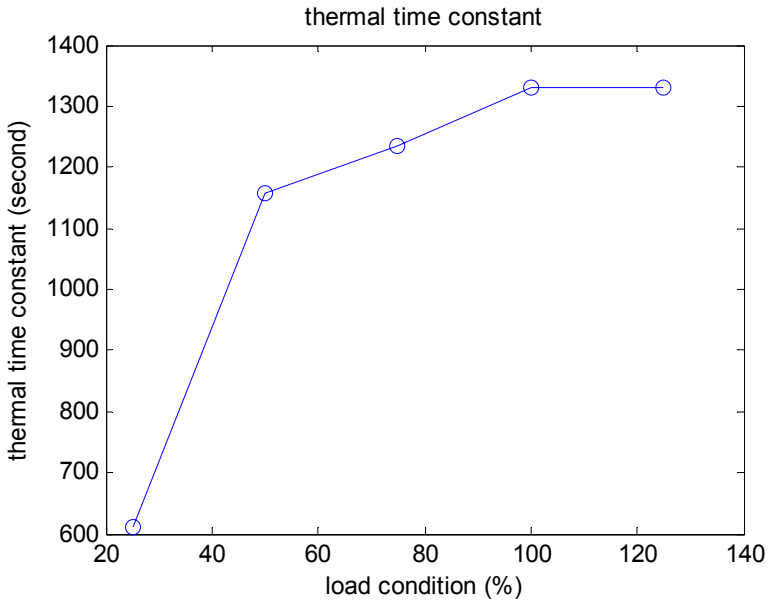


Figure 4.3: Identified thermal time constant for different load conditions.

Table 4.2: Comparison of the Identified Thermal Parameters under Different Load Conditions

| Load conditions | 50% | 75% | 100% | 125% |
|---|---|---|---|---|
| time constant $\tau_1$ (sec.) | 1160 | 1230 | 1330 | 1330 |
| gain $k_1$ (ºC /Amp$^2$) | 0.1427 | 0.1327 | 0.1325 | 0.1380 |

The thermal parameter, $k_1$, in (4.6), can then be estimated assuming that during the load variation testing, the increase of stator temperature is mainly caused by the increase of copper losses, when load conditions are changed as: 50%→75%→100%→125% of the rated load. Therefore, $k_1$ can be calculated as,

$$k_1 = \frac{T_s(\infty) - T_{s,25\%}(\infty)}{I_s^{\,2} - I_{s,25\%}^2}, \tag{4.9}$$

where $I_s$ and $T_s(\infty)$ represent the rms stator current and the stator temperature after the motor reaches thermal balance under 50-120% load conditions; $I_{s,25\%}$ and $T_{s,25\%}(\infty)$ represent the rms stator current and the stator temperature after the motor reaches thermal balance under 25% load conditions. The identified thermal parameters under 50-120% load conditions are compared in Table II. It can be observed that the thermal parameters identified under different load conditions are very close, which confirms the assumption that the thermal transients under 50-125% load conditions are mainly caused by copper losses, $Loss_1$, and therefore have similar thermal characteristics. The $k_1$ and $\tau_1$ in (4.6) and (4.7) are estimated to be 0.1365 ºC/A$^2$ and 1260 seconds, respectively, using the average of the identified parameters under load conditions from 50% to 125%.

With the thermal parameters associated with copper losses identified, the stator temperature rise caused by the other losses, $Loss_2$, can be calculated using the stator temperature under 25% load conditions after cold startup as,

$$T_{s,Loss2}(t) = k_2(1 - e^{-t/\tau_2}) = T_s(t) - k_1 I_s^{\,2}(1 - e^{-t/\tau_1}), \tag{4.10}$$

by removing the stator temperature rise caused by the copper losses. The estimated temperature rise caused by $Loss_2$ under 25% load condition is shown in Figure 4.4. Therefore, the thermal parameters associated with $Loss_2$ can be identified.

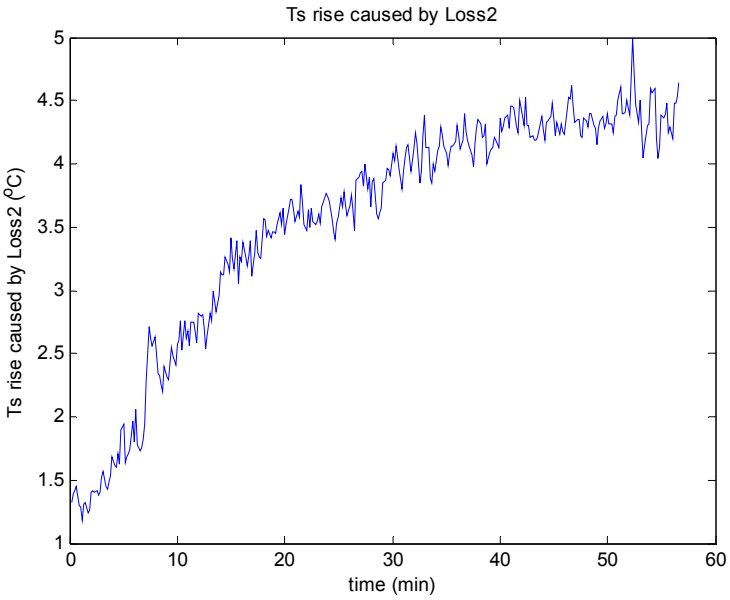


Figure 4.4: Temperature rise caused by $Loss_2$.

### 4.3.3 $T_s$ Estimation using the Proposed Thermal Model from Cold Startup

To test the feasibility of the proposed thermal model, the motor is operated from cold start under 75% and 100% of the rated load, respectively. The average stator temperature is also measured using embedded thermocouples for validation purposes. The proposed thermal model with the identified thermal parameters is used to estimate the stator winding temperature, only based on the phase current measurement. To compare the effectiveness of this proposed thermal model and the first-order thermal model, which is broadly used in conventional overload relays, the stator temperature is also estimated using the first-order thermal model. The thermal parameters in the first-order thermal model are estimated based on the measured stator temperature under 25% load condition.

The stator temperature estimation results, together with the measured average stator temperature under 100% load condition and 75% load condition are shown in Figure 4.5

and Figure 4.6, respectively. It is clearly shown that the $T_s$ estimation accuracy using the proposed thermal model greatly outperforms the accuracy of the first order thermal model.

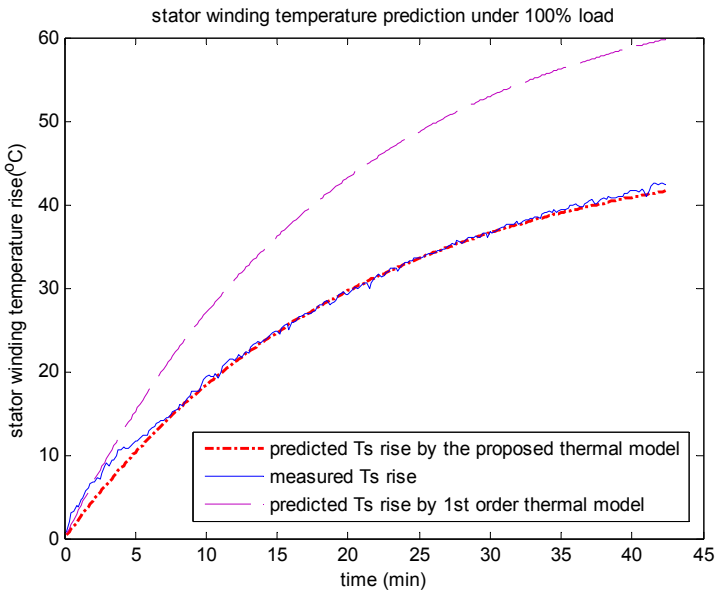


Figure 4.5: Ts estimation under 100% load condition.

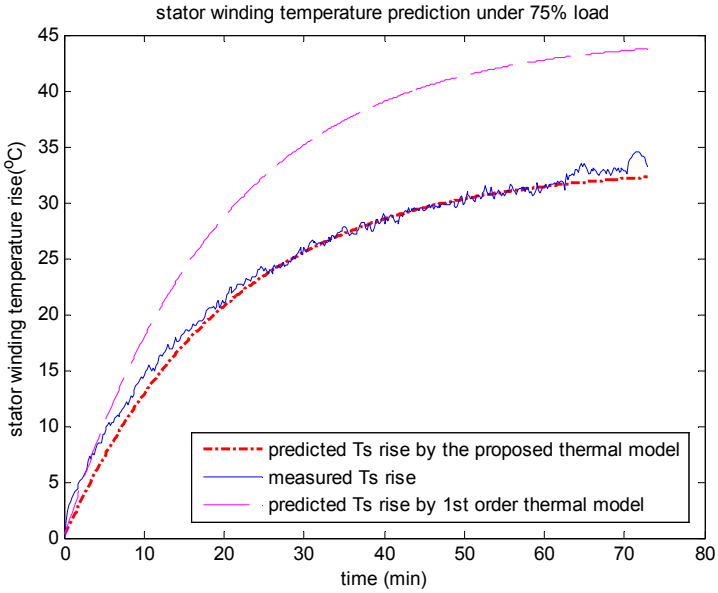


Figure 4.6: Ts estimation under 75% load condition.

The maximum stator temperature estimation error using the proposed thermal model is within 3°C, with the rms error within 1 °C; while the stator temperature estimation error given by the first order thermal model is as large as 25°C. Considering the possible instrumental error, the rms error of the proposed thermal model is within 2°C. The large stator temperature estimation error of the first-order thermal model is mainly caused by the variations of thermal parameters under different load conditions. The machine's thermal behavior is caused by the combined effects of different losses in the machine. Under different operating conditions, the thermal characteristics of induction machines vary largely. Therefore, the thermal parameters in first order thermal models need to be identified under each operating conditions for accurate thermal protection, which is highly impractical for real-time implementation. However, in the proposed simplified thermal model, the variations of the induction machine's thermal characteristics can be accurately modeled with the consideration of different motor losses under different operating conditions.

### 4.3.4 $T_s$ Estimation using the Proposed Thermal Model under Periodic Operating Duty Cycle

To test the feasibility of the proposed thermal model under long time operations, the induction machine is operated under periodic operating duty cycles, as defined in [10]. The induction machine is periodically operated under 50% and 125% of the rated load for 40 minutes. Again, the estimated stator winding temperatures using the proposed thermal model and the first order thermal model are compared with the measured average stator temperature using embedded thermal sensors, as shown in Figure 4.7.

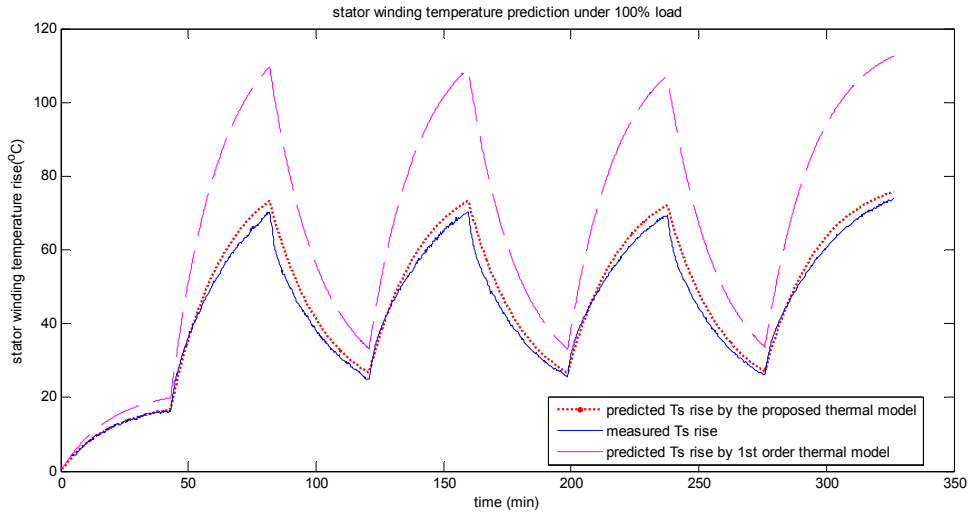


Figure 4.7: Ts estimation under periodic operating duty cycles

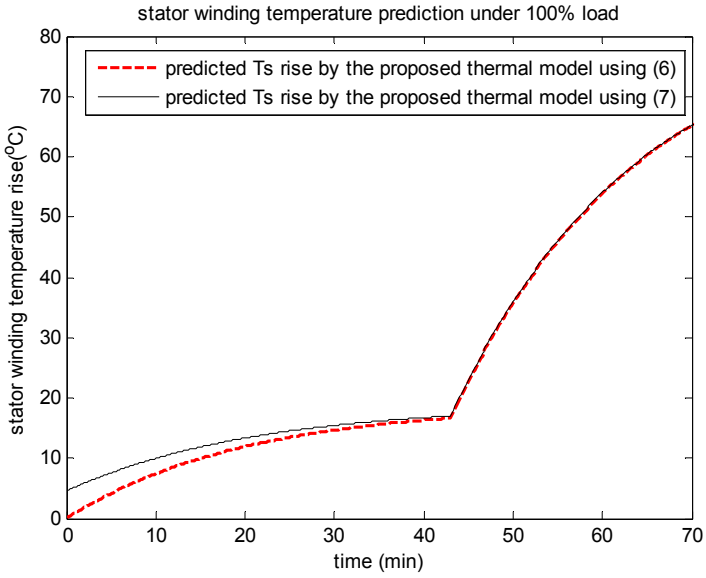


Figure 4.8: Ts estimations using (4.6) and (4.7).

The rms error in the stator winding temperature estimation using the proposed thermal model is within 2°C; while the estimation error using first order thermal model is 25°C. Even when considering the possible instrumental error, the rms error of the proposed thermal model is within 3°C, which is a large improvement compared to first

order thermal model. The proposed thermal model outperforms the first-order thermal model. It should be noted that for this type of long time operation, (4.7) can be used instead of the full model (4.6), since the temperature rise caused by $Loss_2$ reaches steady state after a certain duration of operation, and therefore the thermal transients caused by $Loss_2$ can simply be considered as constant. The estimated stator temperatures using (4.6) and (4.7) are compared in Figure 4.8. It can be observed from Figure 4.8 that (4.6) and (4.7) give the same stator temperature estimation results after a small amount of time (in this case, about 40 minutes). Therefore, for long time operation (4.7) can be used for accurate stator temperature estimation, with only 3 thermal parameters required. This again greatly simplifies the real-time implementation of thermal models in thermal overload relays.

## 4.4 Chapter Summary

In this chapter, a novel simplified thermal model for induction machines has been proposed based on the analysis of machine's thermal behavior. Instead of using lumped thermal networks, a transfer function based approach has been applied, with far less thermal parameters required for accurately modeling the thermal behavior of induction machines. In order to achieve an accurate estimation under different initial operating conditions, the losses in induction machines have been classified into two categories: copper losses, which can be calculated by monitoring the phase currents; the other losses, which are roughly constant under different load conditions. Due to this segregation, the complexity of the thermal model of the induction machine can be greatly reduced.

The proposed simplified thermal model has been validated from experimental testing of a 7.5-hp ODP induction machines under various load conditions, including constant

load testing and periodic operation. The major advantages of the proposed thermal model are summarized as follows:

1. High accuracy. The maximum $T_s$ estimation error from experimental testing is within 4°C, with the rms error within 3 °C;
2. Low calculation effort required. No complex calculation is required, which greatly reduces the cost of overload relays;
3. Easy implementation. Since only current sensors are needed, the proposed thermal model can be easily implemented in thermal overload relays without any requirement on additional hardware.

However, the method also has some disadvantages, which are:

1. Difficulty in parameter identification: thermal parameters in the thermal model need to be identified before the model can be used for online thermal protection;
2. Sensitive to changes in a motor's cooling capability. The thermal parameters can not adapt to the changes in a motor's cooling capability.

Although the proposed thermal model is simple for implementation and has high accuracy, its disadvantages result in the need for thermal protection techniques which can be robust to the changes of a motor's cooling capability.

# CHAPTER 5 Stator Temperature Estimation for Soft-starter-connected Induction Motors

## 5.1 Overview

Accurate stator temperature estimation is crucial to prevent the motor from thermal overload and catastrophic motor failures. Based on the review of existing stator temperature estimation techniques and the thermal model studies presented in the previous chapters, the practical application of thermal model-based techniques is limited due to the difficulties in thermal parameter identification and its sensitivity to the change of a motor's cooling capability. Therefore, dc signal injection-based methods are considered as the candidate methods due to their high accuracy and sensorless nature: only motor terminal quantities are needed.

Soft-starter has been a widely used cost-efficient motor protection device in industry. The soft-starter typically uses solid-state power switches to limit the starting current of induction motors, which leads to a "soft" startup.

In this chapter, a dc signal injection-based stator temperature/resistance estimation technique is presented for soft-starter-connected induction motors. By changing the operation of the power switches in a soft-starter, dc signals can be injected into the stator winding of an induction motor. Therefore, the stator winding resistance and temperature can be estimated. Experimental testing is conducted for the validation of this proposed technique.

## 5.2 Structure of Soft-starter

The soft-starter normally contains multiple anti-parallel solid-state switches (*e.g.*, thyristors) to control the current flow and, in turn, the terminal voltages of the motor.

The soft-starter limits the transient voltages and currents, avoids the inrush currents, and results in a "soft" motor start. After starting, the soft-starter enters the "bypass" mode, when the contactors are closed to minimize the power dissipation. The basic structure of a soft-starter with anti-parallel thyristors is shown in Figure 5.1.

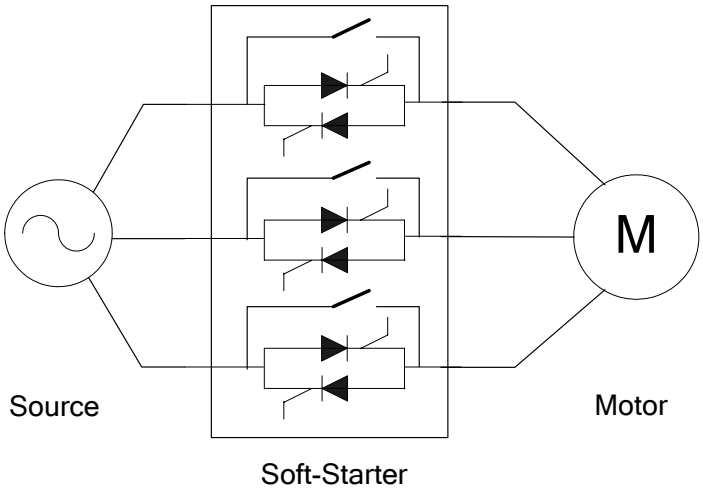


Figure 5.1: Basic structure of soft-starters.

By changing the gate drive signals of the thyristors in the soft-starter, a small *adjustable* dc bias can be intermittently injected to the motor for estimation of the stator winding resistance. Based on online and continuous monitoring of the stator winding resistance, the stator winding temperature can be monitored using only motor voltage and current.

### 5.3 DC Signal Injection using Soft-starter

A new gate drive control mode, namely "*dc injection mode (DIM)*," is proposed in this work to inject dc components in the motor line voltages and phase currents. During the dc injection period, only one contactor (corresponding to only one phase, *e.g.*, phase ***a***) in the soft-starter is kept open, while the other two contactors still work normally as in

bypass mode. Instead of using the *symmetrical operation mode*, a short delay is introduced to the gate drive signal of only the forward- (backward-) conducting thyristor of phase ***a*** ($V_{G1}$), after the phase ***a*** current's rising (falling) zero-crossing. After the DIM period, the phase ***a*** contactor is closed, so that the soft-starter returns to normal bypass operation. Figure 5.2 shows the typical waveforms of the motor line voltage ($v_{ab}$), phase current ($i_a$), while a small delay angle of α (α < 30°) is added.

Therefore, dc signal can be injected by changing the operation of the thyristors to estimate the stator winding resistance and temperature using motor's dc model.

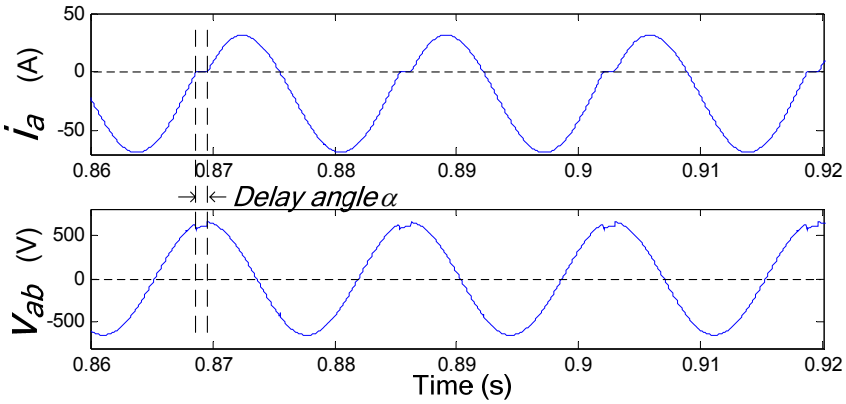


Figure 5.2: Motor line voltage, phase current during DIM.

## 5.4 Stator Temperature Estimation for Soft-starter-connected Induction Motors

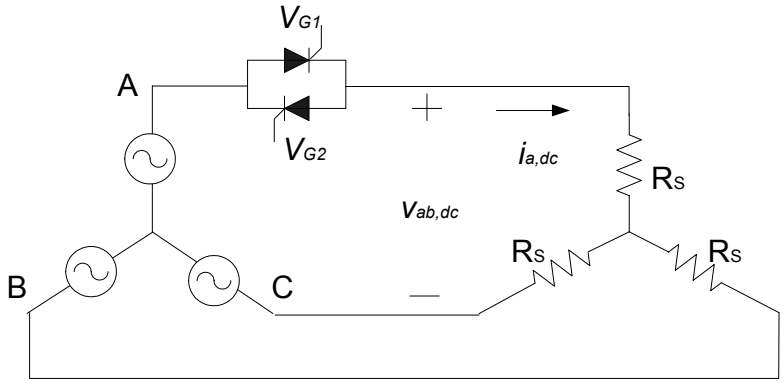


Figure 5.3: DC equivalent circuit of motor, source and soft-starter.

The dc components in the input voltages and currents do not "pass through" the air-gap of the induction motors, and hence have no impact on the rotor circuit. Therefore, the equivalent dc model of the induction motor with a soft-starter can be illustrated as in Figure 5.3. The stator resistance $R_s$ can be estimated from the terminal voltages and currents as

$$R_s = \frac{2 \cdot v_{ab}^{dc}}{3 \cdot i_a^{dc}}, \tag{5.1}$$

where $v_{ab}^{dc}$ and $i_a^{dc}$ are the dc components of the motor line voltage $v_{ab}$ and phase current $i_a$, respectively.

Based on the estimated $R_s$ from dc signal injection, the stator winding temperature $T_s$ can be monitored using equation (2.10).

## 5.5 Evaluation of Torque Pulsation

As shown in Figure 5.2, due to the small delay angle $\alpha$ ($\alpha < 30°$), it can be assumed that $v_{ab}$ only consists of dc component and line frequency ($\omega_e$) component, as

$$v_{ab} \approx v_{ab}^{dc} + v_{ab}^{\omega_e}. \tag{5.2}$$

Similarly, the phase current $i_a$ can be approximately denoted as

$$i_a \approx i_a^{dc} + i_a^{\omega_e}, \tag{5.3}$$

where $i_a^{dc}$ and $i_a^{\omega_e}$ are the dc component and the line frequency component of $i_a$, respectively, as shown in Figure 5.4.

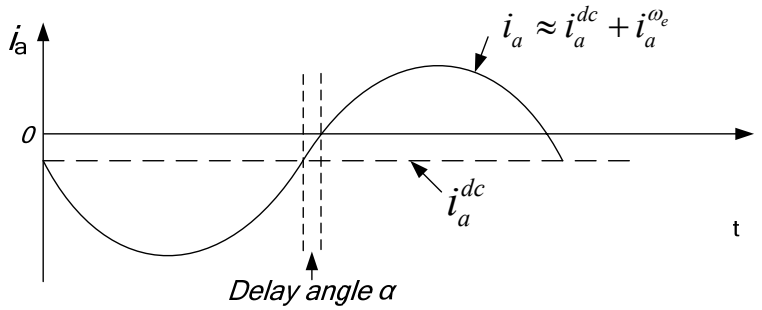


Figure 5.4: Approximation of motor phase current during DIM.

Therefore, the dc component in $i_a$ can be approximately derived as

$$i_a^{dc} \approx -\hat{I}_a^{\omega_e} \sin(\alpha), \tag{5.4}$$

where $\hat{I}_a^{\omega_e}$ is the peak value of the line frequency component in $i_a$.

Let $\vec{v}_{dqs}$, $\vec{i}_{dqs}$, and $\vec{\lambda}_{dqs}$ be the stator voltage, stator current, and total flux linkage space vectors in the d-q stationary reference frame. The air-gap torque, $T_{ag}$, can be calculated as the cross product of $\vec{\lambda}_{dqs}$ and $\vec{i}_{dqs}$, as

$$T_{ag} = \frac{3P}{4}\left|\vec{\lambda}_{dqs} \otimes \vec{i}_{dqs}\right|, \tag{5.5}$$

where $P$ is the number of poles.

The flux linkage vector can be estimated based on the stator voltage and current vectors as

$$\vec{\lambda}_{dqs} = \int (\vec{v}_{dqs} - R_s \vec{i}_{dqs})dt \approx \int \vec{v}_{dqs} dt, \tag{5.6}$$

The flux and current space vectors can be decomposed into vectors at multiples of the fundamental frequency, as

$$\vec{\lambda}_{dqs} = \sum_{n=-\infty}^{+\infty} \vec{\lambda}_{dqs}^{n\cdot 60} \quad and \quad \vec{i}_{dqs} = \sum_{n=-\infty}^{+\infty} \vec{i}_{dqs}^{n\cdot 60}, \quad n \in Z, \tag{5.7}$$

where the superscript of each decomposed vector indicates its rotating direction and angular speed in the vector space, assuming the supply frequency is 60 Hz.

The correlation of each component in the injected signals to the torque pulsation can be evaluated separately based on this decomposition analysis. The frequency of the torque variation caused by flux linkage vector $\vec{\lambda}_{dqs}^{f_1}$ and current vector $\vec{i}_{dqs}^{f_2}$ is $|f_1 - f_2|$. Therefore, the air-gap torque in (5.5) can be extended as

$$\begin{aligned} T_{ag} &= \frac{3P}{4}\left|\left(\sum_{n=-\infty}^{+\infty}\vec{\lambda}_{dqs}^{n\cdot 60}\right)\otimes\left(\sum_{n=-\infty}^{+\infty}\vec{i}_{dqs}^{n\cdot 60}\right)\right| \\ &= \frac{3P}{4}\left|\vec{\lambda}_{dqs}^{60}\otimes\vec{i}_{dqs}^{60}\right| + \frac{3P}{4}\left|\vec{\lambda}_{dqs}^{60}\otimes\vec{i}_{dqs}^{dc}\right| + \xi_T \\ &= T_1^{dc} + T_2^{60} + \xi_T \end{aligned}, \tag{5.8}$$

where $T_1^{dc}$, $T_2^{60}$ represent the dc, 60 Hz major components in the air-gap torque; $\xi_T$ is the remaining high frequency torque components. Neglecting high-order harmonics in the flux linkage and stator current, the dc component and the 60 Hz component in the air-gap torque can be respectively denoted as

$$\begin{aligned} \left|T_{ag}^{dc}\right| &\approx \left|T_1^{dc}\right| \approx \frac{3P}{4}\left|\vec{\lambda}_{dqs}^{60}\otimes\vec{i}_{dqs}^{60}\right| \\ \left|T_{ag}^{60}\right| &\approx \left|T_2^{60}\right| \approx \frac{3P}{4}\left|\vec{\lambda}_{dqs}^{60}\otimes\vec{i}_{dqs}^{dc}\right| \end{aligned}. \tag{5.9}$$

Using (5.8), (5.9) can be derived as

$$\begin{aligned} \left|T_{ag}^{dc}\right| &\approx \left|T_1^{dc}\right| \approx \frac{3P}{4}\left|\vec{\lambda}_{dqs}^{60}\otimes\vec{i}_{dqs}^{60}\right| \\ &\approx \frac{3P}{4}\left|\int\vec{v}_{dqs}^{60}dt\otimes\vec{i}_{dqs}^{60}\right| = \frac{3P}{4}\left|\vec{\lambda}_{dqs}^{60}\right|\left|\vec{i}_{dqs}^{60}\right|\cos(\varphi) \end{aligned}, \tag{5.10}$$

where $\cos(\varphi)$ is the power factor.

The dc component in the air-gap torque is induced by the fundamental frequency component in the phase current, as in bypass mode; while the 60 Hz component in the air-gap torque is the torque distortion caused by the injected dc current. It should be noted that the negative sequence current caused by the dc injection is negligible compared to the injected dc component, so the major harmonic in the air-gap torque is the 60 Hz component caused by the injected dc current.

The percentage torque pulsation can be simply derived using (5.9) and (5.10) as

$$\frac{\left|T_{ag}^{60}\right|}{\left|T_{ag}^{dc}\right|} \approx \frac{\left|\vec{\lambda}_{dqs}^{60} \otimes \vec{i}_{dqs}^{dc}\right|}{\left|\vec{\lambda}_{dqs}^{60} \otimes \vec{i}_{dqs}^{60}\right|} = \frac{\left|\vec{\lambda}_{dqs}^{60}\right|\left|\vec{i}_{dqs}^{dc}\right|}{\left|\vec{\lambda}_{dqs}^{60}\right|\left|\vec{i}_{dqs}^{60}\right| \bullet \cos(\varphi)} = \frac{\sin(\alpha)}{\cos(\varphi)}, \tag{5.11}$$

Therefore, the percentage torque pulsation caused by the injected dc signal can be controlled within an acceptable range by controlling the delay angle $\alpha$.

## 5.6 Improving Stator Temperature Estimation Accuracy

The accuracy of the $R_s$ estimate is highly dependent on the magnitude of the injected dc signal, while a smaller dc signal is preferred to limit the torque distortion. To obtain a more accurate estimate of $T_s$ with a smaller injected dc signal, a filter is necessary to improve the performance of the thermal monitoring. Traditional IIR/FIR filter design techniques, such as *Wiener Filter*, cannot be used due to a lack of training data. Therefore, an adaptive Kalman filter is preferred as no training data are needed.

The design of the adaptive Kalman filter requires a state-space model of the stator winding temperature. Although the high-order thermal model of induction motors can give an accurate estimate of $T_s$, the thermal parameters are hard and sometimes impossible to obtain accurately without installing thermal sensors in the induction motor. Therefore, a simple first-order thermal model is used to model $T_s$. The thermal

capacitance $C_{th}$ and the thermal resistance $R_{th}$ can be approximately obtained from the Trip Class (*TC*) and the Service Factor (SF) of the induction motor, as shown in Chapter 2. Based on equation (2.3), the difference equation for $T_s$ can be derived as,

$$\begin{aligned} T_s(n+1) &= e^{-\frac{\Delta t}{\tau}}[T_s(n)-T_A]+3I^2{}_{rms}R_sR_{th}(1-e^{-\frac{\Delta t}{\tau}})+T_A \\ &=[T_s(n)-T_A]+3I^2{}_{rms}[R_{s0}+\alpha R_{s0}(T_s-T_{s0})]R_{th}(1-e^{-\frac{\Delta t}{\tau}})+T_A \\ &=[e^{-\frac{\Delta t}{\tau}}+3I^2{}_{rms}\alpha R_{s0}R_{th}(1-e^{-\frac{\Delta t}{\tau}})]T_s(n)+\{(1-e^{-\frac{\Delta t}{\tau}})T_A \\ &\quad +3I^2{}_{rms}[R_{s0}-\alpha R_{s0}T_{s0}]R_{th}(1-e^{-\frac{\Delta t}{\tau}})\} \end{aligned} \quad (5.12)$$

The state space model of the system is,

$$\begin{aligned} x(n+1) &= Ax(n)+Bu(n)+w(n) \\ y(n) &= Cx(n)+v(n) \end{aligned} \quad (5.13)$$

where $A=e^{-\frac{\Delta t}{\tau}}+3I^2{}_{rms}\alpha R_{s0}R_{th}(1-e^{-\frac{\Delta t}{\tau}})$, $B$=$C$=1, and $u(n)=(1-e^{-\frac{\Delta t}{\tau}})T_A+3I^2{}_{rms}[R_{s0}-\alpha R_{s0}T_{s0}]R_{th}(1-e^{-\frac{\Delta t}{\tau}})$. The quantity $x$(n) is the estimated stator temperature by the adaptive Kalman filter, denoted as $\hat{T}_{s,AKF}$. The quantity $y$(n) is the estimated stator temperature based on the estimate of $R_s$ from the dc injection, denoted as $\hat{T}_{s,dc}$. Note that $w$(n) is the modeling error of $T_s$, and $v$(n) is the estimation error of $\hat{T}_{s,dc}$.

The update of the Kalman filter is given by equation (5.14), where $P$ is the error covariance matrix, $Q_v$ and $Q_w$ are the autocorrelation matrix of the modeling error and estimation error, respectively.

$$
\begin{aligned}
&\hat{x}(n \mid n-1) = A\hat{x}(n-1 \mid n-1) + Bu(n-1) \\
&P(n \mid n-1) = AP(n-1 \mid n-1)A^T + Q_w(n) \\
&K(n) = P(n \mid n-1)C^T[CP(n \mid n-1)C^T + Q_v(n)]^{-1}. \\
&P(n \mid n) = [I - K(n)C]P(n \mid n-1) \\
&\hat{x}(n \mid n) = \hat{x}(n \mid n-1) + K(n)[y(n) - C\hat{x}(n \mid n-1)]
\end{aligned}
\tag{5.14}
$$

The performance of the adaptive Kalman filter is highly dependent on the selection of $Q_v$ and $Q_w$. Although the mean value of modeling error $w$(n) is not zero, as required by the no bias condition of Kalman filter, a properly selected $Q_w$ can effectively reduce the influence of inaccurate modeling. As the thermal parameters in the Trip Class (*TC*) thermal model are conservative, the modeling error becomes larger due to changes of thermal parameters under higher load conditions. So, $Q_w$ can be roughly approximated as equation (5.15) to compensate for the inaccurate modeling.

$$
Q_w = 25I_{p.u.}(^oC^2), \tag{5.15}
$$

where $I_{p.u.}$ is the per unit value of the phase current in bypass mode. $Q_v$ can be simply estimated as the variance of $\hat{T}_{s,dc}$, when the motor reaches thermal steady state under 100% load condition.

## 5.7 Stator Temperature Estimation Scheme for Soft-starter-connected Induction Motors

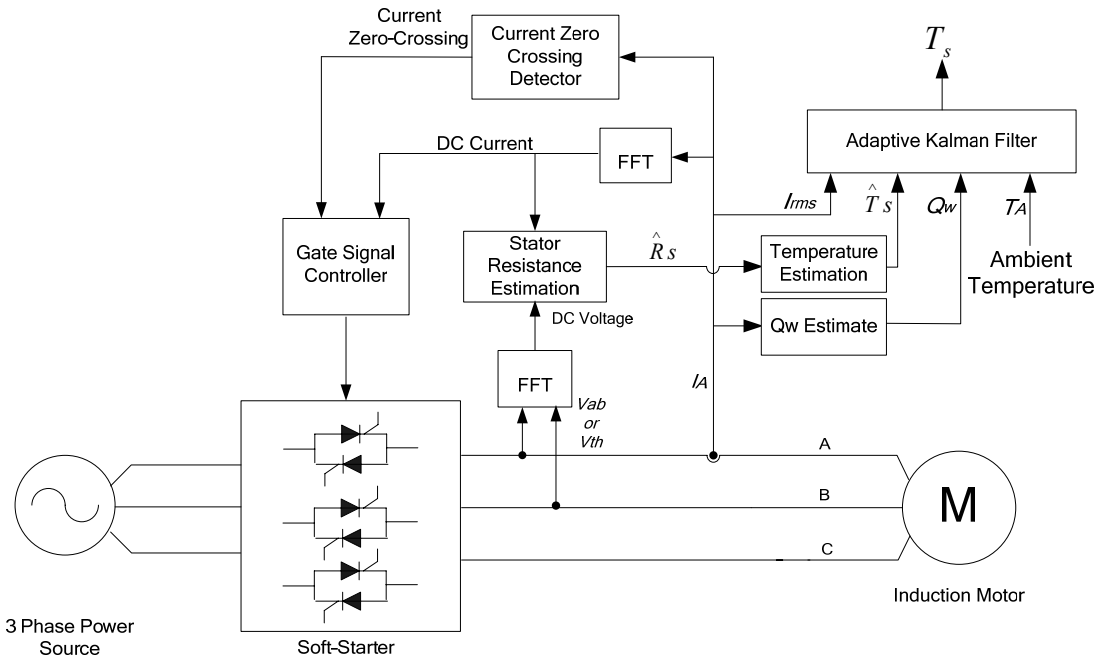


Figure 5.5: $R_s$-based stator temperature estimation scheme using soft-starters.

Once the noise autocorrelation matrix $Q_v$ and $Q_w$ have been determined, the adaptive Kalman filter can produce an optimal estimate of the stator winding temperature. The overall thermal monitoring scheme is shown as in Figure 5.5. The gate signal controller controls the torque distortion under acceptable level by monitoring the magnitude of the injected dc current in DIM. The dc components of $v_{ab}$ (or $v_{th}$ ) and $i_a$ are calculated. Then $\hat{T}_{s,dc}$, $I_{rms}$ and the ambient temperature $T_A$ are used as the inputs to the adaptive Kalman filter, which can reduce the error of $\hat{T}_{s,dc}$.

The advantage of this proposed stator temperature monitoring scheme lies in its non-intrusive and sensorless nature. It is only based on measurements of voltage, current and

ambient temperature. This approach can give an accurate stator winding temperature estimate without any embedded thermal sensor in the motor or any off-line test for thermal parameters.

## 5.8 Implementation Considerations

To implement the proposed $R_s$ estimation method in a soft-starter to achieve remote, sensorless and accurate thermal protection for the motors, the errors caused by the voltage and current measurements, the data acquisition system and the cable resistance have to be evaluated, and reduced if possible.

### 5.8.1 Voltage & Current Measurements

Since $v_{ab}^{dc}$ and $i_a^{dc}$ are obtained from the mean of $v_{ab,}$ and $i_a$, during DIM, the dc offsets in the voltage and current measurements influence the accuracy of the $R_s$ estimate. Therefore, the dc offsets of the measurements must be compensated for.

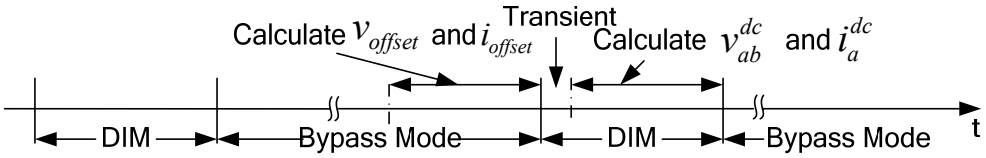


Figure 5.6: Measurement offset compensation.

Assuming that the dc component in the supply voltage can be neglected, the offsets can be calculated by the mean of the $v_{ab,}$ and $i_a$ measurements for an integer number of cycles in the bypass mode before each DIM, when there is no injected dc signal, as shown in Figure 5.6. After compensation for the measurement offsets, equation (2.10) becomes,

$$R_s = \frac{2 \cdot (v_{ab}^{dc} - v_{offset})}{3 \cdot (i_a^{dc} - i_{offset})}. \tag{5.16}$$

### 5.8.2 Sampling Frequency

During the DIM of the soft-starter, the delay angle is normally controlled to be small (10°-25°) so that the torque pulsation caused by the injected dc signal is under some acceptable level. The line-line voltages and phase currents are no longer sinusoidal, with not only dc signal injected, but also multiple harmonics.

Due to the aliasing effect of the spectrum caused by a sampling at a sampling frequency of $f_s$, the dc component in the voltage spectrum is contaminated by the voltage harmonic at 2 $f_s$. The aliasing effect of the voltage spectrum caused by a sampling frequency of 5 kHz is shown in Figure 5.7. It can be seen from Figure 5.7 that the alias effect introduces additional noise, and influence the accuracy of $v_{ab}^{dc}$ measurement. Therefore, the sampling frequency $f_s$ must be high enough that the voltage harmonic at frequency of $2f_s$ is negligible compared to the injected dc component. In the experiment, with a delay angle of 20°, a sampling frequency of 20-50 kHz is needed for accurate measurement. This is obviously undesirable to implement in a real soft-starter. Due to power dissipation considerations, the DSP processing chips in soft-starters normally work at a frequency of 2-5 kHz.

In order to reduce the necessary sampling frequency, a low pass filter is needed to improve the measurement accuracy. Using a low pass filter with cutoff frequency of $f_{cut\text{-}off}$, the voltage harmonic at $f_{cut\text{-}off}$ can be considered negligible. Therefore, a sampling frequency of approximately $f_{cut\text{-}off}/2$ is high enough to provide accurate measurements for voltage and current.

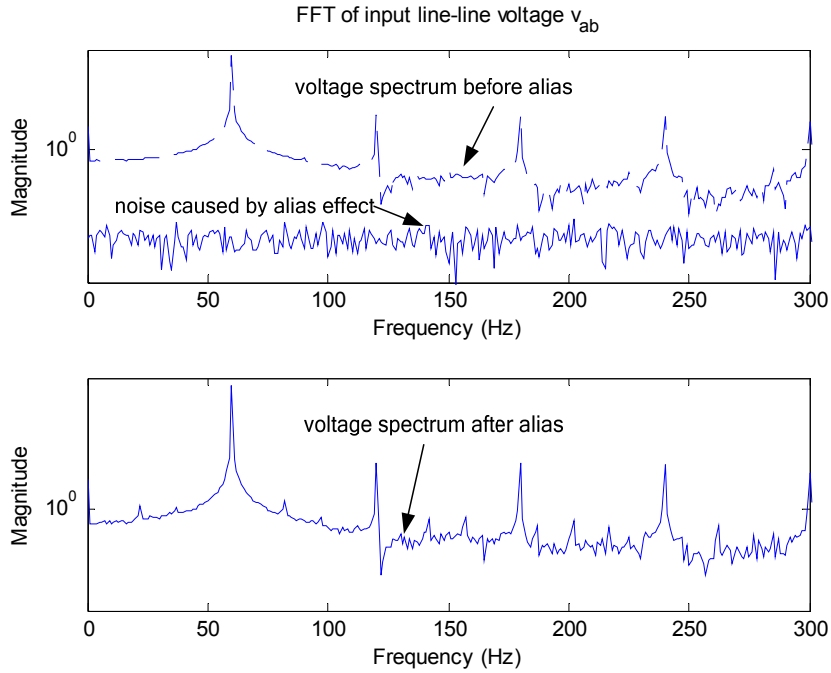


Figure 5.7: The alias effect of the voltage spectrum with $f_s$ of 5 kHz

### 5.8.3 Analog/Digital Conversion Resolution

Another aspect of the data acquisition system that needs to be considered is the A/D conversion resolution. Normally during DIM, due to the small stator resistance of induction motors, the dc component in the line-line voltage is more difficult to measure than the dc component in the phase current.

$$\frac{v_{ab}^{dc}}{v_{ab,peak}} << \frac{i_{ab}^{dc}}{i_{ab,peak}}. \tag{5.17}$$

Therefore, the error caused by A/D conversion is mainly in the voltage measurement. The stator resistance estimation error due to limited A/D conversion resolution can be approximated by

$$\Delta R_s = \frac{2}{3}\frac{\Delta v_{ab}^{dc}}{i_{ab}^{dc}} \le \frac{2}{3}\frac{V_{range}/2^N}{i_{ab}^{dc}}, \tag{5.18}$$

where $N$ is the A/D conversion resolution (bit), and $V_{\text{range}}$ is the max. voltage range of A/D conversion. For instance, when the voltage measurement range is 1500 *volt*s, the error caused by a 12-bit A/D conversion is approximately 0.37 volt, which is not negligible compared to the small injected dc signal. Therefore, to reduce the requirement of the A/D resolution, it is necessary to limit the filter gain at the supply frequency, so that the necessary voltage measurement range is decreased.

Assuming that the filter gain is $H(j\omega)$, equation (5.18) can be rewritten as

$$\Delta R_s = \frac{2}{3}\frac{\Delta v_{ab}^{dc}}{i_{ab}^{dc}} \approx \frac{2}{3}\frac{V_{peak}/2^{N-1}}{i_{ab}^{dc}}|H(j\omega)|_{f=60Hz}, \tag{5.19}$$

where $V_{peak}$ is the peak voltage at the supply frequency of 60 Hz. For instance, with a sampling frequency of 2 kHz, if a simple *RC* filter with cut-off frequency at 20 Hz is used, the magnitude of voltage harmonic at $2f_s$ is reduced to $H(j\omega)|_{f=2fs}$=0.08% of its value before filtering, which means the noise of the dc voltage measurement is greatly reduced. Assuming that the necessary voltage measurement range is 1500 *volts*, if the same *RC* filter is used, the necessary voltage measurement range is reduced to $1500H(j\omega)|_{f=60Hz}$=80 *volts*. The voltage measurement error caused by a 12-bit A/D conversion is reduced from 0.37 *volt* to 0.02 *volt.*

### 5.8.4 Compensation for Cable Resistance

If the soft-starter is installed in the motor control center and the motor terminals are not accessible, the resistance of the cable connecting the induction motor to the soft-starter may not be negligible compared to $R_s$. The $R_s$ estimation equation (2.10) becomes:

$$R_s = \frac{2 \cdot v_{ab}^{dc}}{3 \cdot i_a^{dc}} - R_{cable}\ , \tag{5.20}$$

To obtain an accurate $R_s$ estimation, the cable resistance must be compensated by measurement or estimation of $R_{cable}$. If measuring the cable resistance is not possible, it can be estimated based on the resistivity ρ given by the AWG standard, the approximate length $l$ of the cable, and the ambient temperature $T_A$, as,

$$\hat{R}_{cable} = \rho l + \alpha \rho l (T_A - T_0), \tag{5.21}$$

where α is the temperature coefficient of resistivity; $T_0$ is the room temperature, assuming that the cable temperature is the same as ambient temperature. The error in the $R_s$ estimate caused by an inaccurate estimate of cable temperature is given by,

$$\Delta R_s = \hat{R}_{cable} - R_{cable} = \alpha R_{cable0} \Delta T_{cable}, \tag{5.22}$$

where $\Delta R_s$ is the error of $R_s$ estimate, and $\Delta T_{cable}$ is the actual cable temperature above the ambient temperature.

Table 5.1: Stator Winding Resistance Estimation Error caused by Cable Resistance.

| HP | 2 | 5 | 10 | 20 | 50 |
|---|---|---|---|---|---|
| Typical Rs (Ohm) | 1-2 | 0.3-0.7 | 0.15-0.5 | 0.1-0.3 | 0.05-0.2 |
| Min. Gauge Size (AWG#) | 12 | 9 | 6 | 3 | 00 |
| Cable Resistance (Ohms/1000 feet) | 1.619 | 0.9077 | 0.4028 | 0.2009 | 0.077 |
| Max. ΔRs/Rs caused by cable length of 50 feet (%) | 0.3 | 0.5 | 0.4 | 0.4 | 0.3 |
| Max. ΔRs/Rs caused by cable length of 100 feet (%) | 0.6 | 1.0 | 0.7 | 0.7 | 0.5 |
| Max. ΔRs/Rs caused by cable length of 200 feet (%) | 1.2 | 2.1 | 1.5 | 1.4 | 1.0 |

Table 5.1 shows the typical stator resistance for induction motors rated from 2 hp to 50 hp. The minimum gauge size of the cable is determined considering the rated current for the motor and the current carrying ability of the cable listed by the AWG standard.

For a cable temperature error $\Delta T_{\text{cable}}$ of 10°C, the error of $R_s$ estimate is calculated considering the worst case, using (5.22). It can be seen from Table 5.1 that when the cable resistance is estimated, the $R_s$ estimate error caused by the cable resistance is within acceptable range. Therefore, the proposed scheme can provide remote and reliable $R_s$ estimate even when the motor terminals are not accessible.

## 5.9 Stator Temperature estimation in face of Power Supply Unbalance and Motor Internal Unbalance

### 5.9.1 DC Model of the Soft-starter-connected Motor System

Since most of the motor control/protection devices are installed in the motor control center, normally long cables are used to connect the soft-starter to the motor. The dc model of the soft-starter-connected motor system is shown in Figure 5.8. $R_{line}$ represents the line resistance between the soft-starter and the motor terminal, including cable resistance, fuse resistance, contact resistance, etc; $R_{source,a}$, $R_{source,b}$, $R_{source,c}$ represent the power source resistances in the three phases; $R_{s,a}$, $R_{s,b}$, $R_{s,c}$ represent the motor's stator resistances in the three phases. As the line resistances in three phases normally consist of the same cable resistance, fuse resistance, etc, they are assumed to be balanced. Since the line resistances are normally comparable to the stator resistances of the motor, it is important to compensate for the line resistance before estimating stator temperature using (2.10). Besides, power supply unbalance may be caused by unbalanced load in the system; the electric motor also normally has some internal unbalance. In these cases, when (5.1) is used to estimate stator resistance, the supply unbalance and the motor unbalance may lead to errors in the stator resistance estimation, and thus errors in the stator temperature estimation.

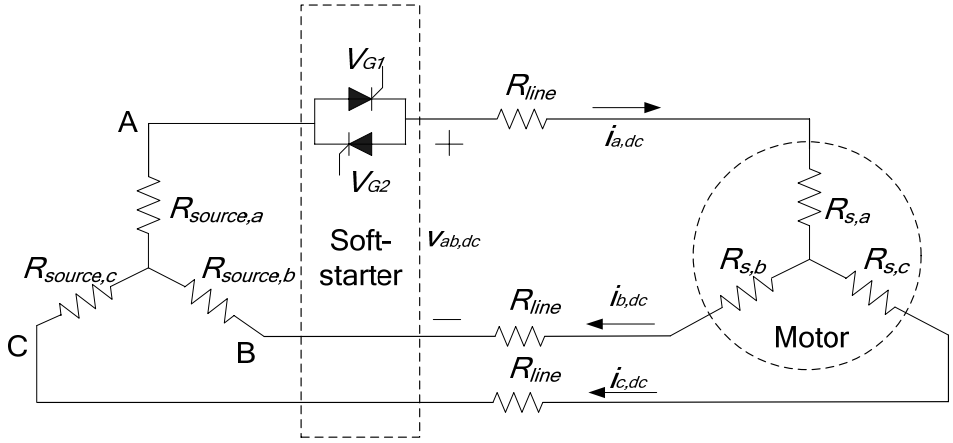


Figure 5.8: DC Model of the motor system with considerations of resistance unbalance.

### 5.9.2 Line Resistance Compensation in face of Motor and Power Supply Unbalance

Based on the dc model of the motor system, the line-line dc voltage $v_{ab,dc}$ can be written as,

$$v_{ab,dc} = R_{line}(i_{a,dc} + i_{b,dc}) + R_{s,a}i_{a,dc} + R_{s,b}i_{b,dc}\,. \tag{5.23}$$

The three phase stator resistances can be measured from motor terminals at room temperature, prior to the installation of the soft-starter, denoted as $R_{s0,a}$, $R_{s0,b}$, and $R_{s0,c}$. The line resistance can then be estimated using the measured $v_{ab,dc}$, $i_{a,dc}$ and $i_{b,dc}$ , right after the starting of the motor, as,

$$R_{line} = \frac{v_{ab,dc} - R_{s0,a}i_{a,dc} - R_{s0,b}i_{b,dc}}{i_{a,dc} + i_{b,dc}}, \tag{5.24}$$

neglecting the temperature rise of the stator winding. The line resistance can be assumed to be constant under normal operating conditions, since the temperature rise in the cable and fuse, etc, is negligible. Therefore, using the measured line-line dc voltage at the soft-

starter terminal, $v_{ab,dc}$, the line-line dc voltage, $v'_{ab,dc}$, at the motor terminal can be estimated as,

$$v'_{ab,dc} = v_{ab,dc} - R_{line}(i_{a,dc} + i_{b,dc}) . \quad (5.25)$$

Based on (5.25), the effect of the line resistances can be compensated, even with supply and motor unbalance.

### 5.9.3 Stator Temperature Estimation in face of Motor and Power Supply Unbalance

With the presence of motor internal unbalance or power supply unbalance, using eqn. (5.1) may lead to non-negligible errors in the stator temperature estimation. Assuming that the differences among the temperatures of the three phases of the stator winding are negligible, the ratio between stator resistances of any two phases becomes constant, as,

$$R_{s0,a} / R_{s0,b} = R_{s,a} / R_{s,b} . \quad (5.26)$$

Using (5.23) and (5.26), (5.25) can be rewritten as,

$$\begin{aligned} v'_{ab,dc} &= v_{ab,dc} - R_{line}(i_{a,dc} + i_{b,dc}) \\ &= R_{s,a} i_{a,dc} + R_{s,b} i_{b,dc} \\ &= \frac{R_{s0,a} i_{a,dc} + R_{s0,b} i_{b,dc}}{R_{s0,a}} R_{s,a} \end{aligned} . \quad (5.27)$$

Therefore, the phase ***a*** stator winding resistance can be estimated as,

$$\begin{aligned} R_{s,a} &= \frac{v'_{ab,dc} R_{s0,a}}{R_{s0,a} i_{a,dc} + R_{s0,b} i_{b,dc}} \\ &= \frac{[v_{ab,dc} - R_{line}(i_{a,dc} + i_{b,dc})] R_{s0,a}}{R_{s0,a} i_{a,dc} + R_{s0,b} i_{b,dc}} \end{aligned} . \quad (5.28)$$

With $R_{s,a}$ estimated, the stator winding temperature can be estimated using (2.10).

## 5.10 Experimental Validation

### 5.10.1 Experimental Setup

The proposed stator temperature monitoring scheme has been validated on 3 induction motors with different power rating. The gate drive control signals of a Cutler-hammer soft-starter are programmed to inject dc signals. The nameplate information of the experimental setup is shown in Table 5.2.

Table 5.2: Nameplate Information of Experiment Setup.

| Induction Motor 1 | | | | |
|---|---|---|---|---|
| **HP** | **Brand** | **CAT. NO.** | **RPM** | **Volts** |
| 5 | Marathon | 184TTFS6026 | 1755 | 460 |
| **SF** | **ENCL.** | **Nom. Eff.** | **F.L. AMPS** | **Rs** |
| 1.15 | ODP | 90.2 | 6.2 | 1.36 (Ω) |
| Induction Motor 2 | | | | |
| **HP** | **Brand** | **CAT. NO.** | **RPM** | **Volts** |
| 30 | Lincoln | TV2632 | 1765 | 230/460 |
| **SF** | **ENCL.** | **Nom. Eff.** | **F.L. AMPS** | **Rs** |
| 1.15 | TEFC | 88.5 | 74/37 | 0.329 |
| Induction Motor 3 | | | | |
| **HP** | **Brand** | **CAT. NO.** | **RPM** | **Volts** |
| 7.5 | Emerson | H7E1D | 3515 | 230/460 |
| **SF** | **ENCL.** | **Nom. Eff.** | **F.L. AMPS** | **Rs** |
| 1.15 | TEFC | 88.5 | 18.4/9.2 | 0.15 (Ω) |
| Soft-Starter for Experimental Testing | | | | |
| **Brand** | | **CAT. NO.** | **Volts** | |
| Cutler-Hammer | | IT.S811N | 200/230/460/575 | |
| **HP** | | **Max. AMPS** | **Working Freq. Hz** | |
| 10/10/25/30 | | 37 | 47-63 | |

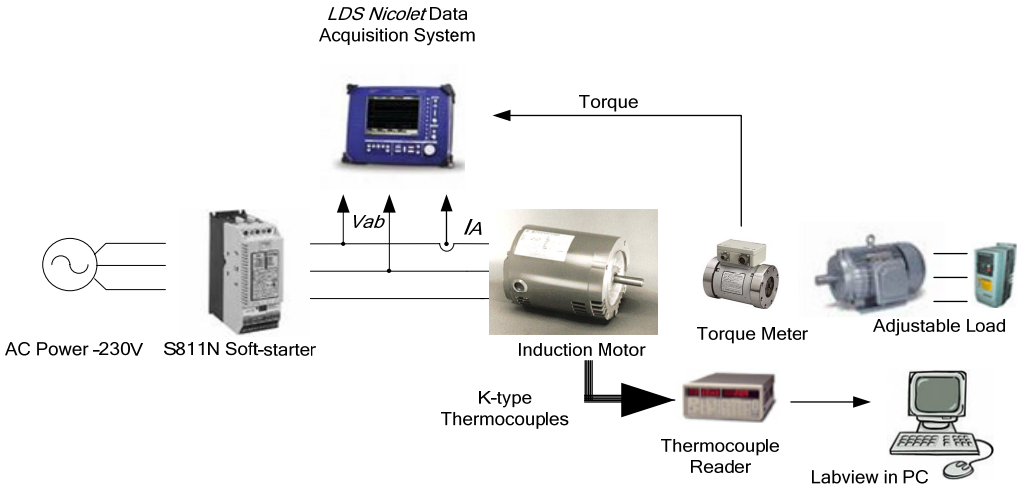


Figure 5.9: The experimental setup for motor 1 and motor 2.

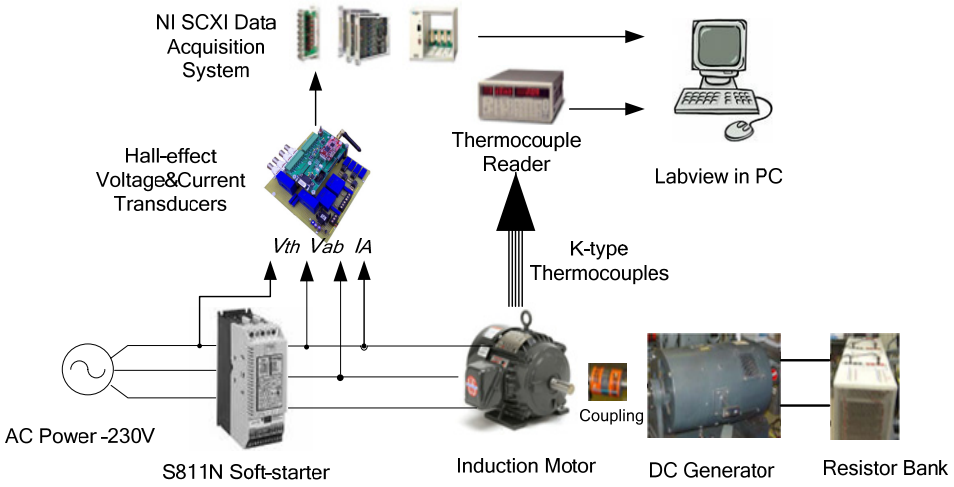


Figure 5.10: The experimental setup for motor 2.

The experimental setup for motor 1 and motor 2 is shown in Figure 5.9. The motor terminal voltages, phase currents are measured and stored using an *LDS Nicolet* data acquisition system, with 16-bit analog-to-digital conversion resolution at a sampling frequency of 100 kHz. A 30-hp drive-connected induction generator serves as adjustable load. A *Himmelstein* digital torque meter is connected between the induction motor and

the load to measure the output torque for torque pulsation analysis. The motor is instrumented with 6 K-type thermocouples at different locations in the stator winding to record its average winding temperature for validation purpose, as shown in Figure 5.9.

The experimental setup of motor 3 is shown in Figure 5.10. A 10-hp dc generator supplying a resistor bank is coupled to the tested motor to vary the load conditions by adjusting the resistance of the resistor bank. The motor terminal voltages, phase currents and the voltage across the soft-starter are measured using Hall-effect sensors. The data are acquired and stored using a *NI/LabView* data acquisition system with 16-bit A/D conversion at 100 kHz sampling frequency. The motor is instrumented with 8 K-type thermocouples at different locations in the stator winding to record its average winding temperature for validation purpose. Another K-type thermocouple is installed to measure the ambient temperature. The overall experimental setup is shown in Figure 5.10.

### 5.10.2 Torque Pulsation Analysis

In order to test the induced torque pulsation by the injected dc signal, Motor 1 is operated under 80% of the rated load with a dc-injection delay angle of 20°. The FFTs of the $v_{ab}$, $i_a$, and the output torque are normalized with respect to the 60-Hz components in $v_{ab}$, $i_a$, and the dc component of the output torque, respectively, as shown in Figure 5.11. It can been seen from Figure 5.11 that the high frequency components in $i_a$ and $v_{ab}$ can be neglected compared to the dc and 60-Hz components, which confirms the assumption in equation (5.3). The major components in the output torque are the dc and 60 Hz components, induced by the 60 Hz and dc components in phase current, respectively.

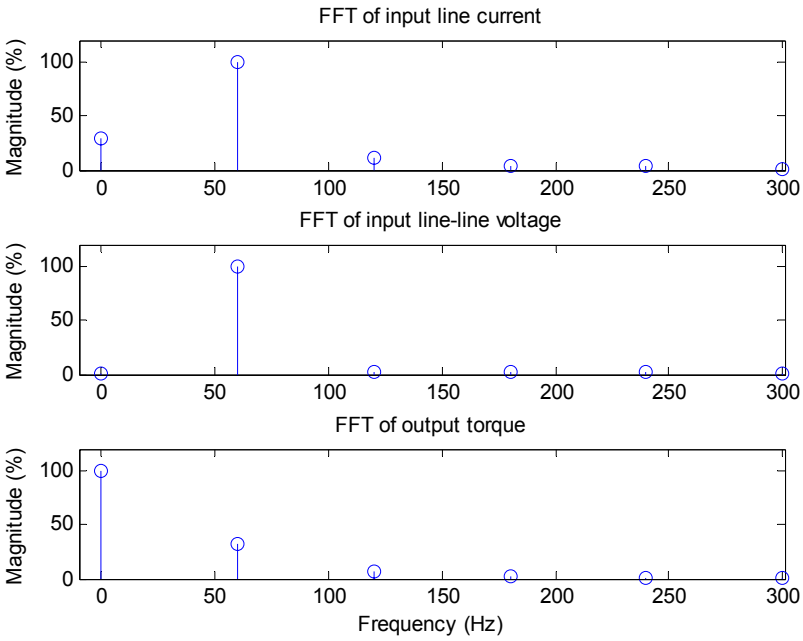


Figure 5.11: Normalized FFTs of voltage, current and output torque.

The percentage torque pulsation of the measured output torque caused by the injected dc signal is 36.8%, while the estimated torque pulsation from delay angle α by equation (5.11) gives sin(20°)/cos(φ)=43.3%, with the measured power factor cos(φ)=0.79. This shows that using (5.11), the maximum delay angle α can be adjusted online given an acceptable torque pulsation level.

It should be noted that torque pulsation is only induced in DIM, in which the motor is only operated for 0.5 sec. every 60 sec. In the bypass mode, the motor performance is not affected.

### 5.10.3 Stator Temperature Estimation

After determining the maximal delay angle to limit the torque pulsation under an acceptable level, the stator winding temperature $T_s$ can be monitored using (2.10) based

on the stator resistance estimation from dc injection. It should be noted that the $T_s$ estimation accuracy is dependent on the level of the injected dc signal.

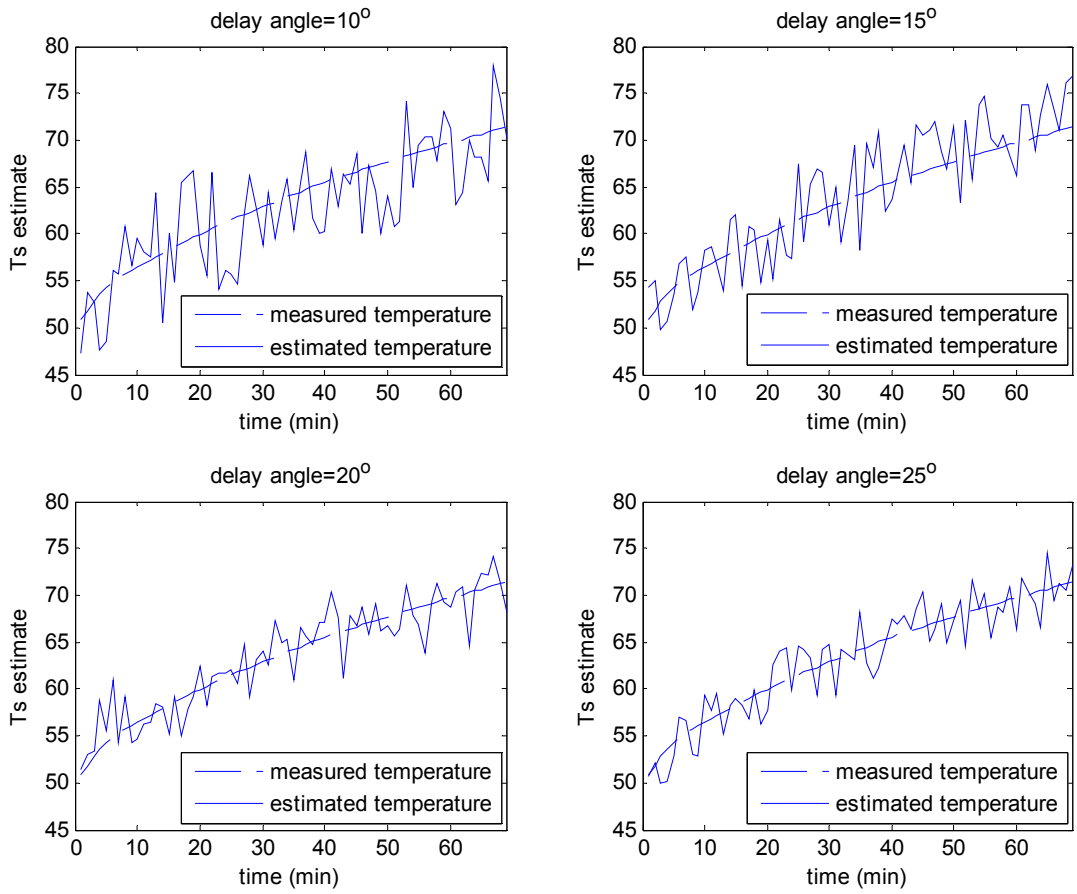


Figure 5.12: Stator winding temperature estimation results (motor 1).

The estimated $T_s$ based on dc injection for Motor 1 and Motor 2 are shown in Figure 5.12 and Figure 5.13, respectively. The tested motors are operated under full load with different delay angles (10°, 15°, 20°, 25°). The measured temperatures are calculated using the average temperature measured from the pre-installed thermocouples for validation purposes. It can be seen from Figure 5.12 and Figure 5.13 that the accuracy of $T_s$ estimate improves for a larger delay angle. However, from (5.11), the torque pulsation

caused by the delay angle also increases as delay angle increases. Therefore, determining delay angle is a tradeoff between stator temperature accuracy and torque pulsation. Figure 5.14 and Figure 5.15 shows the mean square error (MSE) of the $T_s$ estimation under full-load condition, and the percentage torque pulsation as functions of delay angle, for Motor 1 and Motor 2, respectively.

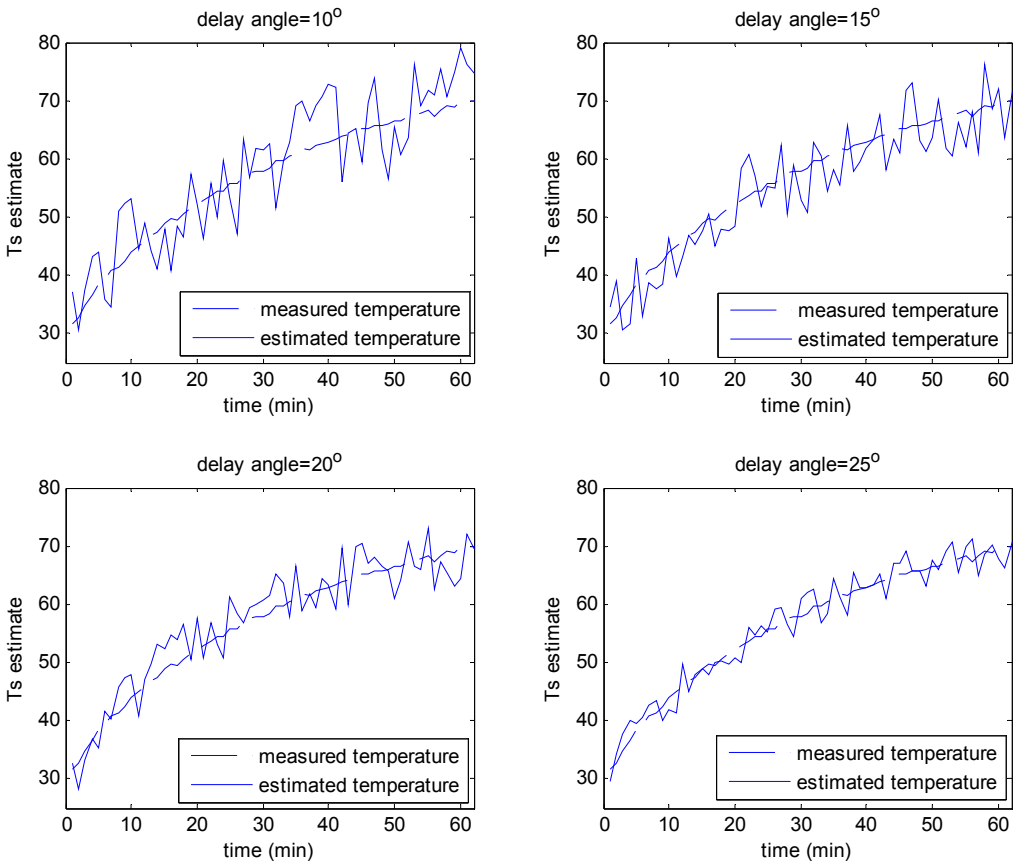


Figure 5.13: Stator winding temperature estimation results (motor 2).

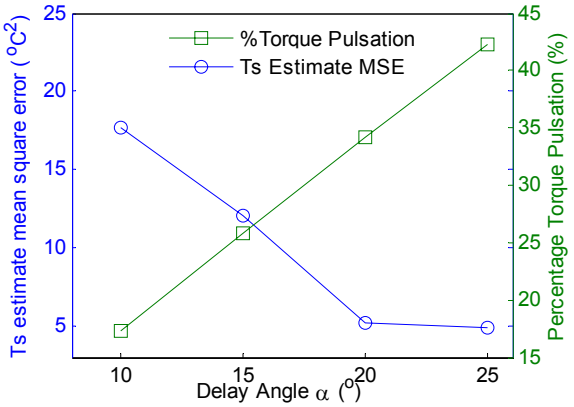


Figure 5.14: MSE of $T_s$ estimation and %torque pulsation (motor 1).

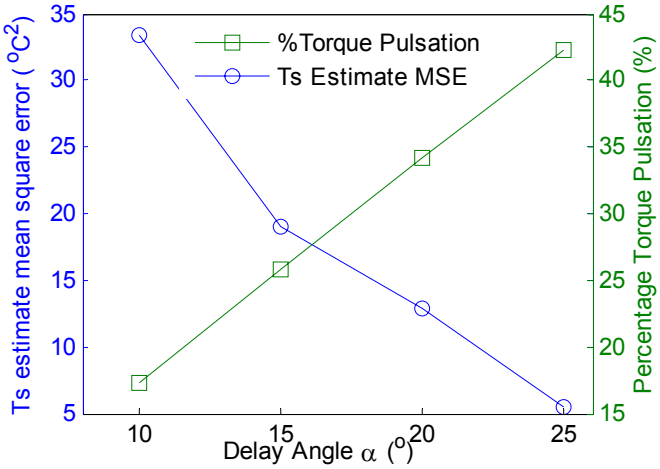


Figure 5.15: MSE of $T_s$ estimation and %torque pulsation (motor 2).

### 5.10.4 Performance of Adaptive Kalman Filter

The performance of the adaptive Kalman filter is tested on Motor 3. The value of $Q_v$ is estimated as the variance of $\hat{T}_{s,dc}$, when thermal steady state is reached at full load. In this experiment with a delay angle of 15°, $Q_v$ is identified as $9.2\,^{\circ}C^2$. Then, the thermal model is roughly derived based on the Trip Class and the Service Factor of the motor. The thermal resistance $R_{th}$ and the time constant $\tau$ are identified as 0.47 $K \cdot W^{-1}$ and 534 s, respectively.

To test the performance of the adaptive Kalman filter, the motor is operated under variable load conditions (0% → 100% → 50% → 75% rated load) with a delay angle of 15°. Figure 5.16-(a) and (b) show the estimated $T_s$ from dc injection before filtering, and the estimated $T_s$ after filtered by the adaptive Kalman filter, respectively. The mean value of the measured $T_s$ from the thermocouples is also shown for validation purpose. Figure 5.16-(c) and (d) show the $T_s$ estimation error before, and after filtering, respectively. The mean square error is reduced from $21.2\,^{o}C^{2}$ to $5.2\,^{o}C^{2}$.

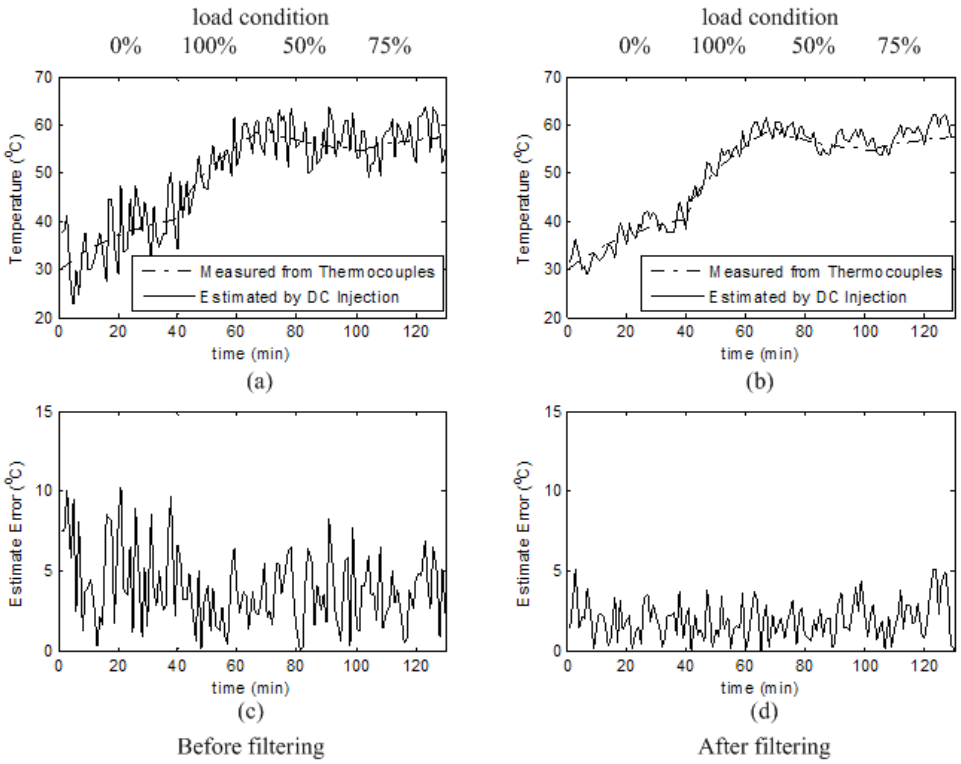


Figure 5.16: Performance of the adaptive Kalman filter.

### 5.10.5 Performance of the Overall Stator Temperature Monitoring Scheme

In order to test the performance of the proposed stator temperature monitoring scheme with different magnitudes of the injected dc signal, Motor 3 is operated with delay angles of 10°, 15°, 20°, 25°, respectively. At each delay angle, the motor is

operated under various load conditions (0%→100%→50% →75% rated load). For each delay angle, $Q_w$ is identified as described in the last section. In comparison, the parameters of the first-order thermal model are also identified from the measured temperature. The thermal resistance $R_{th}$ and the time constant τ are identified as 0.48 $K{\cdot}W^{-1}$ and 1073 sec., respectively.

Figure 5.17-(a), (b), (c) and (d) show the performances of the proposed thermal monitoring scheme with delay angles of 10°, 15°, 20°, 25°, respectively. It can be observed in Figure 5.17 that the proposed thermal monitoring method can accurately estimate $T_s$ under load variation, even with inaccurate thermal parameters in the model.

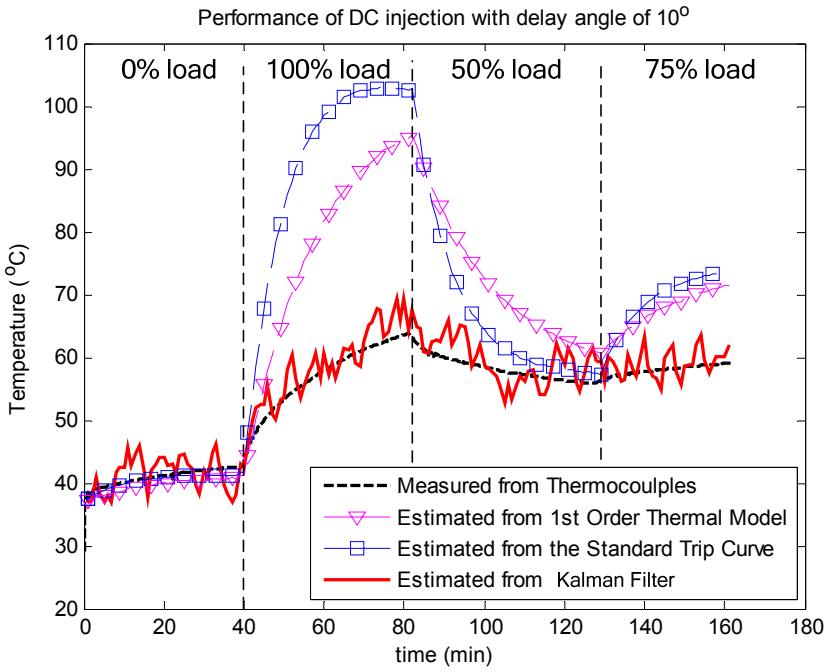


(a)

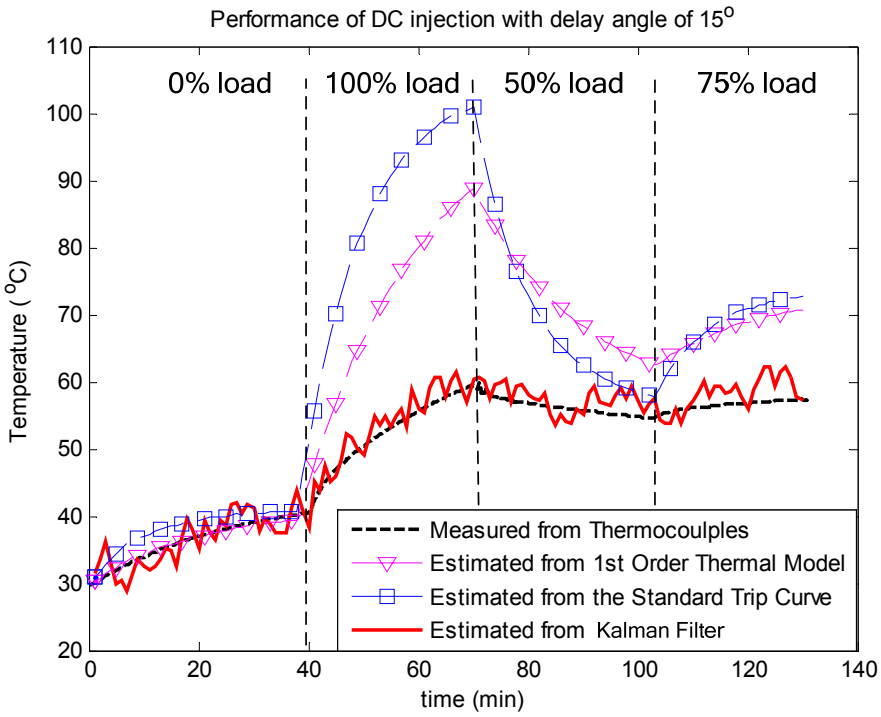
Performance of DC injection with delay angle of 15o
0% load
100% load
50% load
75% load
Temperature (oC)
time (min)
Measured from Thermocoulples
Estimated from 1st Order Thermal Model
Estimated from the Standard Trip Curve
Estimated from Kalman Filter

(b)

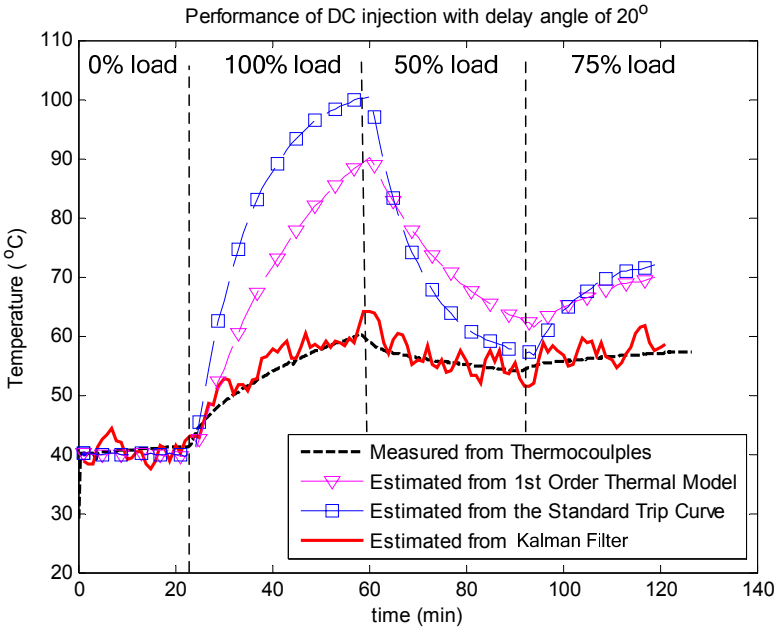
Performance of DC injection with delay angle of 20o
0% load
100% load
50% load
75% load
Temperature (oC)
time (min)
Measured from Thermocoulples
Estimated from 1st Order Thermal Model
Estimated from the Standard Trip Curve
Estimated from Kalman Filter

(c)

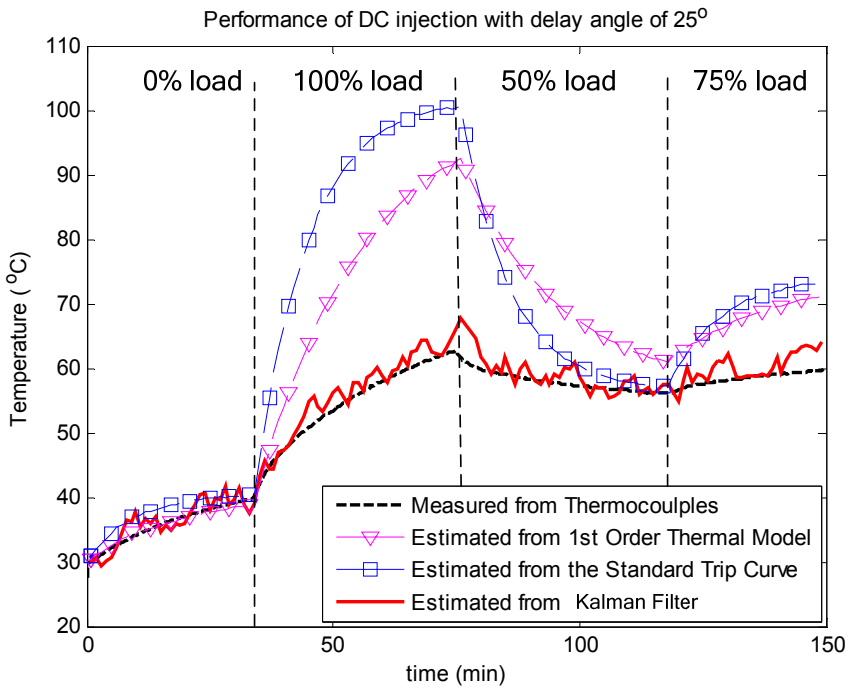


(d)

Figure 5.17: Performance of the stator temperature estimation scheme.

The Standard Trip Curve, which is widely used in induction motor thermal relays, is too conservative, giving an error as large as 40°C, under 100% load. It should also be noted that even for the "accurate" first-order thermal model, whose thermal parameters are identified from the measured temperature by thermocouples, the estimation error is still large. This is because the stator winding temperature change is a complex result of distributed thermal capacitances and resistances excited by distributed heat sources. It is simply not accurate enough to lump the other thermal capacitances, resistances and heat sources into one thermal capacitance and one thermal resistance. However, the performance of the proposed thermal monitoring scheme shows its robustness, despite the inaccurate modeling of induction motor thermal behavior.

### 5.10.6 Influence of Cable Resistance

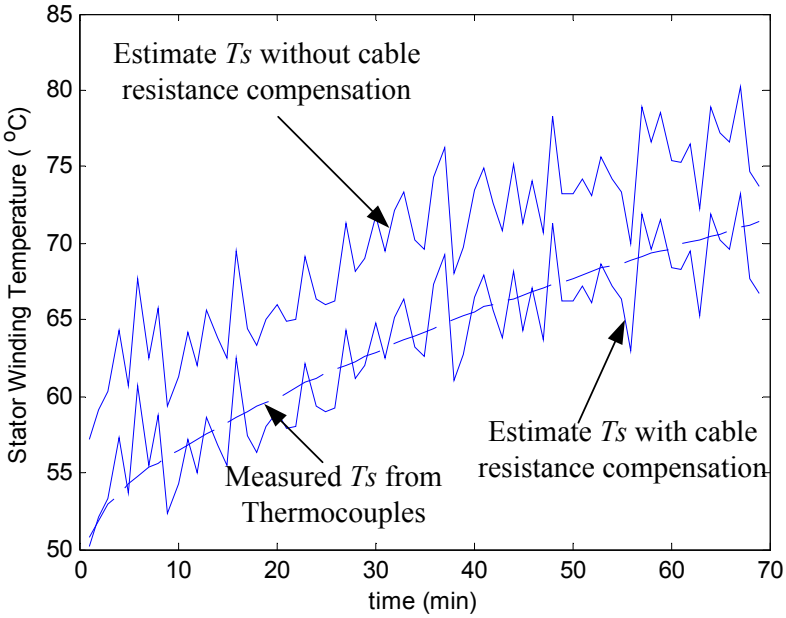


Figure 5.18: $T_s$ Estimation with and without cable resistance compensation.

To test the influence of the cable resistance, a 48-feet 12 AWG cable is installed from supply power to Motor 1. From the AWG standard, the resistivity of the 12 AWG cable is 1.588 ohms/1000 feet. Using (5.21), the cable resistance at room temperature is calculated as 0.0762 ohm. Motor 1 is operated under full-load condition with a delay angle of 20°. The $T_s$ estimation results with and without cable resistance compensation are compared in Figure 5.18. It can be seen from Figure 5.18 the proposed cable resistance compensation method can effectively reduce the $T_s$ estimation error caused by the cable resistance, which allows remote thermal monitoring of the motors.

### 5.10.7 Stator Temperature Estimation in face of Resistance Unbalance

The proposed stator temperature estimation method in face of power source and motor unbalance is tested on Motor 3. An additional 30-meter AWG 6 cable, (the cable

resistance is about 45 m ohm), is connected in phase ***c*** between the soft-starter and the power supply, with short cables used in phase ***a*** and ***b***, to emulate the power supply unbalance in the practical implementation environment.

With the motor's three phase resistances measured under room temperature, the line resistance is estimated using (5.24), right after the starting of the motor under no load condition. The estimated line resistance per phase is 17 m ohm. In comparison, the measured line resistance per phase is 15.6 m ohm. Therefore, using (5.24), the line resistance can be accurately estimated and compensated.

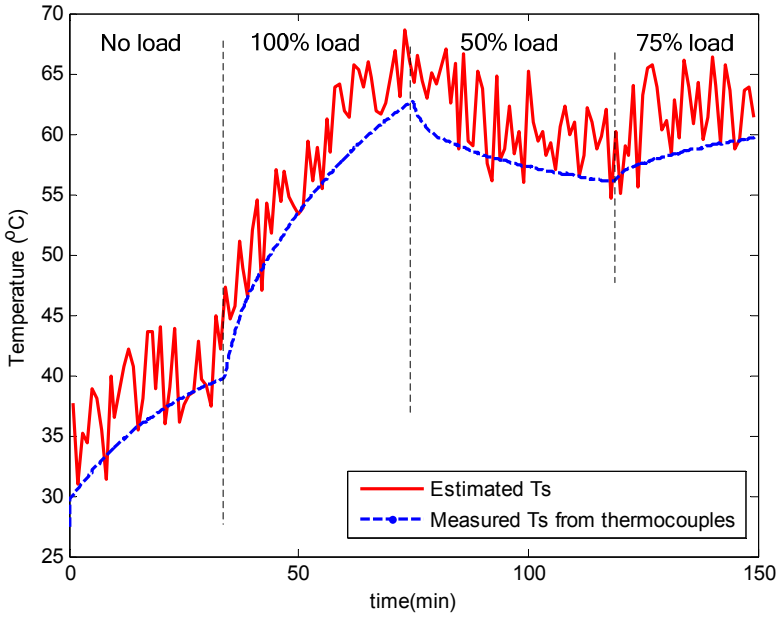


Figure 5.19: $T_s$ Estimation in face of resistance unbalance.

With line resistance compensated, the stator winding resistance can be estimated using (5.28) and the stator winding temperature can therefore be estimated using (2.10). To test the feasibility of the proposed stator temperature estimation method, the motor is operated under variable load condition: 0%→100%→50%→75% of the rated load. The

estimated stator winding temperature and the measured stator winding temperature from embedded thermocouples are compared in Figure 5.19. The stator temperature estimation error is within 10ºC.

## 5.11 Chapter Summary

In this chapter new non-intrusive stator winding resistance/temperature estimation technique for thermal overload protection has been proposed for soft-starter-connected induction motors. Based on the continuously monitoring of $R_s$, the stator winding temperature is estimated. An adaptive Kalman filter has been designed to reduce the temperature estimation error via dc injection. The performance of the adaptive Kalman filter has been validated by experiment, decreasing the mean square error by more than 75%. The proposed thermal monitoring scheme has been validated by experimental results from 3 different motors under various load conditions. In addition, the influence of the cable resistance is investigated, and the compensation method is suggested.

The main contribution of this new stator temperature monitoring scheme lies in its remote and sensorless nature.

- Sensorless - the stator winding temperature can be estimated using only the motor line voltage and phase current measurement (already existing in soft-starter) without additional sensors attached on the motor.
- Remote - using the proposed cable resistance compensation method, the motor winding resistance/temperature can be accurately determined remotely at the soft-starter. As a result, remote motor winding thermal monitoring and protection becomes feasible.

- Accurate - from the experimental results, the rms error of the stator winding temperature estimation using the proposed methods is within 2.5 °C at 25° delay angle when the winding temperature varies from 30°C to 70°C.
- Flexible - the torque pulsation caused by the dc injection and the estimation accuracy are found to be both related to the delay angle. The delay angle can be optimally controlled to compromise between the estimation accuracy and the induced torque pulsation during the resistance/temperature estimation.

# CHAPTER 6 Stator Temperature Estimation for Variable-frequency Drive-fed Induction Motors

## 6.1 Overview

Aside from solid-state motor starters, variable-frequency motor drive is another type of broadly used motor control devices. As motor losses are functions of input frequency, voltage magnitude, and speed, etc, loss estimation for drive-fed motors is more difficult than that of soft-starter-connected motors, which makes it difficult to estimate stator temperature using thermal models. Therefore, this chapter proposes signal injection-based stator temperature estimation techniques for variable-frequency drive-fed motors.

Similar to the soft-starter case, DC signals can be injected into the stator winding of an induction motor by changing the operation of the power switches in a motor drive. A modified space vector PWM pattern is proposed for the dc signal injection. The stator winding temperature can be continuously monitored using only current measurements. Experimental results are shown for the validation of the proposed techniques.

## 6.2 DC Signal Injection using Motor Drives

### 6.2.1 Schematic of Open-loop Motor Drives

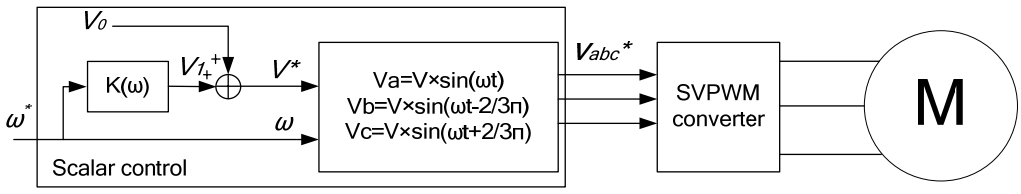


Figure 6.1: Typical scalar control scheme for induction motors.

The structure of a typical open-loop motor drive using the scalar control method, which is also known as constant *V/f* control, is shown in Figure 6.1. The three phase input voltage control signal, $v_{abc}^{*}$, is calculated based on the input frequency command, $\omega^{*}$. Using the d-q transform, the three phase voltage control signal, $v_{abc}^{*}$, can be transformed to the d-q voltage control vector, $\vec{v}_{dqs}$. Then, given the voltage control vector, the SVPWM can achieve accurate input voltage control by controlling the power switches in the converter.

To add a dc signal in the input voltages, a dc voltage command can be added to the voltage control signals, $v_{abc}^{*}$. With such implementation, the SVPWM can automatically inject dc components in addition to the original voltage signals by altering the switching of the power electronics switches.

### 6.2.2 Schematic of Closed-loop Motor Drives

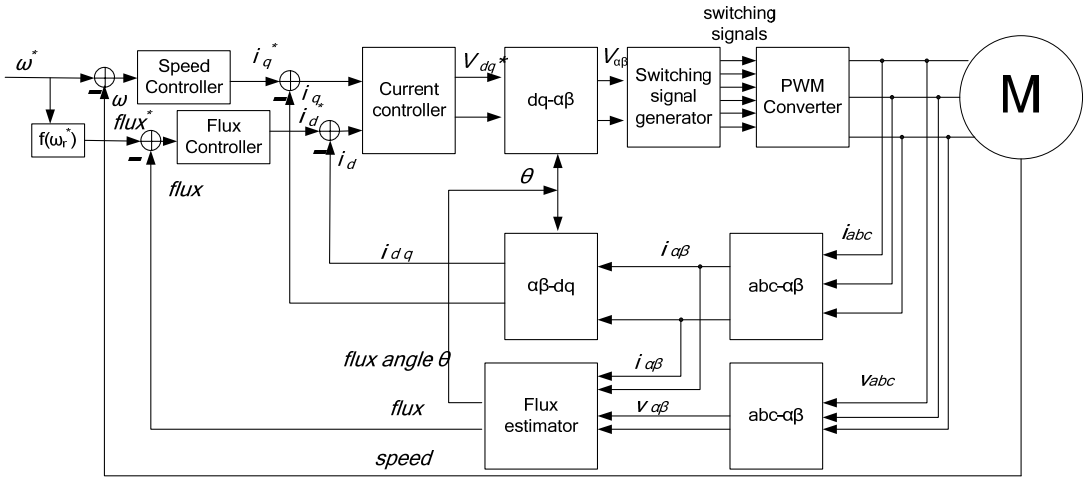


Figure 6.2: Field-oriented control scheme of AC motors.

The most popular type of closed-loop speed control scheme, field-oriented control, is shown in Figure 6.2. The synchronous reference frame used in this scheme is aligned with the rotor flux so that the d-q currents can be decoupled as the flux command and torque command, as in dc motor drives. By controlling the three phase motor currents, the output torque and thus rotor speed can be controlled to the desired value for different applications. In closed-loop speed control scheme, the three phase stator currents are controlled by adjusting the voltage commands. Due to the dynamic performance of the overall control loop, the accurate injection of a desired dc voltage or current is difficult with the presence of the controllers.

However, in steady-state, the three phase voltages given by the motor drives are constant. In such conditions, the voltage command can be kept constant with the control loop disconnected, which does not affect the operation of the motor system. DC signals can therefore again be injected by adding a dc voltage command to the original voltage command given by the control scheme, which is identical to the open-loop case. After each signal injection duration, the dc voltage command is removed and the control loop is put back in operation so that the motor's speed can be dynamically controlled.

Therefore, the dc signal injection for both open-loop and closed-loop motor drives can be achieved in the same approach.

### 6.2.3 DC Signal Injection using Motor Drives

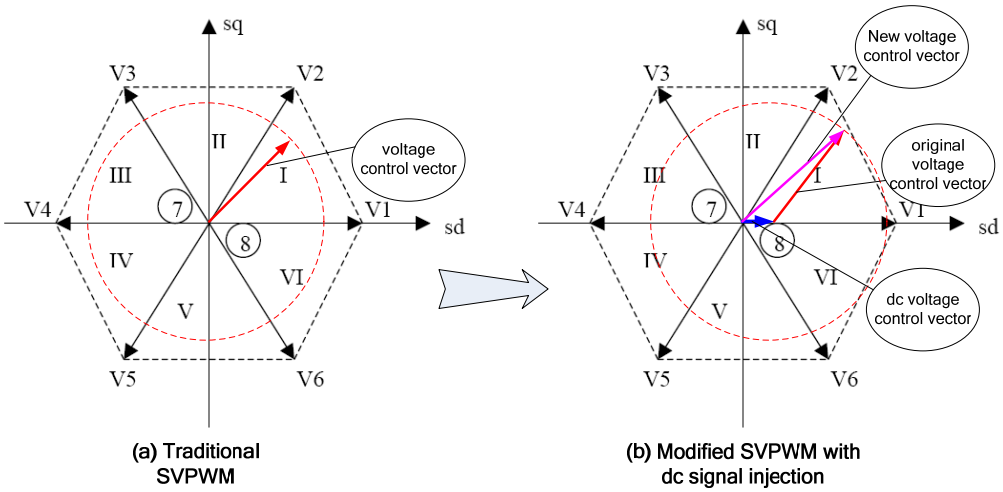


Figure 6.3: Modified space vector PWM for dc signal injection.

To inject dc signals, a dc voltage control vector, $\vec{v}_{dc,dqs}$, is added to the original voltage control vector, $\vec{v}_{dqs}$, in the stationary d-q reference frame. When a dc voltage, $v_{dc}$, is injected between *phase a* and *phase b, c*, the dc voltage control vector can be calculated as,

$$\vec{v}_{dc,dqs} = \sqrt{\frac{2}{3}}\begin{bmatrix} 1 & -\frac{1}{2} & -\frac{1}{2} \\ 0 & -\frac{\sqrt{3}}{2} & \frac{\sqrt{3}}{2} \end{bmatrix}\begin{bmatrix} v_a \\ v_b \\ v_c \end{bmatrix} = \sqrt{\frac{2}{3}}\begin{bmatrix} \frac{1}{2}v_{dc} + \frac{1}{2}v_{dc} \\ -\frac{\sqrt{3}}{2}\times 0 \end{bmatrix} = \sqrt{\frac{2}{3}}\begin{bmatrix} v_{dc} \\ 0 \end{bmatrix}. \qquad (6.1)$$

By intermittently adding the dc voltage control vector, a controllable dc voltage can be injected into the motor for thermal protection purposes. Meanwhile the original voltage control vector, which is given by the scalar control, is still controlled to maintain the normal operation of the motor. The modified SVPWM is shown in Figure 6.3. Since the magnitude of the dc voltage control vector is typically much smaller than that of the original voltage vector, the operating region of the SVPWM is not largely affected. To

reduce the impact of the injected dc signal on the motor and the motor drive, the dc signal is injected for 1 second every 1 minute.

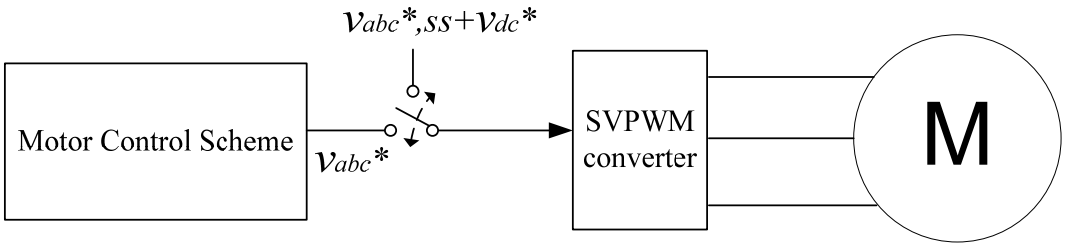


Figure 6.4: Periodic operation of a motor drive.

After each dc signal injection, the voltage command given by the control scheme is fed to the SVPWM without dc voltage control vector so that the normal operation can be re-stored. Such operation is illustrated in Figure 6.4. The motor control scheme can be different types of motor control algorithms in motor drives for output voltage control. $v_{abc\ ss}^{*}$ represents the output of the motor control scheme under steady state.

### 6.3 Evaluation of Torque Pulsation

While the fundamental-frequency current induces a constant output torque, the injected dc signal induces an output torque oscillating at the fundamental frequency. Let $\vec{i}_{dqs}$ and $\vec{\lambda}_{dqs}$ be the stator current and total flux linkage space vectors in the d-q stationary reference frame. The air-gap torque, $T_{\text{ag}}$, can be calculated as the cross product of $\vec{\lambda}_{dqs}$ and $\vec{i}_{dqs}$, as,

$$T_{ag} = \frac{3P}{4}\left|\vec{\lambda}_{dqs} \otimes \vec{i}_{dqs}\right|. \tag{6.2}$$

where $P$ is the number of poles. It is shown in [45] that the torque pulsation caused by the injected dc signal and the constant torque induced by the fundamental-frequency current can be respectively evaluated as,

$$\begin{aligned} \left|T_{ag}^{dc}\right| &\approx \frac{3P}{4}\left|\vec{\lambda}_{dqs}^{\omega} \otimes \vec{i}_{dqs}^{\omega}\right| \\ \left|T_{ag}^{\omega}\right| &\approx \frac{3P}{4}\left|\vec{\lambda}_{dqs}^{\omega} \otimes \vec{i}_{dqs}^{dc}\right| \end{aligned}, \tag{6.3}$$

where ω is the fundamental frequency. Therefore, the relative torque pulsation can be shown as,

$$\frac{\left|T_{ag}^{\omega}\right|}{\left|T_{ag}^{dc}\right|} \approx \frac{\left|\vec{\lambda}_{dqs}^{\omega} \otimes \vec{i}_{dqs}^{dc}\right|}{\left|\vec{\lambda}_{dqs}^{\omega} \otimes \vec{i}_{dqs}^{\omega}\right|} = \frac{\left|\vec{\lambda}_{dqs}^{\omega}\right|\left|\vec{i}_{dqs}^{dc}\right|}{\left|\vec{\lambda}_{dqs}^{\omega}\right|\left|\vec{i}_{dqs}^{\omega}\right| \bullet \cos(\varphi)} = \frac{I_{a,dc}}{I_{a,peak}\cos(\varphi)} , \tag{6.4}$$

where cos(φ) is the power factor; $I_{a,dc}$ and $I_{a,peak}$ represents the magnitude of the dc component and the peak value of the ac component in phase *a* current, assuming that the dc signal is injected between phase *a* and phase *b*, *c*.

Therefore, by using (6.4), the torque pulsation can be evaluated by monitoring the dc current and the power factor. Since the injected dc current can be controlled by adjusting the dc voltage command, $v_{dc}$, given the allowable relative torque pulsation, the torque pulsation can be controlled within acceptable range.

## 6.4 Stator Temperature Estimation for Inverter-fed Motors

With the dc signal injected using the modified SVPWM, when $T_s$ is represented in *Kelvin* temperature, $T_s$ and $R_s$ can be calculated as,

$$\hat{R}_s = \frac{2 \cdot v_{ab}^{dc}}{3 \cdot i_a^{dc}} \quad . \tag{6.5}$$

$$\hat{T}_s = T_{s0} + \frac{(\hat{R}_s - R_{s0})}{\alpha R_{s0}} . \tag{6.6}$$

where $i_a^{dc}$ and $v_{ab}^{dc}$ represent the dc component in the phase current, $i_a$, and line to line voltage, $v_{ab}$, respectively; $T_{s0}$ and $R_{s0}$ represents $T_s$ and $R_s$ at room temperature; and $\hat{T}_s$ and $\hat{R}_s$ are the estimated $T_s$ and $R_s$ from the dc signal injection; and α is the temperature coefficient of resistivity with respect to $T_{s0}$.

As only current sensors are present in most of the motor drives, it is preferred to avoid using voltage measurements. Because of the non-ideal switching of the IGBTs, such as the dead time and dwell time, the actually injected dc voltage does not accurately follow the dc voltage command. The compensation of the non-ideality of the switching is difficult, which make it difficult to accurately estimate the injected dc voltage from the dc voltage command [46]. However, under constant load condition, the injected dc voltage is found to be nearly constant from the experimental results. Therefore, it can be assumed that the injected dc voltage remains constant under constant load conditions. Based on this assumption, voltage measurements can be avoided during the estimation of stator resistance, as,

$$\hat{T}_s = T_{s0} - \frac{1}{\alpha} + \frac{\hat{R}_s}{\alpha R_{s0}} = T_{s0} - \frac{1}{\alpha} + \frac{1}{\alpha} \bullet \frac{v_{ab}^{dc} / i_a^{dc}}{v_{ab}^{dc} / i_{a0}^{dc}} = T_{s0} - \frac{1}{\alpha} + \frac{1}{\alpha} \bullet \frac{i_{a0}^{dc}}{i_a^{dc}}, \tag{6.7}$$

where $i_{a0}^{dc}$ represents the dc component in the phase current when the stator temperature is $T_{s0}$. Therefore, the stator winding temperature can be estimated using only the magnitude of the injected dc current under constant load condition. Typically, the stator temperature can be considered as the room temperature right after cold start, and therefore, the dc current right after starting can be estimated as $i_{a0}^{dc}$.

In the case of load change, the injected dc voltage changes. This is because the variations of the magnitude of the current may lead to the variations of the injected dc voltage, due to the non-ideality of the switching of IGBTs. However, it can be assumed that before and after the load change, the stator winding temperature variations can be neglected. Under such assumption, based on (6.7), the ratio of dc currents under the same load condition remain unchanged. Therefore, the change of the magnitude of the injected dc current caused by the load change can be compensated using a rescaling process, as,

$$i_a^{dc} = i_{a,load2}^{dc} \frac{i_{a,load1}^{dc}(t_0-)}{i_{a,load2}^{dc}(t_0+)}, \tag{6.8}$$

where $i_{a,load1}^{dc}$ and $i_{a,load2}^{dc}$ represent the measured dc current under load 1 and load 2 conditions, respectively; $t_0$ represents the time when the load condition is changed from load 1 to load 2; $i_{a,load1}^{dc}(t_0-)$ and $i_{a,load2}^{dc}(t_0+)$ are the dc currents measured right before and after the load change; $i_a^{dc}$ is the rescaled dc current after compensation for the load change, which is periodically updated for the estimation of stator winding resistance and temperature. Based on this, the stator winding temperature can be monitored under the new load condition using (6.7).

For continuous load variation conditions, however, it is difficult to estimate the stator winding temperature only based on the stator current measurement. This is due to the inaccurate injection of the dc voltage signal, which is because of the non-ideal switching of the power switches. In the case of continuous load variation applications, additional voltage sensors are required for measuring the injected dc voltage. With the

measurement of both dc voltage and current, the stator winding resistance and temperature can be continuously monitored online.

## 6.5 Compensation for Series Resistances

Since the motor drives are normally installed in the motor control centre, long cables may be present between the motor and motor drives. The cable resistance and the internal resistance of motor drives may be comparable to the stator resistance, which may significantly decrease the accuracy of stator temperature estimation when (6.7) is used. Therefore, the compensation of series resistances, including motor drive internal resistance and cable resistance is crucial for the accurate estimation of stator temperature. The dc model of the motor drive system is shown in Figure 6.5, neglecting contact resistances. $R_{cable}$ represents the cable resistance; $R_{drive}$ represents the internal resistance of motor drives.

As suggested in [8, 45], the cable resistance can be estimated based on the length and the size of the cable. It is shown in [45] that the stator temperature estimation error can be neglected after the compensation of cable resistance for small- to medium-size induction motors. For more accurate estimation of the cable resistance, the cable resistance can be experimentally measured during the installation of the motor drives with the motor terminals shorted. Such testing can be one of the initial tests required during the installation of motor drives for obtaining parameters of the motor system. Therefore, the stator temperature can be remotely monitored in the motor control centre.

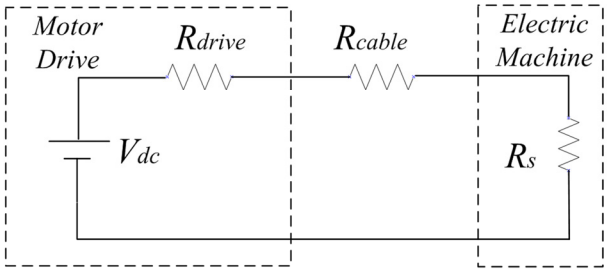

Figure 6.5: DC model of the motor drive system.

The internal resistance of motor drives consists of the equivalent resistance of IGBT, cable resistance and contact resistance, etc. The cable resistance and contact resistance can be assumed constant under normal operating conditions. The equivalent resistance of IGBT may vary slightly with different temperature, different magnitude of the gate signal, and different magnitude of the phase current. For some applications, these variations may be negligible compared to the stator resistance. Therefore the internal resistance of motor drive can be assumed constant and predetermined before installation. However, for some other applications, these variations might not be negligible. Therefore, the internal resistance of motor drive needs to be predetermined with different magnitudes of input current and different temperatures to form a lookup table for online compensation. Since temperature sensors are typically attached to the IGBT modules to monitor their temperature in motor drives, the temperature of IGBT and the magnitude of the phase current can both be monitored online. Therefore, the internal resistance of motor drives can be estimated online using the predetermined lookup table. The pretesting of the internal resistance of motor drives is only required once for each model of motor drives, and stored in the signal processing chip for online compensation.

Under constant load condition, it can be assumed that the injected dc voltage is constant, as,

$$i_a^{dc}(R_s + R_{cable} + R_{drive}) = i_{a0}^{dc}(R_{s0} + R_{cable} + R_{drive0}), \tag{6.9}$$

where $R_{drive}$ and $R_{drive0}$ represent the internal resistance of motor drives when the stator resistance is $R_s$ and $R_{s0}$, respectively. Based on the estimation of cable resistance and internal resistance of motor drives, the stator temperature can be estimated as,

$$\begin{aligned} \hat{T}_s &= T_{s0} + \frac{\hat{R}_s}{\alpha R_{s0}} - \frac{1}{\alpha} \\ &= T_{s0} - \frac{1}{\alpha} + \frac{i_{a0}^{dc}(R_{s0} + R_{cable} + R_{drive0}) - i_a^{dc}(R_{cable} + R_{drive})}{i_a^{dc} R_{s0}} \end{aligned} . \tag{6.10}$$

Therefore, the effects of the series resistances can be compensated for improving the accuracy of the stator temperature estimation.

## 6.6 Overall Thermal Protection Scheme for Inverter-fed Induction Motors

The overall thermal protection scheme for open-loop drive-fed induction motors is shown in Figure 6.6. The dc signals are injected by using the modified SVPWM, as shown in Section 6.2. The relative torque pulsation caused by the injected dc signal can be estimated using (6.4) by monitoring the phase current. Therefore, the relative torque pulsation can be controlled within acceptable range by adjusting the dc voltage command. On the other hand, it is understandable that the accuracy of the stator temperature estimation is highly dependent on the magnitude of the injected dc voltage. Therefore, the determination of the dc voltage command is a trade-off between acceptable torque pulsation and the accuracy of the stator temperature estimation.

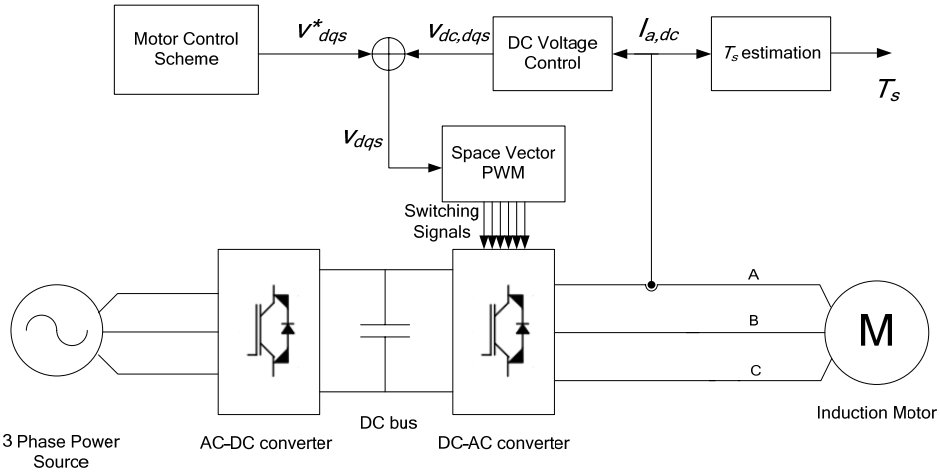


Figure 6.6: Stator temperature estimation scheme for inverter-fed induction motor.

Since dc signal injection causes undesirable torque pulsation, it is not necessary to inject the dc signal and estimate the stator temperature and resistance continuously. DC signals can be periodically injected for a minimal time interval which is sufficient to obtain an accurate estimate of the stator temperature, while small enough not to cause unacceptable torque pulsation. From the experimental results of this work, it is suggested to inject dc signals for 1 second each time to obtain an accurate estimate of the stator temperature. Given a typical motor thermal time constant, a period of 5-10 minutes for the stator temperature update is sufficient for thermal protection purposes, depending on the requirements of practical application. Therefore, the motor performance is only affected by dc signal injection for 1 second every 5-10 minute. In this work, for validation purposes, the dc signals are injected for 1 second every 1 minute.

The importance of the proposed thermal protection scheme lies in its non-intrusive nature: only current sensors are required for implementation; normal operation of the motor is not interrupted.

## 6.7 Experimental Validation

### 6.7.1 Experimental Setup

The proposed thermal monitoring scheme is tested on two induction motors, whose ratings and parameters are shown in Table 6.1. An Eaton SPX9000 motor drive is programmed to inject the dc signal using modified SVPWM, as stated in Section 6.2. The switching frequency of the inverter is set as 5k Hz. A 10-hp dc generator supplying a resistor bank is connected to the tested motor to vary the load conditions by adjusting the resistance of the resistor bank. The motor phase current is measured using Hall-effect sensors. The data are then acquired and stored using a *NI LabView* system with 16-bit A/D conversion at 100 kHz sampling frequency. The motors are each equipped with 9 K-type thermocouples at different locations (3 in each phase) in the stator windings to record the average stator winding temperature for validation purposes, as shown in Figure 6.7.

Table 6.1: Nameplate Information of Experiment Setup.

| Induction Motor 1 | | | | | | | | |
|---|---|---|---|---|---|---|---|---|
| HP | Brand | CAT. NO. | RPM | Volts | SF | ENCL | Nom. Eff. | F.L. AMPS |
| 7.5 | Emerson | H7E1D | 3515 | 230/460 | 1.15 | TEFC | 88.5 | 18.4/9.2 |
| Induction Motor 2 | | | | | | | | |
| HP | Brand | CAT. NO. | RPM | Volts | SF | ENCL. | Nom. Eff. | F.L. AMPS |
| 7.5 | Leeson | G140417 | 1760 | 230/460 | 1.15 | ODP | 88.5 | 20/10 |
| Motor Drive for Experimental Testing | | | | | | | | |
| Brand | CAT. NO. | Input Volts | HP | Max. Output AMPS | | Output Freq. Hz | | |
| Eaton | SPX9000 | 380-500 | 20 | 23 | | 0-320 | | |

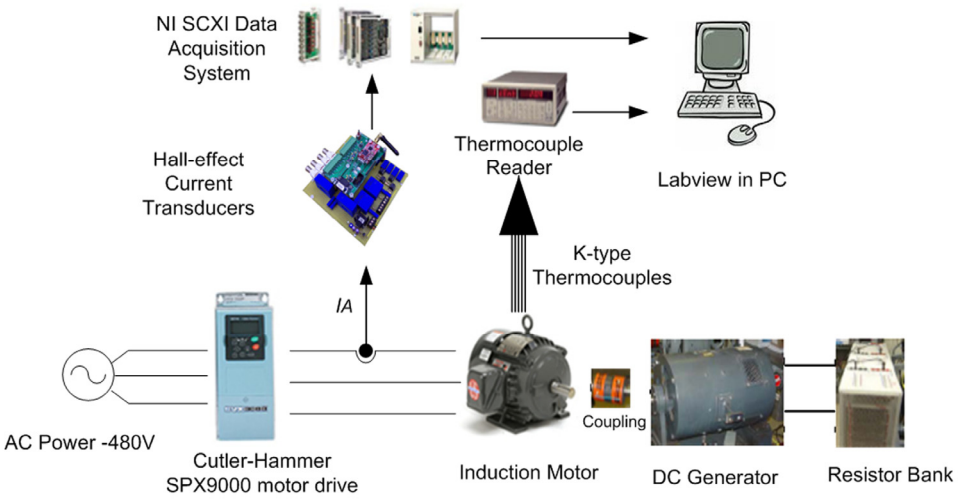


Figure 6.7: Experimental setup for inverter-fed induction motor.

### 6.7.2 Motor Current during DC Signal Injection

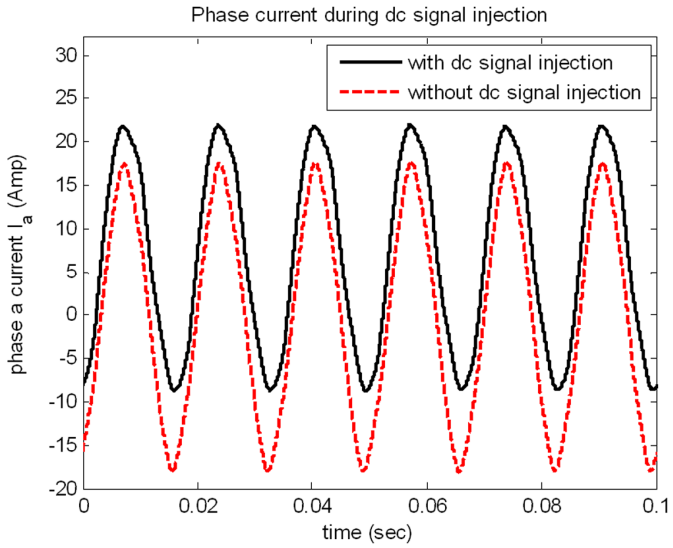


Figure 6.8: Stator current with dc signal injection.

The stator phase current of motor 1 during dc signal injection is shown in Figure 6.8. A low-pass filter with a cut-off frequency of 500 Hz is used to remove the current harmonics caused by the switching of IGBTs. It can be observed that by using the modified SVPWM, a dc signal is successfully injected into the motor. While the dc

voltage command is set as 5 volts, the injected dc current is around 7 amps. Therefore, based on the dc signal injection, the stator winding resistance and temperature can be estimated using the motor's dc model.

### 6.7.3 Stator Temperature Estimation under Constant Load Condition

Based on the monitoring of the stator current, the stator winding temperature can be determined. The internal resistance of motor drive is assumed constant, and must be predetermined or estimated *a priori*, together with the cable resistance. The effects of the series resistances can be compensated using (6.10). The estimated stator winding temperature based on dc injection for motor 1 under constant load condition is shown in Figure 6.9. The tested motor is operated under no load, 30%, 60% and 90% of the rated load with rated input frequency command of 60 Hz. The estimated stator winding temperature for motor 1 with input frequency of 30 Hz is shown in Figure 6.10, where the motor is operated under 30% and 45% of the rated load, respectively. The measured temperatures are calculated using the average temperature measured from the pre-installed thermocouples for validation purposes. It can be seen from Figure 6.9 and Figure 6.10 that the stator winding temperature can be accurately monitored using only the current measurements under constant load condition with different input frequencies. The maximum error of $T_s$ estimation is within 8 ºC.

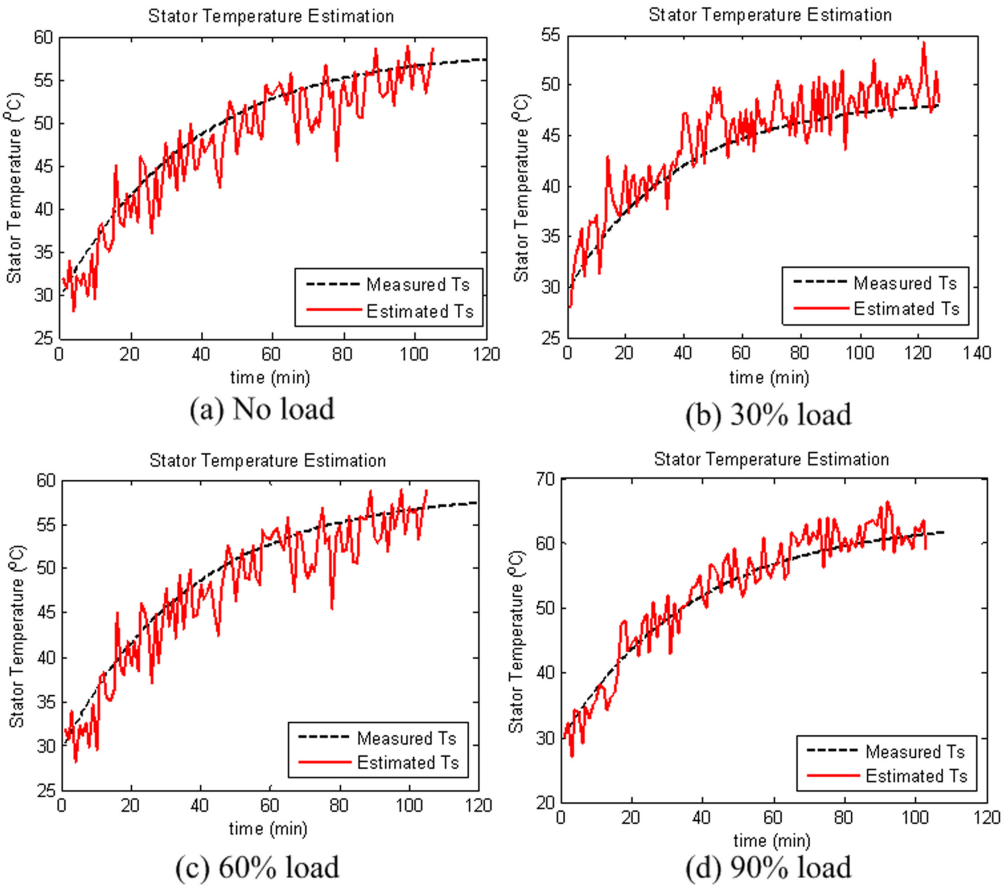


Figure 6.9: Stator temperature estimation with input frequency of 60 Hz (motor 1).

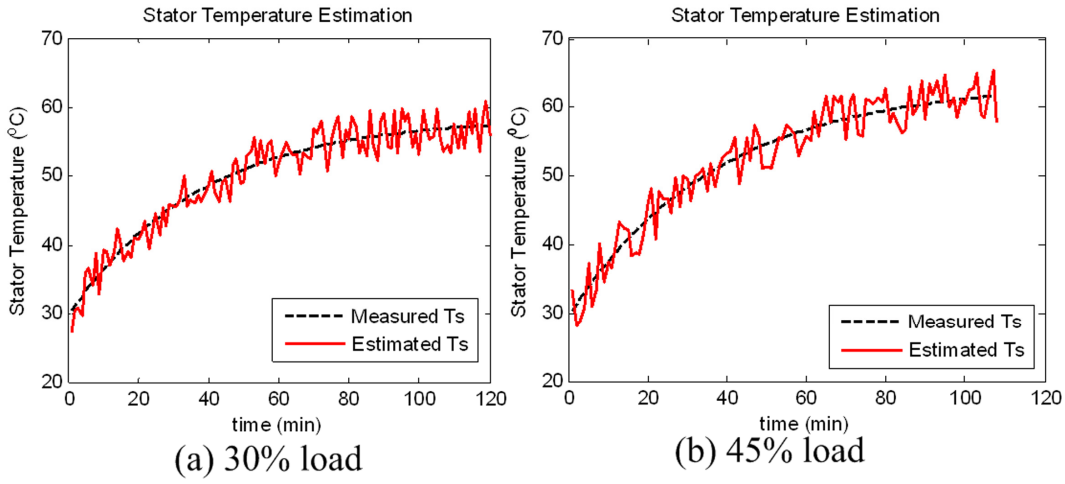


Figure 6.10: Stator temperature estimation with input frequency of 30 Hz (motor 1).

### 6.7.4 Stator Temperature Estimation under Variable Load Condition

To test the feasibility of the proposed stator temperature estimation scheme under variable load conditions, motor 2 is operated under variable load conditions (no load →100%→50% →75% of the rated load). The effects of the load change on the dc signal injection are compensated using (6.8) for each load change. To remove effects of the measurement noise, the measured currents before and after the load change for rescaling are obtained by nonlinear curve fitting of the dc current measured under each load condition. The stator temperature estimation results are shown in Figure 6.11. The maximum error in the stator temperature estimation is within 7 ºC. It can be observed in Figure 6.11 that by using (6.8) the proposed thermal protection scheme is capable of providing accurate estimation of the stator temperature under variable load conditions.

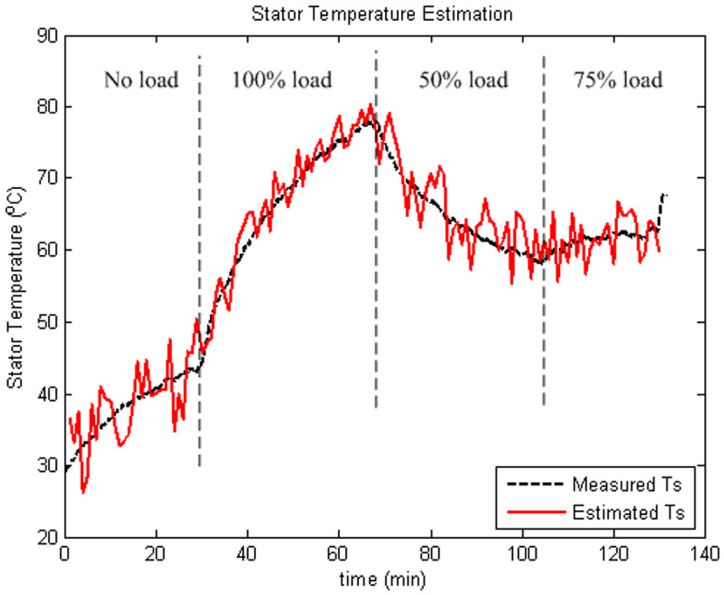


Figure 6.11: Stator temperature estimation under variable load conditions (motor 2).

### 6.7.5 Stator Temperature Estimation with Impaired Cooling

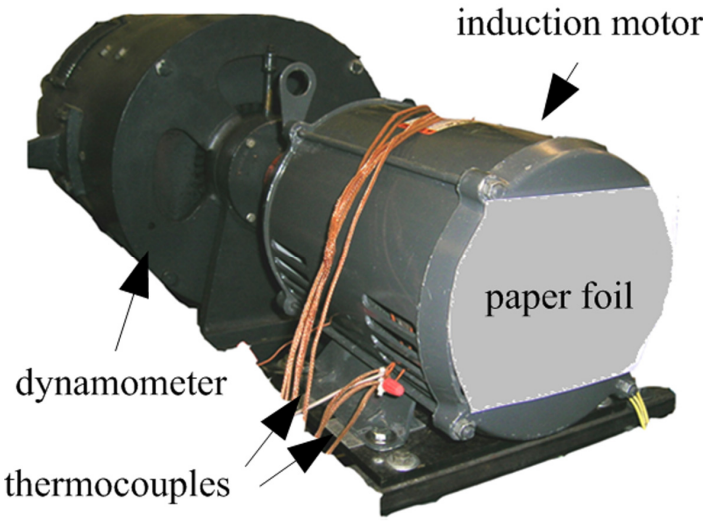


Figure 6.12: Impaired cooling by blocking ventilation (motor 2).

It is crucial that the stator temperature can be accurately estimated when the motor's cooling capability is deteriorated, so that the user can be warned for inspection or repair of the motor with impaired cooling. To test the feasibility of the proposed stator temperature estimation scheme in the case of impaired cooling, a paper foil is attached to the end of motor 2 to partly block the ventilation, as shown in Figure 6.12.

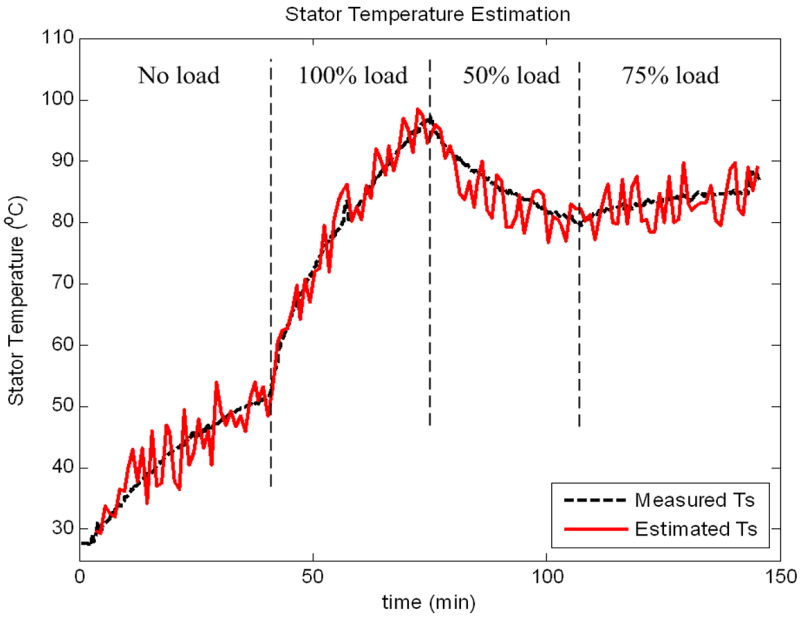


Figure 6.13: Stator temperature estimation with impaired cooling (motor 2).

For comparison purposes, the motor is again operated under variable load conditions (no load→100%→50% →75% of the rated load). The stator temperature estimation results are shown in Figure 6.13. It can be observed that the proposed stator temperature estimation scheme can provide accurate estimation of the stator temperature, for determining whether the cooling capability of the motor is healthy or impaired. It can be observed from the comparisons of Figure 6.11 and Figure 6.13 that impaired cooling induces an increased stator temperature rise under the same load condition. Therefore, the stator temperature estimation, in addition to improved traditional protection, can also be used to detect abnormal cooling capability of the motor, so that the user can be warned for inspection or repair of the induction motor. The development of such impaired cooling detection technique will be discussed in more detail in Chapter 8. From Figure 6.13, it can be observed that the proposed technique can provide accurate stator

temperature estimation under impaired cooling conditions, which is essential for the online detection of impaired cooling.

## 6.8 Chapter Summary

An active stator temperature estimation scheme has been proposed in this Chapter for the thermal protection of inverter-fed induction motors. DC signals are intermittently injected into the motor using a modified space vector pulse width modulation (SVPWM) pattern. The stator winding temperature can then be estimated based on the monitoring of only the stator phase current under both constant and variable load conditions.

The torque pulsation caused by the injected dc signals has been evaluated so that the torque pulsation can be controlled within an acceptable range by adjusting the dc voltage command in the modified SVPWM. In addition, a compensation technique for series resistances, including the internal resistance of motor drives and cable resistances, has been suggested to improve the accuracy of the stator temperature estimation.

The proposed stator temperature estimation scheme has been validated from experimental results on two induction motors with different ratings. It has been shown that the proposed stator temperature estimation scheme is capable of providing accurate stator temperature estimation under both constant and variable load conditions, and both healthy and impaired cooling conditions. The errors in the stator winding temperature estimation from experimental testing are within 8ºC under different operating conditions.

The proposed stator temperature estimation scheme can provide reliable protection of inverter-fed induction motors under both healthy and impaired cooling conditions, which makes it feasible for impaired cooling detection.

The proposed technique can be directly implemented in a motor drive, since only current sensors are required for implementation, which are typically available in motor drives.

# CHAPTER 7 Magnetic Effects of DC Signal Injection on Induction Motors

## 7.1 Overview

Although proven to work for stator winding temperature estimation, the effects of the dc signal injection have not yet been thoroughly studied. The injected dc signals induce a non-rotational pulsating magnetic flux. The overlap of the non-rotational flux and the rotating flux induced by the ac components may result in an unbalanced motor magnetic saturation within each cycle. Such magnetic saturation may increase the losses in the stator and rotor core. Therefore, it is crucial to analyze and evaluate the effects of magnetic saturation on a motor's performance and thermal behavior. In addition, since such saturation condition is aggravated under a higher load condition or with larger dc signals injected. It is crucial to theoretically prove the feasibility of the stator resistance and temperature estimation techniques with considerations of magnetic saturation.

## 7.2 An Analysis of Magnetic Saturation during DC Signal Injection

### 7.2.1 Magnetic Saturation during Normal Operation

During normal operation without dc signal injection, the total flux is induced by the three phase currents, denoted as $\Psi$, which rotates at synchronous speed. Normally, the induction motor is designed so that under full load condition, only slight magnetic saturation is present, as shown in Figure 7.1. This is for reducing the cost of the core while limiting the possible losses and maintaining the performance of induction motors during normal operation. Since the magnitude of the rotating magnetic flux is constant during normal operation, the level of magnetic saturation is also constant under constant

load conditions. Neglecting the stator tooth saturation, the magnetic flux $\Psi$ with and without the considerations of saturation are shown in Figure 7.2-(a) (solid line: with saturation; dashed line: without saturation). It can be observed that with considerations of saturation, the magnitude of the magnetic flux is reduced. But since the magnitude of the rotating flux is constant, the effect of saturation is consistent within each cycle. Therefore, even with saturation, the stator inductance, rotor inductance and mutual inductance are constant, as the saturation condition is the same.

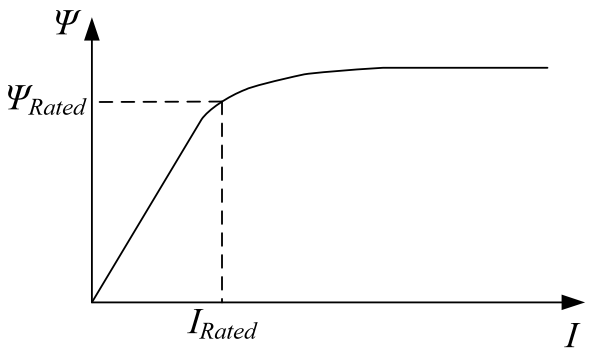


Figure 7.1: Typical current-flux curve.

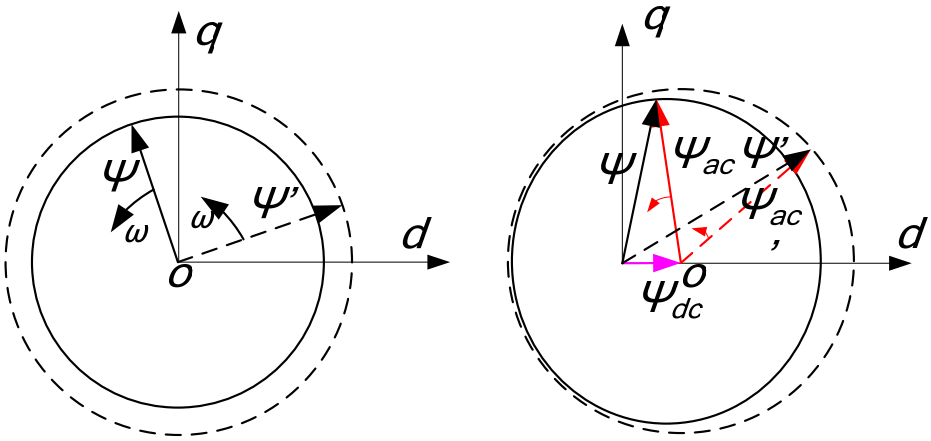


(a) normal operation (b) during dc signal injection

Figure 7.2: Magnetic flux with and without considerations of saturation.

### 7.2.2 Magnetic Saturation during DC Signal Injection

Unlike the normal operation, the injected dc signals induce a bias in both the stator current and the magnetic flux, as shown in Figure 7.2-(b). The actual magnetic flux, $\Psi$, now consists of the stationary flux, $\Psi_{dc}$, and the rotating flux, $\Psi_{ac}$. As a result, in each cycle, the magnitude of the flux is varying, due to the injected dc bias. Therefore, different levels of saturation are induced in each cycle: when the magnitude of the total flux is smaller, a lower level of saturation is induced; when the magnitude of the total flux is larger, a higher level of saturation is induced. As a result, the magnetic inductance periodically varies within each cycle. The typical inductance varying with different values of the magnitude of the magnetizing current is shown in Figure 7.3.

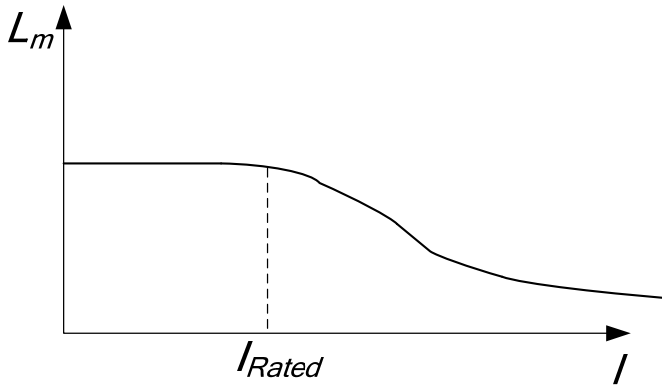


Figure 7.3: Typical current-inductance curve.

### 7.2.3 The Effects of Magnetic Saturation

Compared to normal operation, the magnitude of the flux decreases when the rotating flux is in phase with the stationary flux; the magnitude of the flux increases when the rotating flux is in the opposite phase against the stationary flux. Therefore, assuming that dc signals are injected from phase ***a*** to phase ***b*** and ***c***, compared to normal operation,

a higher level of saturation is induced around the positive peak of phase ***a*** current; a lower level of saturation is induced around the negative peak of phase ***a*** current. As a result, the absolute values of all three phase currents increase when the positive peak of phase ***a*** current appears; the absolute values of all three phase currents decrease when the negative peak of phase ***a*** current appears. The effects of the saturation variations are aggravated when the magnitude of the injected dc signal increases, or under a higher load condition. Such analysis is validated by simulation and experimental results.

Due to the effects of saturation, multiple harmonics at even orders are induced in both the stator current and the air-gap flux, including the $2^{nd}$ harmonics, $4^{th}$ harmonics, $8^{th}$ harmonics, etc. The interaction between these harmonics and the fundamental frequency induces output torque pulsation, mainly at 60 and 180 Hz.

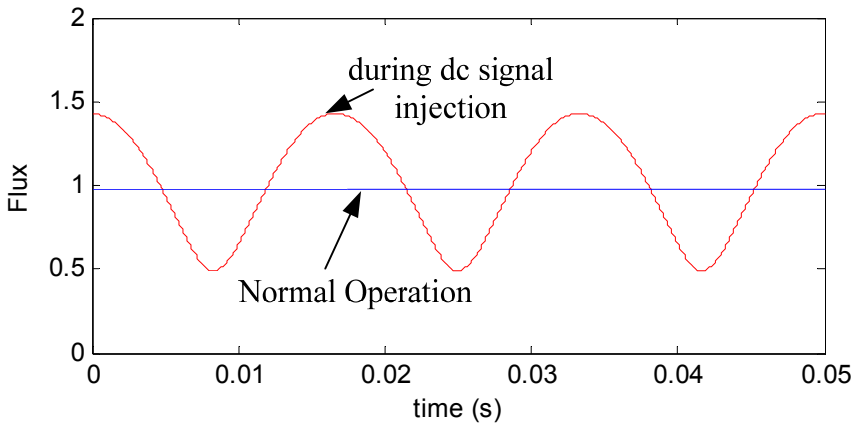


Figure 7.4: Typical flux waveform.

In addition, the magnetic saturation also increases the core losses. As shown in Figure 7.2, the magnitude of the air-gap flux varies in each cycle during dc signal injection. The typical values of the air-gap flux for one pole during dc signal injection and normal operation are compared in Figure 7.4. In normal operation, the magnitudes of

the rotating flux at different locations of the core are almost the same. However, as the flux is biased, the magnitudes of the rotating flux at different locations of the core are different. Therefore, the heat dissipation in the core is not uniformly distributed any more. The extra heat dissipation caused by the injected dc signal and the unbalanced distribution of the core losses may cause some thermal issue on the core. To ease this thermal stress, the dc signals are typically injected *intermittently* for a small amount of time, which is sufficient to obtain an accurate estimation of the stator temperature.

### 7.2.4 Model of Induction Motors during DC Signal Injection with considerations of Magnetic Saturation

The dynamic model of induction motors in stationary reference frame is shown as,

$$\begin{aligned} v_{ds} &= R_s i_{ds} + \frac{d}{dt}(L_s i_{ds} + L_m i_{dr}) \\ v_{qs} &= R_s i_{ds} + \frac{d}{dt}(L_s i_{qs} + L_m i_{qr}) \\ 0 &= R_r i_{dr} + \frac{d}{dt}(L_m i_{ds} + L_r i_{dr}) \\ 0 &= R_r i_{qr} + \frac{d}{dt}(L_m i_{qs} + L_r i_{qr}) \end{aligned}, \qquad (7.1)$$

where $v_{ds}$, $v_{qs}$ are the stator input voltages in d- and q-axis; $R_s$ and $R_r$ are the stator and rotor resistances; $i_{ds}$, $i_{qs}$, $i_{dr}$ and $i_{qr}$ represent the stator and rotor currents in d- and q-axis; $L_s$, $L_r$ and $L_m$ are the stator, rotor and mutual inductances.

During the dc signal injection, the inductances vary when the magnetizing current changes, as shown in Figure 7.3. Therefore, the mutual inductance, $L_m$, can be modeled as a nonlinear function of the magnetizing current, as,

$$L_m = L_m(I_m) = L_m\left(\sqrt{(i_{ds} + i_{dr})^2 + (i_{qs} + i_{qr})^2}\right). \qquad (7.2)$$

Neglecting the variations of the leakage inductances, the model of induction motor can be rewritten as,

$$\begin{aligned} v_{ds} &= R_s i_{ds} + \frac{d}{dt}[L_{ls} i_{ds} + L_m(I_m)\bullet(i_{ds} + i_{dr})] \\ v_{qs} &= R_s i_{ds} + \frac{d}{dt}[L_{ls} i_{qs} + L_m(I_m)\bullet(i_{qs} + i_{qr})] \\ 0 &= R_r i_{dr} + \frac{d}{dt}[L_{lr} i_{dr} + L_m(I_m)\bullet(i_{ds} + i_{dr})] \\ 0 &= R_r i_{qr} + \frac{d}{dt}[L_{lr} i_{qr} + L_m(I_m)\bullet(i_{qs} + i_{qr})] \end{aligned}, \tag{7.3}$$

where $I_m$ is the magnitude of the magnetizing current, as,

$$I_m = \sqrt{(i_{ds} + i_{dr})^2 + (i_{qs} + i_{qr})^2} \ . \tag{7.4}$$

By using (7.3), the dynamic performance of induction motors during dc signal injection can be modeled with considerations of magnetic saturation.

### 7.2.5 Effects of Magnetic Saturation on the Estimation of Stator Resistance and Temperature

For the estimation of stator winding resistance and temperature, the dc components in the input current and voltage need to be calculated. Assuming that dc signals are injected from phase ***a*** to phase ***b*** and ***c***, only the dc components in the d-axis stator voltage and current need to be calculated, as,

$$v_{ds} = R_s i_{ds} + \frac{d}{dt}\lambda_{ds} , \tag{7.5}$$

where $\lambda_{ds}$ is the d-axis stator flux. Therefore, the dc component in the d-axis stator voltage can be estimated as,

$$v_{ds}^{dc} = \frac{1}{T}\int_{T} v_{ds}\,dt = \frac{1}{T}\int_{T} R_s i_{ds}\,dt + \frac{1}{T}\lambda_{ds}\Big|_{0}^{T}, \tag{7.6}$$

where $T$ is the period of the fundamental frequency. In stead state, as the saturation varies periodically, the stator flux is still periodic at the fundamental frequency. Therefore,

$$v_{ds}^{dc} = \frac{1}{T}\int_{T} R_s i_{ds}\,dt + \frac{1}{T}\lambda_{ds}\Big|_{0}^{T} = R_s\,\frac{1}{T}\int_{T} i_{ds}\,dt + 0 = R_s i_{ds}^{dc}, \tag{7.7}$$

where $i_{ds}^{dc}$ is the dc component in the d-axis stator current. Therefore, even considering the magnetic saturation, the stator winding resistance can still be estimated as,

$$R_s = \frac{v_{ds}^{dc}}{i_{ds}^{dc}}. \tag{7.8}$$

This validates the feasibility of previous proposed active thermal protection techniques, even with considerations of the magnetic saturation under different load conditions.

### 7.2.6 Induction Machine Losses during DC Injection

DC injection induces additional losses in the motor, which may cause temperature rise during dc injection mode. Hence, it is necessary to have good knowledge of the additional losses in order to ensure that the winding insulation system is not harmed by dc injection.

The induction machine losses can be briefly divided into several components, namely the stator copper loss, the rotor copper loss, the core loss, the windage loss and the stray loss, which are all affected by the injected dc current.

The injected dc current, $i^{dc}$ induces additional stator copper loss. For the dc injection for inverter-fed machines, the additional copper losses can be estimated as,

$$P_{s,copper} = \frac{3}{2} {i_{DC}}^2 R_s , \tag{7.9}$$

where $R_s$ is the stator phase armature resistance. As for the dc injection for mains-fed and soft-starter induction machines, the additional copper loss is higher than $\frac{3}{2} {i_{DC}}^2 R_s$ because of the harmonics injected along with the dc current. However, since the stator current is measured and the stator resistance is calculated, the additional stator copper loss can be always directly calculated.

Seen from the rotor, the magnetic field produced by the dc current is rotating at a frequency of *(1-s)f*, where *s* is the slip and *f* is the main frequency. This rotating magnetic field induces additional current in the rotor bar and results in additional rotor copper losses, which can also be estimated.

The rotor equation of the dynamic induction machine model in the rotor reference frame is as follows:

$$\begin{aligned} 0 &= R_r i_{dr} + \frac{d}{dt}(L_m i_{ds} + L_r i_{dr}) \\ 0 &= R_r i_{qr} + \frac{d}{dt}(L_m i_{qs} + L_r i_{qr}) \end{aligned} \tag{7.10}$$

where $R_r$ is the rotor resistance, $L_m$ and $L_r$ are the mutual inductances. The dc component of the stator current in the rotor reference frame is as follows:

$$\begin{aligned} i_{ds} &= \frac{3}{2} i_{dc} \sin(\omega_{dc} t + \phi) \\ i_{qs} &= \frac{3}{2} i_{dc} \cos(\omega_{dc} t + \phi) \end{aligned} \tag{7.11}$$

where $\omega_{dc} = 2\pi(1-s)f$ is the angular frequency of the DC current in the rotor reference frame.

By solving (7.10) and (7.11), it can be found that both the steady state solution of $i_{dr}$ and $i_{qr}$ are sinusoidal and have a magnitude of $\frac{3}{2}\frac{\omega_{dc}L_m I_{dc}}{\sqrt{R_r^2+(\omega_{dc}L_r)^2}}$. As a result, the additional rotor copper loss by the dc injection is

$$P_{r,copper} = \frac{3}{2}\frac{(\omega_{dc}L_m)^2}{R_r^2+(\omega_{dc}L_r)^2} I_{dc}^2 R_r \tag{7.12}$$

Note that $R_r$ is the rotor equivalent resistance considering the skin effect at frequency *(1-s)f*. Induction machines with deep rotor slots have higher skin effect and thus more additional rotor copper losses. Again this additional rotor copper loss is higher for the dc injection for mains-fed and soft-starter induction machines.

In the stator core, additional magnetic field is added to the original field, which causes the flux density distribution in the stator core and possible saturation. The stator core loss may be increased. However, because the injected dc current is small compared to the rated current, the increase of stator core loss is small.

The injected dc current also causes flux fluctuations in the rotor core when the rotor rotates and thus the additional rotor core loss. However, because the rotor cores in induction motors are also laminated and the magnetic field by the injected dc current is small, the rotor core loss is also small.

To sum up, the additional losses induced by the dc injection are primarily the additional copper loss in the stator and rotor, which can be both estimated with the machine parameters. Hence, the thermal effect of dc injection can be estimated to

prevent possible winding insulation damage caused by the temperature due to additional losses.

## 7.3 Simulation Results

The analysis of the effects of magnetic saturation is first validated through finite-element simulation results using Maxwell. The simulated motor has the same rating as the one in the experiment: 7.5 HP, 230/460 V, 60 Hz. Although the exact design parameters of the motor for the experiment are unknown, classical design rules and methods such as are applied and the designed motor has a normal efficiency of 85 %, normal power factor of 0.85 and a rated slip of 0.04, which is close to the performance of the actual motor for the test. M19-29G from AK Steel, a type of non-oriented electric steel typically used for stator and rotor core material is use in the simulation. The peak flux densities in the stator teeth, rotor teeth, stator core and rotor core, are designed to be around 1.45 T, which is approximately knee point in the B-H curve of M19-29G. During transient simulations, the rotor slip is kept to be the rated value and rated voltage is applied to the motor.

The Flux density during normal operation and dc signal injection are shown in Figure 7.5-(a) and (b), respectively. A higher level of magnetic saturation is induced during dc signal injection, due to flux bias caused by the injected dc signals.

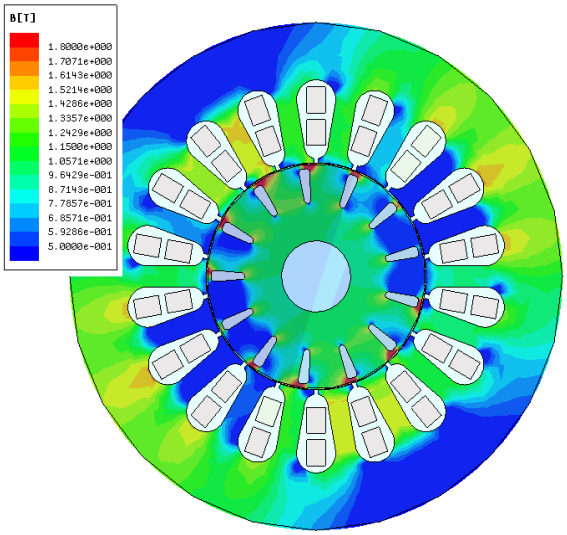


(a) normal operation

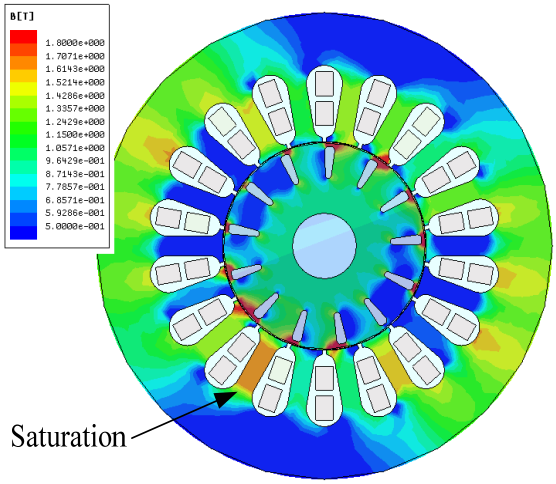


(b) dc signal injection

Figure 7.5: Flux density.

To compare the waveforms of the stator currents during dc signal injection and the normal operation, the dc bias in the stator currents during dc signal injection is removed, as shown in Figure 7.6. To better show the effects of magnetic saturation on the waveforms of the stator currents, the phase ***a*** currents are amplified, as shown in Figure 7.7. It can be observed from Figure 7.7 that during dc signal injection, the positive peak

value of the phase a current is increased due to a higher level of saturation compared to normal operating condition; the negative peak value is reduced due to a lower level of saturation. However, the change of waveform of the stator current does not have any impact on its dc component.

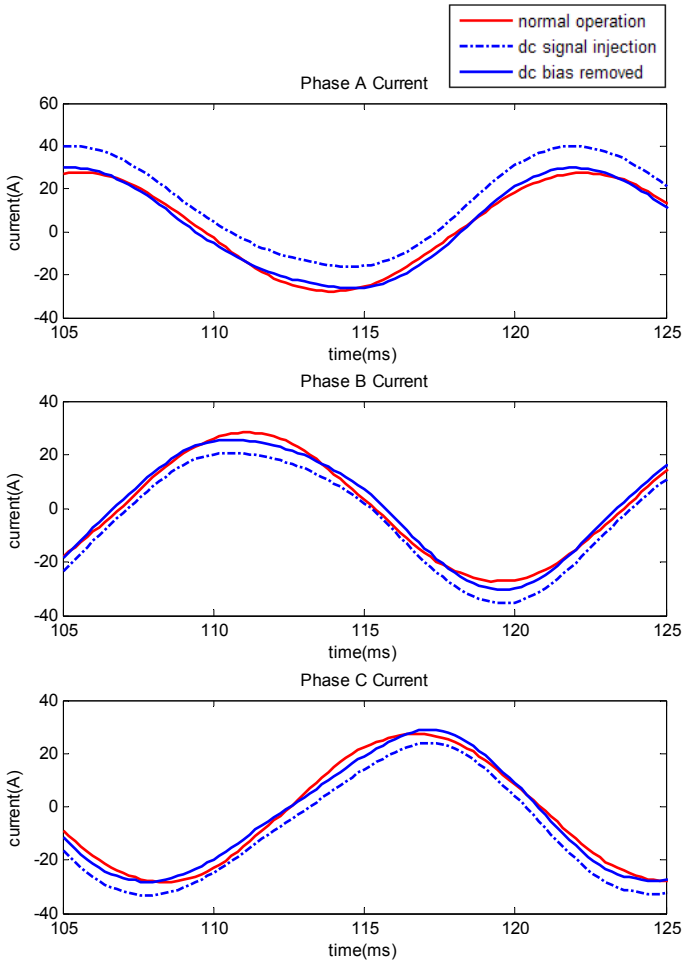


Figure 7.6: Simulated stator currents during dc signal injection and normal operation.

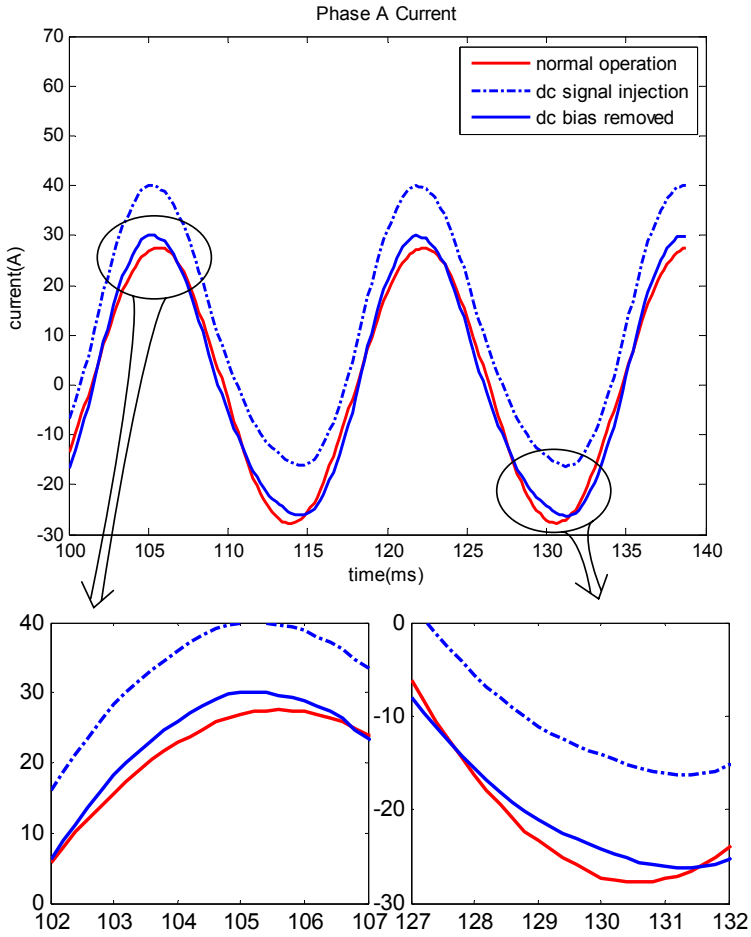


Figure 7.7: Simulated phase a current during dc signal injection and normal operation.

In addition to simulation results on magnetic flux and current during dc signal injection, the different losses in the induction machine are simulated with different magnitudes of the injected dc signals, as compared in Table 7.1. The dc signals are injected at 0, 0.9, 3.6, and 6.3 amps, with respect to the rated current of 19 amps. It can be shown from table I that the increase of copper losses is dominant compared to the core losses when the injected dc signal increases. This is due to the fact that the magnetic saturation is unbalanced in each cycle as discusses in Section 7.2.6, and the average losses remain almost the same for different magnitudes of dc signal injection.

Additional stator and rotor copper losses under normal operating condition versus $i_{dc}^2$ for the three simulated case are plotted in Figure 7.8. It can be observed that both the stator and rotor copper losses increase proportionally with the increase of $i_{dc}^2$, which agrees with the theoretical analysis in Section 7.2.6.

Table 7.1: Motor Losses with Different Magnitudes of the Injected DC Signals

| | Vdc=0 V | Vdc=0.3 V | Vdc=1.2 V | Vdc=2.1 V |
|---|---|---|---|---|
| Phase A DC current (A) | 0 A | 0.9 A | 3.6 A | 6.3 A |
| Stator copper loss (W) | 123.9 | 124.2 | 128.9 | 139.3 |
| Rotor aluminum loss (W) | 263.2 | 264.0 | 275.0 | 299.2 |
| Core loss (W) | 73.7 | 73.7 | 74.3 | 76.1 |

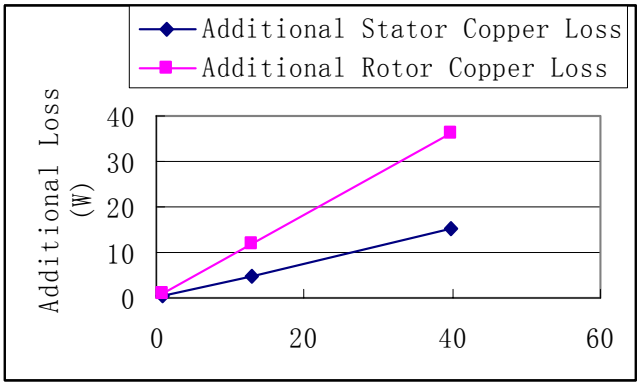


Figure 7.8: Additional stator and rotor copper losses vs. square of dc current

## 7.4 Experimental Results

The experimental testing is conducted on an ODP induction motor, using the same setup as shown in Section 6.7.1.

The waveforms of the stator currents under normal operation and during dc signal injection are compared in Figure 7.9. A dc current of 7 amps is injected when the motor is operated under full load. For comparison purposes, the dc component in the phase ***a*** current during dc signal injection is removed. A low pass filter with a cutoff frequency

of 1000 Hz is applied to remove the noise caused by the switching of IGBTs. An amplified figure of the phase ***a*** current is in Figure 7.10. The effects of magnetic saturation on the waveform of the stator current can be observed, which agrees with the analysis and the simulation results.

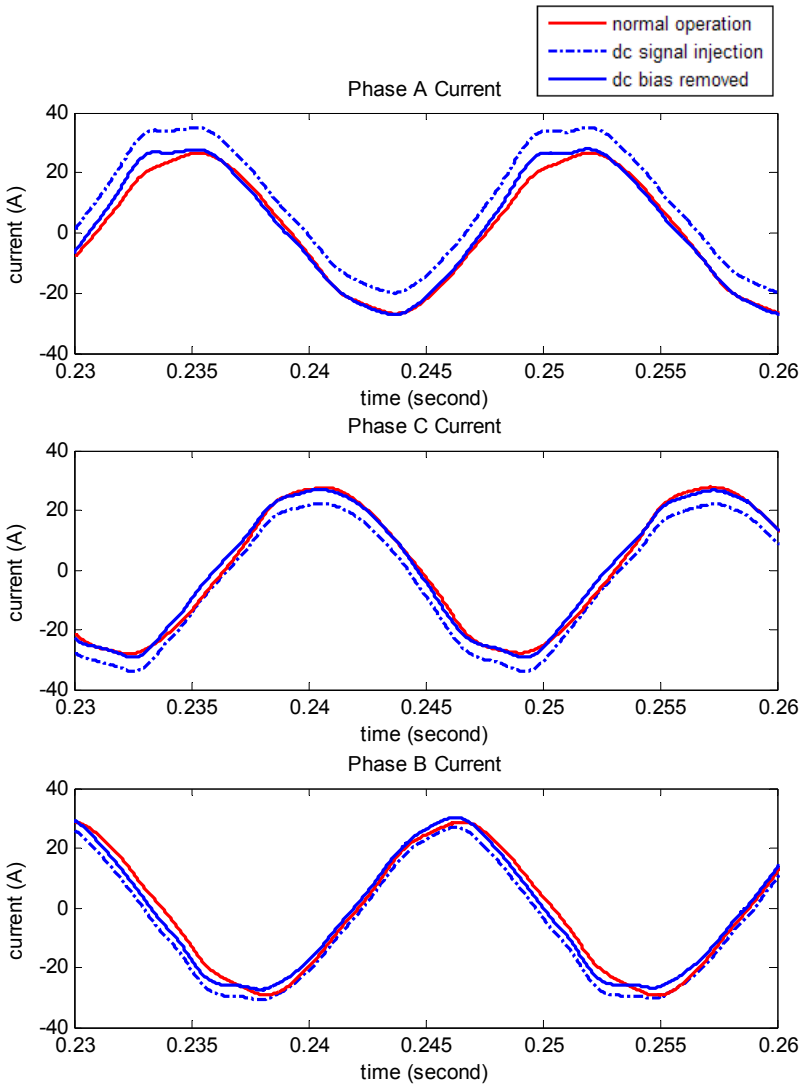


Figure 7.9: Stator currents during dc signal injection and normal operation.

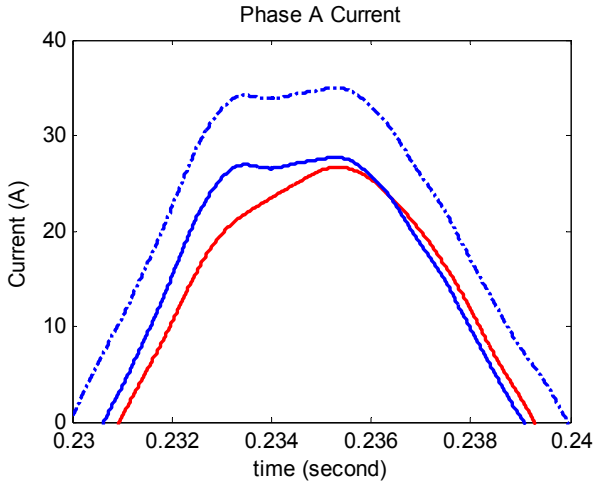


Figure 7.10: Amplified phase a current during dc signal injection and normal operation.

## 7.5 Chapter Summary

Active thermal protection techniques have been proposed for the thermal protection of induction motors in Chapter 5 and 6. The stator resistance and temperature can be monitored using the dc model of induction motors via dc signal injection.

This chapter has presented a detailed analysis of magnetic saturation caused by the dc signal injection with its effects discussed. Due to the bias in the flux caused by the injected dc signals, the level of magnetic saturation varies within each cycle. Such varying magnetic saturation degrades the performance of induction motors, induces torque pulsation, and increases the losses in the motors. The effects of the magnetic saturation on the motor currents, the motor's thermal behavior and the estimation accuracy of stator resistance and temperature have been analyzed. Finite-element simulation results and experimental results have been presented to illustrate the analysis. It has been shown that although the magnetic saturation affects the waveforms of the stator currents, it does not have any impact on their dc components. Therefore, the

accuracy of the stator resistance and temperature estimation can be guaranteed even with presence of magnetic saturation under different conditions.

# CHAPTER 8 A Cooling Capability Monitoring Scheme

## 8.1 Overview

The stator temperature estimation techniques for in-service induction motors are presented in Chapter 5 and Chapter 6. However, the monitoring of the stator winding temperature is not sufficient for the complete thermal protection of induction motors. The thermal overload of motors can be caused not only by motor overload, but also by impaired cooling capability. Impaired cooling capability causes additional motor temperature rise, and accelerate the deterioration of induction motor components. Therefore, in the case of impaired cooling capability, it is important to detect the problem as early as possible, so that the motor can be inspected and repaired proactively to avoid catastrophic process downtime and extend the motor life.

In this chapter, a novel cooling capability monitoring scheme is proposed by monitoring the thermal parameters of the motor's first-order thermal model. The thermal parameters are identified online using an extended Kalman filter approach based on the estimated stator temperature via dc signal injection. The proposed cooling capability monitoring scheme, together with the stator winding temperature estimation scheme provides a complete thermal protection for in-service induction motors.

## 8.2 First-order Thermal Model for Detecting Impaired Cooling Capability

The mathematical representation and detailed analysis of the first-order thermal model of induction motors are presented in Chapter 2. The first-order thermal model is not an accurate representation of the thermal behavior of the induction motor, since the other losses, such as core loss, rotor loss, etc., are neglected, as discussed in Section 4.2.

The equivalent thermal resistance, $R_{th}$, and the equivalent thermal time constant, τ, are not constant under different operating conditions with different load, speed, input frequency, etc, when such models are used. However, this simplified thermal model provides a tool to monitor the cooling capability of the induction motor by identifying the equivalent thermal parameter of the thermal model. In the case of impaired cooling capability, the equivalent thermal resistance increases since the motor's ability to transfer heat is obstructed. Therefore, the impaired cooling capability of induction motors can be detected based on monitoring the equivalent thermal resistance of the first-order thermal model.

## 8.3 Impaired Cooling Capability Detection

Based on the first-order thermal model and the estimated $T_s$ via dc signal injection, the thermal parameters can be identified online to monitor the cooling capability of the motor. Because of the nonlinearity of the first-order thermal model, an extended Kalman filter (EKF) approach is used for its simplicity and online nature.

The state-space model of the thermal parameters is given by,

$$x_n = \begin{bmatrix} R_{th} \\ T_{s0} \\ 1/\tau \end{bmatrix}_n = \begin{bmatrix} 1 & 0 & 0 \\ 0 & 1 & 0 \\ 0 & 0 & 1 \end{bmatrix} \begin{bmatrix} R_{th} \\ T_{s0} \\ 1/\tau \end{bmatrix}_{n-1} + w = x_{n-1} + w \quad , \tag{8.1}$$

where $w$ is the modeling error, identified as 0, since the thermal parameters remain constant under constant load condition; $x_n$ represents the thermal parameters at the $n^{th}$ iteration. To avoid singularity, 1/τ, instead of τ, is used in the space model. The initial states of the thermal parameters are estimated based on the Trip Class (*TC*) and the Service Factor (*SF*) of the induction motor as shown in Chapter 2.

The observation model is given by,

$$\begin{aligned} z_n &= \hat{T}_s = P_{loss} R_{th}(1-e^{-t/\tau}) + T_{s0} e^{-t/\tau} + T_A + v_n \\ &= h(x_n) + v_n \end{aligned}, \tag{8.2}$$

where $v_n$ is measurement error, which is the $T_s$ estimation error. The variance matrix $Q_v$, is estimated as the variance of the estimated $T_s$ at full load after the motor reaches thermal balance.

The Jacobian matrix of the function *h(x)* is given by,

$$H_n = \left.\frac{\partial h}{\partial x}\right|_{x_{n-1}} = \left.\begin{bmatrix} P_{loss}(1-e^{-t/\tau}) \\ e^{-t/\tau} \\ t(P_{loss}R_{th} - T_{s0})e^{-t/\tau} \end{bmatrix}^T\right|_{x_{n-1}}. \tag{8.3}$$

In each iteration step, the EKF first gives an initial prediction, as,

$$\hat{x}_{k|k-1} = \hat{x}_{k-1|k-1}. \tag{8.4}$$

$$P_{k|k-1} = P_{k-1|k-1} + Q_w. \tag{8.5}$$

The EKF then updates the prediction as,

$$K_k = P_{k|k-1} H_k^T (H_k P_{k|k-1} H_k^T + Q_v)^{-1}, \tag{8.6}$$

$$\hat{x}_{k|k} = \hat{x}_{k|k-1} + K_k(z_k - h(\hat{x}_{k|k-1})), \tag{8.7}$$

$$P_{k|k} = (I - K_k H_k) P_{k|k-1}. \tag{8.8}$$

Equations (8.4) to (8.8) are repeated for each step of the iteration to provide an estimation based on all available information.

Using the EKF approach, the thermal parameters of the induction motor can be estimated to monitor the cooling capability of the induction motor, under constant load

condition. The change of thermal parameters implies the change of the motor cooling capability. More specifically, the increase of $R_{th}$ implies the deterioration of cooling capability of the motor, since $R_{th}$ represents the cooling capability of the stator winding.

### 8.4 Overall Thermal Protection Scheme for In-service Induction Motors

The overall thermal protection scheme for soft-starter-connected induction motors is shown in Figure 8.1. By modifying the operation of thyristors in the soft-starter, the dc signals are injected intermittently to estimate the stator winding resistance over time. The thermal protection scheme is also feasible for induction motors fed by motor drives. The stator winding temperature, $T_s$, is estimated based on the estimated stator winding resistance, $R_s$. The thermal resistance, $R_{th}$, in the simplified thermal model, is then estimated based on the estimated $T_s$ via dc signal injection. Using the $R_{th}$ estimated at normal cooling capability as threshold, the increase of $R_{th}$ indicates the deterioration of the cooling capability.

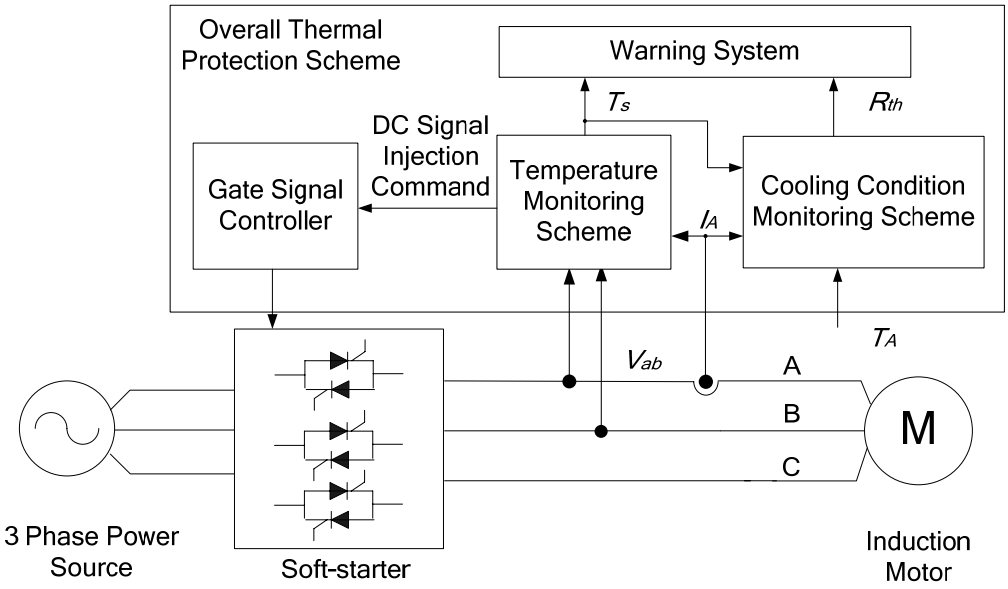

Figure 8.1: Overall thermal protection scheme for soft-starter-connected induction motors.

The overall thermal protection system can therefore warn the user not only of the stator winding overheating, but also of the deterioration of the cooling capability in a proactive manner. This allows the user to turn off the motor in the case of stator winding overheating, and also to inspect, repair the motor or schedule maintenance for cooling capability deterioration when necessary. The significance of the thermal protection scheme lies in its non-intrusive and sensorless nature: only voltage and current sensors are used; the motor can be well protected without any embedded thermal sensor, or any off-line test.

## 8.5 Experimental Validation

### 8.5.1 Experimental Setup

The proposed cooling capability monitoring scheme is tested on motor 3, whose nameplate information is shown in Table 5.2. The overall setup is the same as shown in Figure 5.10. The dc signal is injected for 0.5 second every 1 minute with a delay angle of 30º. To test the feasibility of the proposed cooling capability monitoring system, three different cooling capabilities are tested: 1) the motor is firstly operated with normal cooling capability; 2) the motor fan is removed to emulate the broken cooling fan condition; 3) a fiberglass thermal insulation foil is used to cover part of the induction motor frame to emulate the impaired cooling caused by motor frame dust build-up. The induction motor setups with the impaired cooling capabilities are shown in Figure 8.2.

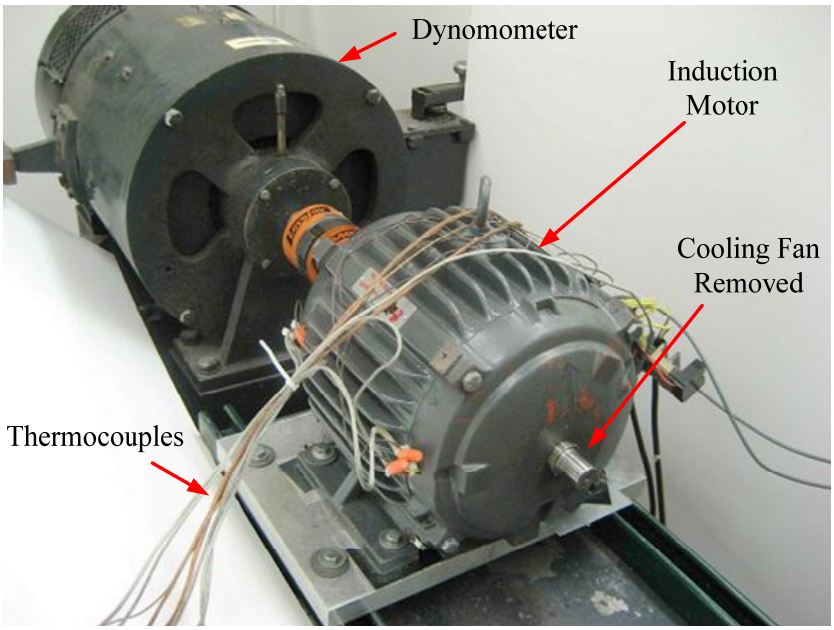


(a) Impaired cooling capability with cooling fan removed

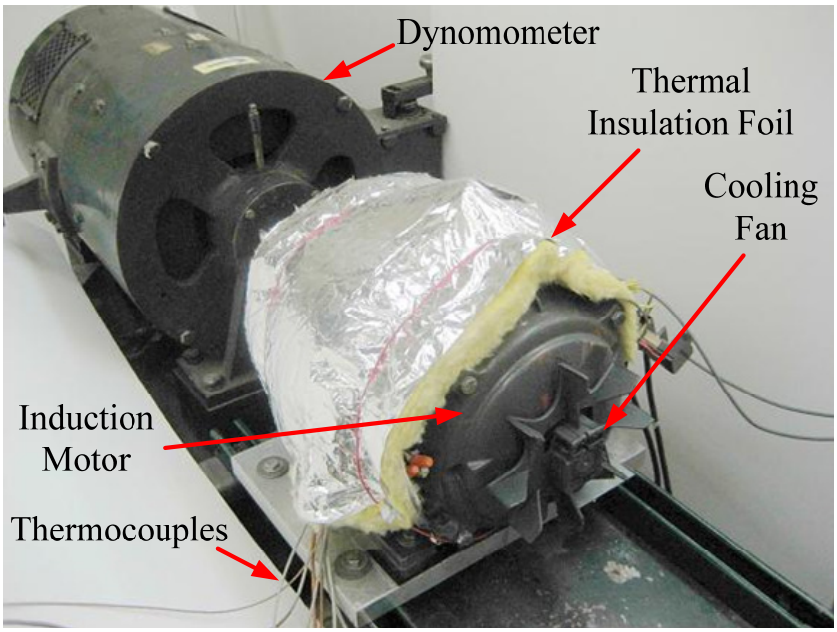


(b) Impaired cooling capability with additional thermal insulation

Figure 8.2: Experimental setup of impaired cooling capabilities.

### 8.5.2 Stator Temperature Estimation

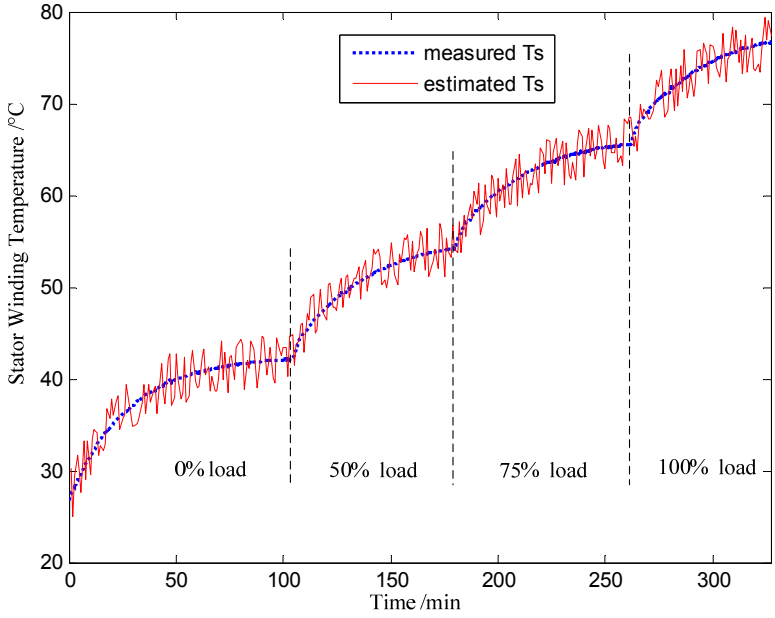


(a) Normal cooling capability

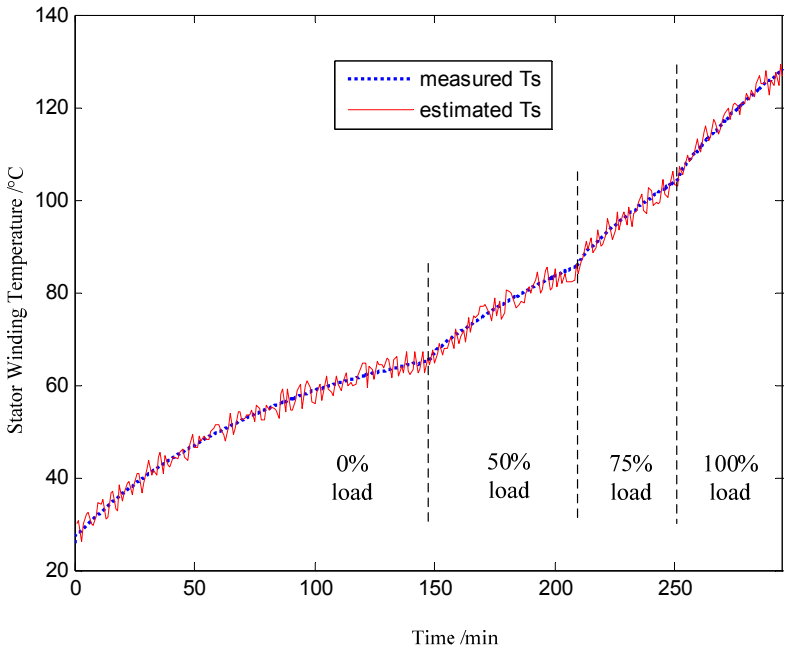


(b) Impaired cooling capability with cooling fan removed

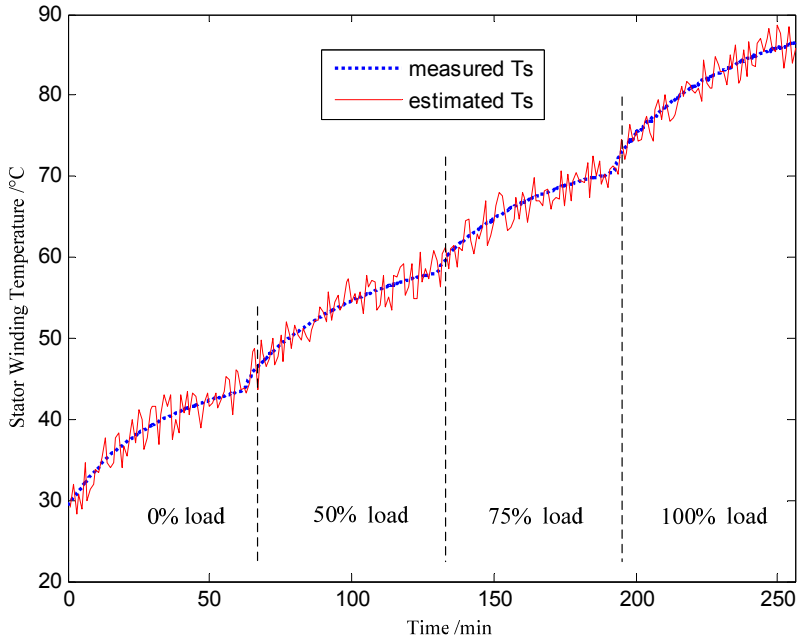


(c) Impaired cooling capability with additional thermal insulation

Figure 8.3: Experimental results of $T_s$ estimation.

The stator winding temperature estimation results with different cooling capabilities and under different load conditions are shown in Figure 8.3. Figure 8.3 (a), (b) and (c) show the $T_s$ estimation results with three different cooling capabilities, respectively: the normal cooling capability; the impaired cooling capability with a broken cooling fan; and the impaired cooling capability with additional thermal insulation. Under each cooling condition, variable load conditions, 0%→50%→75%→100% of the rated load, are tested. The stator winding temperature is estimated with all the contact resistances and cable resistances measured and compensated. In a practical application, the inaccurate compensation can lead to an "offset" in the $T_s$ estimation, but this does not affect the effectiveness of the proposed cooling capability monitoring scheme.

It is clearly shown in Figure 8.3 that the dc signal injection-based $T_s$ estimation method is capable of providing accurate monitoring of the stator winding temperature under variable load conditions and different cooling capabilities. This feature is of great significance since the stator winding of the motor can be reliably protected with different cooling capabilities and under different operating conditions. Besides, because of its independence on the cooling capabilities, dc-signal-injection-based $T_s$ estimation method provides a tool for monitoring the motor cooling capabilities.

### 8.5.3 Cooling Capability Monitoring

Based on the estimated $T_s$ using dc signal injection, the cooling capability can be monitored using the EKF approach. The initial thermal parameters, the thermal resistance, $R_{th}$, and the time constant, $\tau$, are identified as 0.47 $K \cdot W^{-1}$ and 534 $s$, respectively, based on the Trip Class and the Service Factor of the motor. After the initialization, the EKF updates the thermal parameters automatically based on the estimated $T_s$ from the injected dc signals. The covariance of the observation error, $Q_v$, is measured as the variance of the estimated $T_s$ under full load after the motor reaches thermal balance, which is identified as $3.5\,^{o}C^{2}$.

To test the effectiveness of the proposed thermal parameter estimation method, the motor thermal parameters are also calculated from the measured stator winding temperature from the thermocouples, for validation purposes. The experimental results of the $R_{th}$ estimated under variable load conditions and different cooling capabilities are shown in Figure 8.4. Figure 8.4 (a), (b), and (c) show the comparisons of the estimated $R_{th}$ from EKF approach based on dc signal injection, and the calculated $R_{th}$ from measured $T_s$ under normal cooling capability, the impaired cooling capability with broken

cooling fan, and the impaired cooling capability with additional thermal insulation, respectively. Under each cooling condition, the motor is operated under variable load conditions: 0%→50%→75%→100% of the rated load. When the load changes, the covariance matrix of the initial thermal parameters is reset to allow EKF to search for new thermal parameters under the new load condition. It is clearly shown in Figure 8.4 that the EKF approach is capable of giving accurate estimation of the thermal parameters, based on the dc-injection-based $T_s$ estimation, under variable load conditions and different cooling capabilities. The thermal parameter estimation error is within 3% after convergence. The EKF approach converges within 30-50 iterations/updates. The required convergence time can be further reduced by increasing the $T_s$ estimation update frequency.

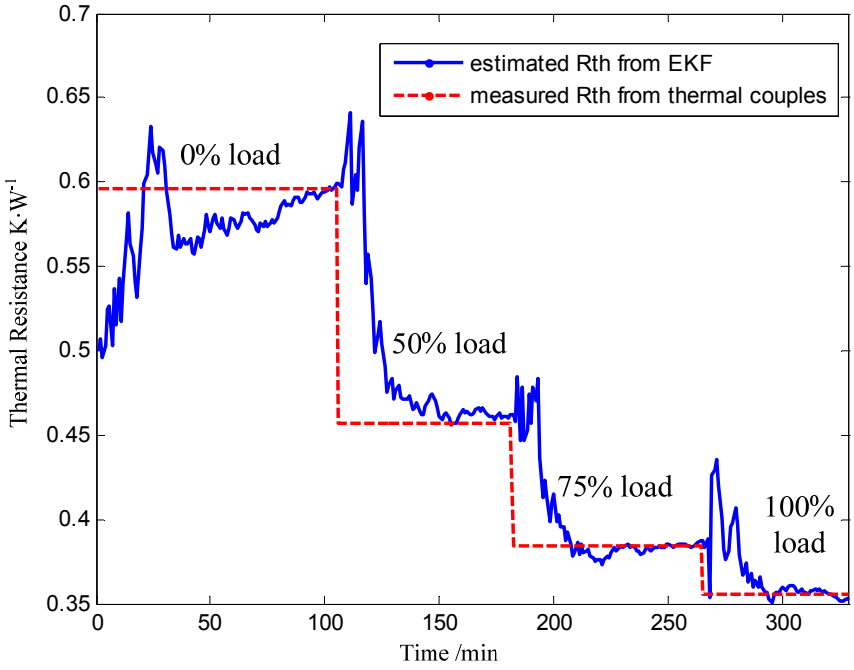


(a) Normal cooling capability

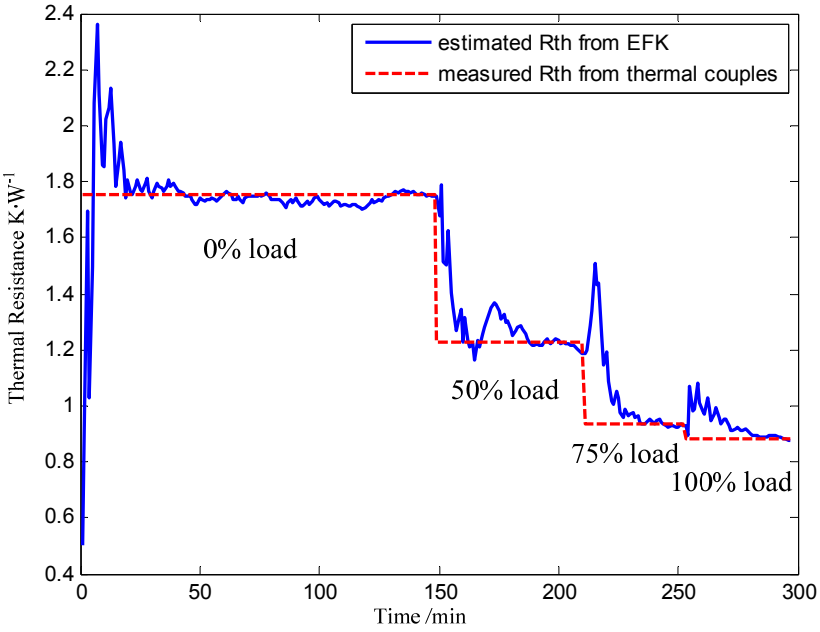


(b) Impaired cooling capability with cooling fan removed

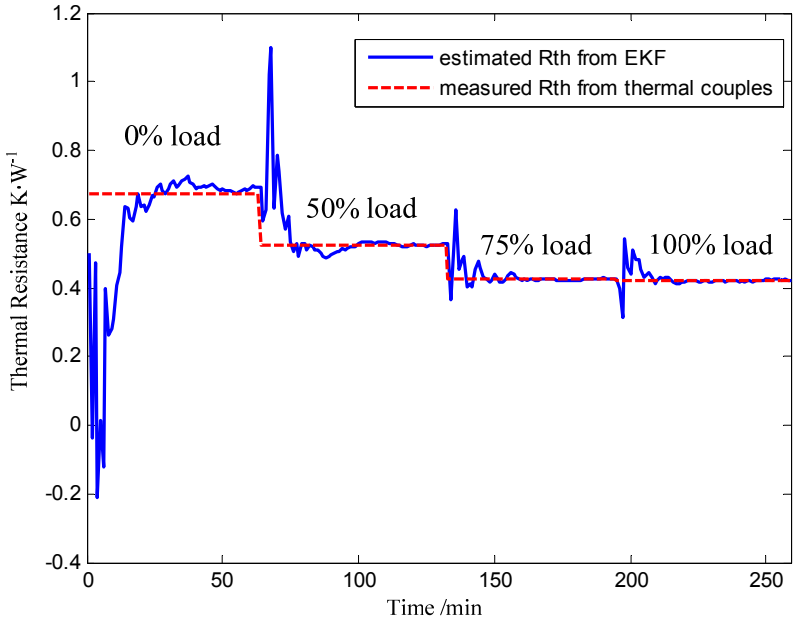


(c) Impaired cooling capability with additional thermal insulation

Figure 8.4: Experimental results of cooling capability monitoring.

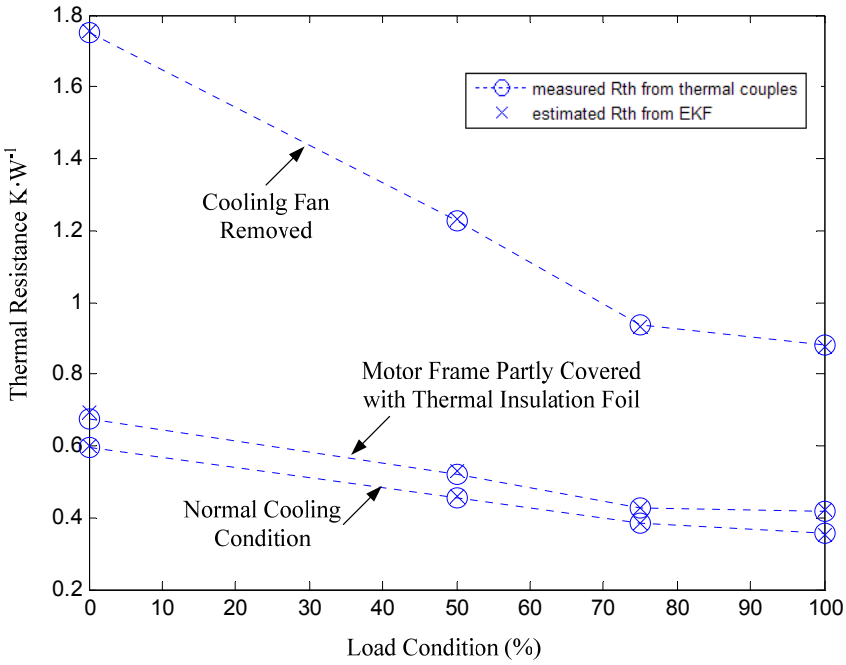


Figure 8.5: Comparison of thermal resistance $R_{th}$.

With the thermal resistance $R_{th}$ estimated from the proposed EKF approach, the cooling capability of the induction motor can be monitored. Figure 8.5 shows the comparison of the values of $R_{th}$ under different load conditions and with different cooling capabilities. It clearly shows that the increase of thermal resistance, $R_{th}$, indicates the deterioration of the cooling capability of the induction motor. Therefore, by monitoring the thermal resistance, $R_{th}$, using the proposed cooling capability monitoring scheme, the deterioration of cooling capability can be detected to alert the user for further inspection and repair.

## 8.6 Chapter Summary

This chapter has proposed a dc-injection-based cooling capability monitoring scheme for in-service induction motors. Via continuously monitoring of the values of $R_s$, the

stator winding temperature, $T_s$, can be estimated, as proposed in Chapter 5 and Chapter 6. The cooling capability of the motor can be monitored based on the estimate stator temperature. An extended Kalman filtering approach has been proposed to identify the thermal parameters of a simplified thermal model for induction motors, which are used as indicators of motor cooling capability.

The feasibility of the proposed cooling capability monitoring system has been validated from experimental results under variable load conditions and different cooling capabilities. Two different impaired cooling capabilities have been created: 1) the cooling fan is removed to emulate the broken cooling fan condition; 2) a thermal insulation foil is used to cover a part of the motor frame to emulate the impaired cooling capability caused by motor frame dust build-up. From the comparison of experimental results between normal cooling capability and the impaired cooling capabilities, it has been validated that the proposed cooling capability monitoring scheme is capable of providing accurate indication of the motor cooling capability. The thermal parameter estimation error from the EKF approach is within 3% after convergence. With both the stator winding temperature and the motor cooling capability monitored, the overall thermal protection scheme will trip the motor in the case of stator winding overheat, and warn the user for proactive inspections or maintenance in the case of cooling capability deterioration. Therefore, the proposed overall thermal protection scheme can provide complete, reliable thermal protection for soft-starter-connected induction motors.

# CHAPTER 9 Improving Thermal Recovery Time for Induction Motors in Intermittent Periodic Duty Cycles

## 9.1 Overview

Active stator winding temperature estimation techniques have been proposed in the previous Chapters for the thermal protection of in-service induction motors. However, in some applications, stator winding temperature estimation is also needed for de-energized induction motors for assisting motor system management. In many industrial processes, induction motors need to operate with intermittent periodic duty cycles, where the motors do not operate continuously. Under such operating conditions, a motor must be periodically de-energized for certain duration to allow the motor's temperature to recover back to a predetermined value before the next startup, which prevents the heat from accumulating in the motors. Therefore, the accurate stator winding temperature estimation for de-energized induction motors is important to accurately determine the required minimum thermal recovery time and thus assist the management of the industrial processes.

The thermal characteristics of de-energized ac motors are largely different from those of operating ac motors. For ac motors operated with intermittent periodic duty cycles, conventional techniques generally overestimate the required thermal recovery time in each operating cycle, which results in the reduction of utilization and efficiency of industrial processes.

This chapter proposes a non-intrusive stator winding resistance and temperature estimation technique for soft-starter-connected ac motors at standstill. By changing the operation of the solid-state power switches in the soft-starter, a dc signal can be

intermittently injected into the ac motor when de-energized, with no output torque induced. The stator winding resistance and temperature can therefore be monitored based on the dc model of ac motors, when the motors are de-energized. Based on the monitoring of the stator winding temperature, the required thermal recovery time can be accurately determined, which can greatly reduce the required time of each operating cycle and improve the usage of the industrial process. The proposed technique is validated through experimental testing.

## 9.2 Introduction

The major objective of thermal protection for induction motors is to avoid thermal overload depending on the thermal limit of the stator insulation. The thermal protection of continuously operated induction motors has drawn a lot of attention in the past several decades. However, in many industrial applications, such as pumps in petroleum industry, sewage treatment, mining, etc., instead of continuous constant load operation, denoted as duty type S1 by [10], ac motors are operated with intermittent periodic duty cycles, designated as duty type S3 [10]. Each cycle of this duty type typically consists of a time of operation at constant load, and a time of de-energization to allow the motor to cool down before the next startup, which is also known as thermal recovery time.

Since embedded thermal sensors are considered costly, especially for small- to medium-size ac motors, thermal overload relays are widely used to provide thermal protection of ac motors and prolong a motor's lifetime. Conventional overload protection devices, including dual-element time-delay fuses and eutectic alloy overload relays, are normally designed based on the thermal limit curves, which define the safe operating time for different magnitudes of input currents under both transient and running overload

conditions [13]. Since the effects of the initial temperature of a motor before startup are generally neglected, these conventional protection devices are not suitable for the protection of motors operated with intermittent periodic duty type.

Microprocessor-based thermal overload relays, which represent the state of the art in thermal protection devices, typically use a simplified first-order thermal model to emulate the thermal characteristics of ac motors during operation [14]. These thermal overload relays are primarily designed for the protection of motors operated under continuous constant load condition. However, the thermal characteristics of ac motors during operation are largely different from those at standstill. The cooling capability of de-energized ac motors is highly reduced for both Totally-Enclosed Fan-Cooled (TEFC) and open drip-proof (ODP) motors, since the cooling fan or rotor blades are also at rest. In the case of under-estimation of the thermal recovery time, the motor cannot be completely cooled down before startup, which may result in the accumulation of heat dissipation and therefore a higher motor temperature [47]. For thermal protection purposes, the thermal recovery time is typically estimated conservatively to avoid the unexpected motor temperature rise and the resultant deterioration of a motor's key components. However, this conservative estimation may largely increase the required thermal recovery time, and therefore reduce the overall usage of the industrial process and its productivity.

In this Chapter, a novel dc signal injection-based technique is proposed to estimate stator winding temperature of de-energized ac motors for assisting the thermal protection of intermittently operated ac motors, reducing the thermal recovery time and optimizing the overall usage of the industrial processes. The thermal characteristics of ac motors

operated with intermittent duty cycles are firstly discussed. A dc signal injection-based stator temperature estimation approach for de-energized ac motors using soft-starters is then proposed. The proposed signal injection technique does not interrupt the operation of ac motors, since no output torque is induced.

## 9.3 Thermal Behavior of AC Motors with Intermittent Periodic Duty Type

### 9.3.1 Operation of AC Motors with Intermittent Periodic Duty Type

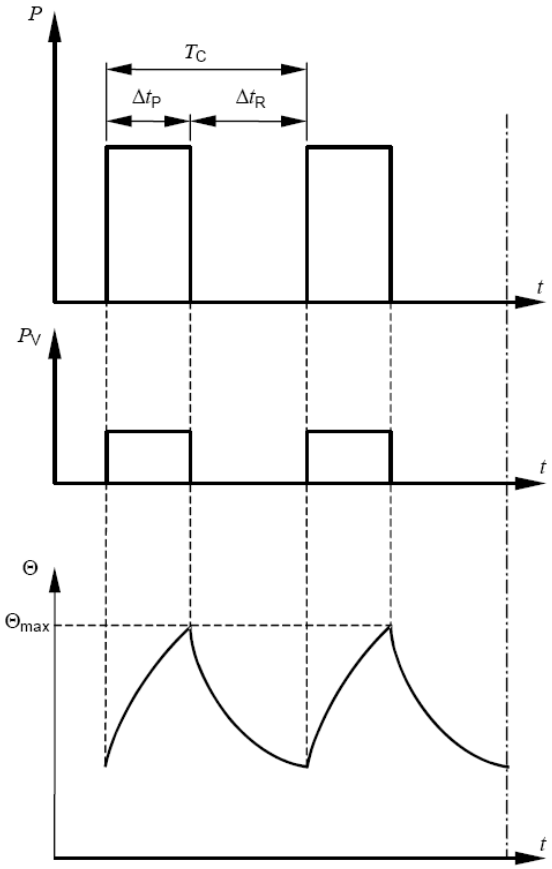


Figure 9.1: Intermittent periodic duty type-S3 [10].

For intermittent periodic duty type, denoted as S3 duty type [10], each operating cycle consists of two periods of operation: a time of constant load operation, and a time

de-energized and at rest, as shown in Figure 9.1. In this duty type, it is assumed that the time of constant load is long enough so that the effects of the high starting current on the motor temperature rise can be neglected. The duration of each cycle is denoted as $T_C$; $\Delta t_P$ and $\Delta t_R$ represent the duration of operation and the duration of de-energization, also known as the thermal recovery time; $P$ is the motor's load; $P_V$ represents the motor losses; $\Theta$ is the motor temperature; $\Theta_{max}$ is the maximum motor temperature attained. It is important that the thermal recovery time is sufficient so that the temperature of the motor drops below some predetermined value before next startup, so that the accumulation of heat dissipation can be avoided.

### 9.3.2 Thermal Behavior of AC Motors with S3 Duty Type

It is a common practice to model the thermal behavior of ac motors under constant operating conditions, e.g. constant load condition or standstill, using a simplified thermal model with one single thermal time constant, as,

$$T_s(t) = T_s(\infty)(1 - e^{-t/\tau}) + T_{s0}e^{-t/\tau}, \qquad (9.1)$$

where $T_s(t)$ represents the stator temperature rise; $T_s(\infty)$ is the stator temperature rise when a thermal equilibrium is reached; $T_{s0}$ is the initial stator temperature rise; $\tau$ is the equivalent thermal time constant.

Equation (9.1) is a rough model of the motor's thermal characteristics under constant operating conditions. Since the stator temperature rise is an accumulative result of different losses in different locations of ac motors, the thermal behavior of ac motors can also be represented in a transfer-function form, as,

$$T_s(s) = \sum Z_i(s) \bullet P_{loss}(s), \qquad (9.2)$$

where $P_{loss}$ represents the losses in different locations in ac motors; $Z_i$ is the transfer function from different losses to the stator temperature rise. For simplicity, each $Z_i$ can be approximated using a single time constant, as,

$$Z_i(s) = \frac{\alpha_i}{s + 1/\tau_i}, \tag{9.3}$$

where $\alpha_i$ is the gain; $\tau_i$ is the time constant. The time constants, corresponding to different losses in the motor, are largely different. Therefore, under different operating conditions, the equivalent time constant, $\tau$, as in (9.1), changes. For instance, under high load condition, the thermal time constants corresponding to the higher losses dominate the thermal response.

For motors operated with S3 duty type, even when the motor is operated under constant load condition during the operating duration $\Delta t_P$, the equivalent thermal time constant still changes with different lengths of $\Delta t_P$. For a longer $\Delta t_P$, the slow thermal transients with larger thermal time constants dominate the thermal response of the motor, and therefore, the equivalent thermal time constant increases. When the simplified thermal model with a single thermal time constant is used, as shown in (9.1), the thermal time constant needs to be adjusted under different load conditions and with different values of $\Delta t_P$, which is highly difficult for practical applications without embedded thermal sensors. On the other hand, when the motor is de-energized during $\Delta t_R$, the equivalent thermal time constant can be assumed constant. However, the accurate estimation of the thermal time constant at standstill is still difficult without embedded thermal sensors, and normally, no such information is provided by the manufacturers. In addition, the thermal parameters for both $\Delta t_P$ and $\Delta t_R$ vary when the cooling capability of

ac motors changes, for instance, with motor surface dust build-up, which further decrease the accuracy of stator temperature estimation when simplified thermal model is used.

### 9.3.3 Practical Considerations for Thermal Overload Relays

Most of the thermal overload relays use the simplified thermal model to estimate the stator temperature, using (9.1). Since the thermal time constant is difficult to estimate, methods have been proposed to roughly estimate these thermal parameters based on the motor's *Service Factor* and *Trip Class* [14]. However, these approaches are highly conservative, and therefore trip the motor long before the thermal limit is reached [48].

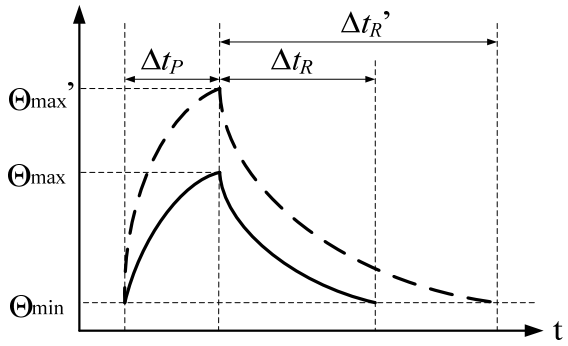


Figure 9.2: Comparison of the estimated and actual stator temperature when operated with duty type S3.

When thermal overload relays are used to protect the ac motors with duty type S3, because of the conservative estimation of both the stator temperature during operation and the thermal time constant during de-energization, a much longer thermal recovery time, $\Delta t_R$, is required. The typical estimated stator temperature (dashed line) and the actual stator temperature (solid line) are shown in Figure 9.2. $\Theta_{min}$ is the predetermined minimum stator temperature rise before each startup; $\Theta_{max}$ is the actual maximum stator temperature rise; while $\Theta_{max}$' is the estimated maximum stator temperature rise; $\Delta t_R$' is

the estimated required thermal recovery time; while $\Delta t_R$ is the actually required thermal recovery time. Because of the conservative estimation of the stator temperature, even though the thermal time constant during de-energization is accurately known, $\Delta t_R$' is still much longer than $\Delta t_R$, which increase the required time of each cycle and reduces the usage of the industrial process.

Therefore, accurate stator temperature estimation during both operation and de-energization is crucial for both thermal protection purposes and improving the overall usage of industrial process.

## 9.4 A Stator Temperature Estimation Technique for De-energized AC Motors

### 9.4.1 DC Injection Method for De-energized AC Motors

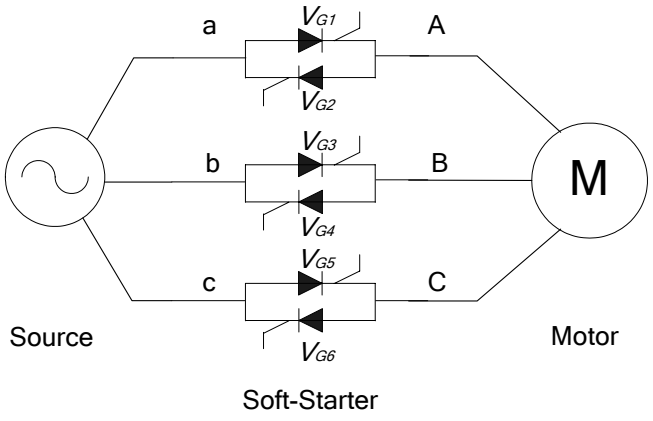


Figure 9.3: Basic structure of soft-starters.

The basic structure of a soft-starter with anti-parallel thyristors is shown in Figure 9.3. In order to inject dc signals without inducing any output torque, one phase of the soft-starter is kept open, e.g., phase ***a***. To inject a dc signal from phase ***b*** to phase ***c***, only two thyristors, one in each of these two phases, e.g. $V_{G3}$, $V_{G6}$, are turned on before the

falling zero-crossing of the line-line power source voltage, $v_{bc}$. This creates a current path for the dc signal injection, without inducing any output torque. The thyristors are turned off automatically when the phase ***b*** current drops to zero. During dc signal injection, all the other four thyristors are kept off. The typical current and voltage waveforms during dc signal injection are shown in Figure 9.4. $V_{bc}$ is the line-line power source voltage between phase ***b*** and phase ***c***; $I_b$ is the phase current of phase ***b***; α is the firing angle before the falling zero-crossing of $V_{bc}$.

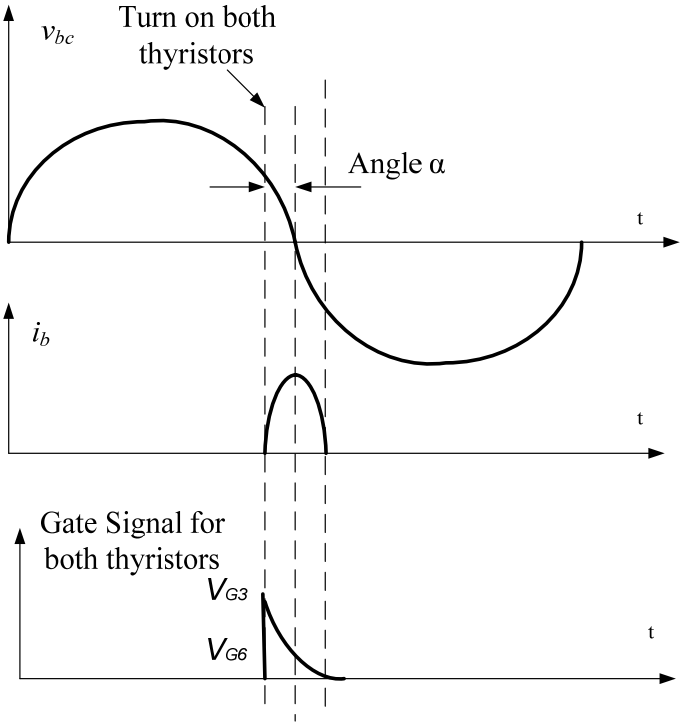


Figure 9.4: Typical waveform of the input voltage, current and the gate drive signal for thyristors during dc signal injection.

To reduce the extra heat dissipation in both soft-starters and ac motors, dc signals can be intermittently injected. After each dc signal injection, all six thyristors are kept open until the next dc signal injection period. The period of dc signal injection is typically around 3-5 minutes, depending on the requirement of practical application.

### 9.4.2 Stator Resistance and Temperature Estimation

Since the dc signals do not "pass through" the air-gap, the dc model of ac motors only consists of the three-phase stator resistances. The dc model of the motor system during dc signal injection is shown in Figure 9.5. Based on the dc signal injection, the stator resistance can be estimated using the dc model of ac motors, as,

$$R_s = \frac{v_{bc}^{dc}}{2 \cdot i_b^{dc}}, \tag{9.4}$$

where $i_b^{dc}$ is the dc component in the phase ***b*** current; $v_{bc}^{dc}$ is the dc component in the line-line voltage between phase ***b*** and phase ***c***, measured from motor terminals. Based on the monitoring of the stator resistance, the average stator winding temperature can be estimated using (2.10). Therefore, the stator winding resistance and temperature can be monitored using only voltage and current measurements, which guarantee the non-intrusive nature of the proposed technique. Based on the monitoring of the stator winding temperature, the required thermal recovery time can be minimized, and the usage of the industrial process can be improved.

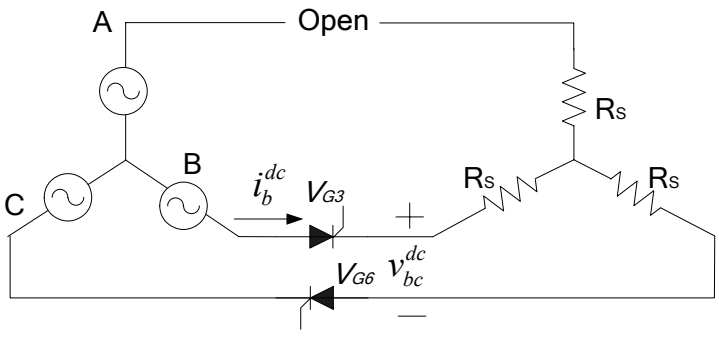


Figure 9.5: DC model of the motor system during dc signal injection.

DC signals can be intermittently injected for a minimal amount of time, which is sufficient for acquiring an accurate estimation of the stator temperature. Typically, a dc signal injection duration of 0.5-1 second is sufficient for accurate estimation of the stator temperature. The required frequency of the stator temperature estimation update depends on the practical applications, given a motor's typical thermal time constant. In this research, dc signals are injected for 1 second every 1 minute for validation purposes.

### 9.4.3 Analysis of the Output Torque during DC Signal Injection

The three phase input currents, $i_a$, $i_b$, $i_c$, can be represented in the stationary d-q reference frame with d-axis aligned with phase a, as,

$$\begin{bmatrix} i_{ds} \\ i_{qs} \end{bmatrix} = \sqrt{\frac{2}{3}} \begin{bmatrix} 1 & -\frac{1}{2} & -\frac{1}{2} \\ 0 & -\frac{\sqrt{3}}{2} & \frac{\sqrt{3}}{2} \end{bmatrix} \begin{bmatrix} i_a \\ i_b \\ i_c \end{bmatrix} = \begin{bmatrix} 0 \\ -\sqrt{2} i_b \end{bmatrix}, \tag{9.5}$$

where $i_{ds}$ and $i_{qs}$ are the stator current in the stationary d-q reference frame; $i_a$=0; $i_c$=-$i_b$, as phase ***a*** is kept open. In the d-axis of the rotor,

$$0 = R_r i_{dr} + \frac{d}{dt}\lambda_{dr} = R_r i_{dr} + \frac{d}{dt}(L_m i_{ds} + L_r i_{dr}), \tag{9.6}$$

where $\lambda_{dr}$ is the d-axis rotor flux; $L_m$ is the mutual inductance; $L_r$ is the rotor inductance; $i_{dr}$ is the d-axis rotor current; $R_r$ is the rotor resistance. From (9.5), $i_{ds}$=0, and therefore, using (9.6), $i_{dr}$=0. The d-axis stator flux, $\lambda_{ds}$, can therefore be represented as,

$$\lambda_{ds} = L_s i_{ds} + L_m i_{dr} = 0. \tag{9.7}$$

The air-gap torque can be represented as,

$$T = \frac{3}{2}\frac{Poles}{2}(\lambda_{ds} i_{qs} - \lambda_{qs} i_{ds}) = \frac{3}{2}\frac{Poles}{2}(0 \bullet i_{qs} - \lambda_{qs} \bullet 0) = 0 \quad (9.8)$$

As a result, no output torque is induced during dc signal injection. Therefore, the motor's condition is not interrupted by the dc signal injection.

### 9.4.4 Analysis of the Input Phase Current

Since no output torque is induced during the dc signal injection, the equivalent circuit of the ac motor is obtained as shown in Figure 9.6.

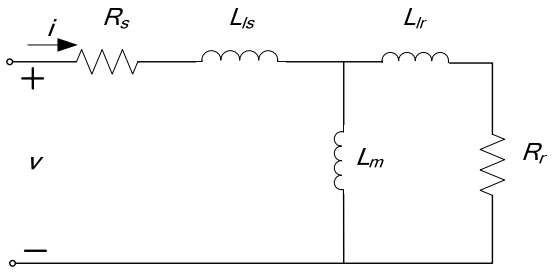


Figure 9.6: Equivalent circuit of ac motors during dc signal injection.

Assuming $L_m >> L_{lr}$ and $L_{ls}$ and neglecting the voltage drop on $R_s$ and $R_r$, during the signal injection, $i_b$ can be approximately calculated as,

$$i_b(t) \approx \begin{cases} \frac{1}{2\omega(L_{ls}+L_{lr})} V_p[\cos(\alpha-\omega t)-\cos\alpha] & (\frac{2n\pi}{\omega} \le t \le \frac{2\alpha+2n\pi}{\omega}) \\ 0 & \text{(else)} \end{cases}, \quad (9.9)$$

where $V_p$ is the peak value of $v_{bc}$.

The magnitude of the dc component can be calculated as,

$$i_b^{dc} = \frac{\omega}{2\pi}\int_{t=0}^{2\alpha/\omega} i_b(t)dt \approx \frac{1}{2\pi\omega(L_{ls}+L_{lr})} V_p[\sin\alpha - \alpha\cos\alpha] \quad (9.10)$$

Therefore, the magnitudes of both the phase current and its dc component are highly dependent on the value of the firing angle α. It is understandable that a better accuracy of the stator temperature estimation can be obtained for a larger injected dc signal; while a larger injected dc current yields higher heat dissipation in both the soft-starter and ac motor. Therefore, the determination of the firing angle α is a tradeoff between heat dissipation in the soft-starter and ac motor, and the accuracy of stator temperature estimation. Typically, a firing angle $\alpha>10°$ is sufficient to acquire an accurate estimation of the stator temperature.

Since only voltage and current measurements are required for the proposed stator temperature estimation technique, and the motor's condition is not interrupted with no output torque produced, the proposed stator temperature estimation technique for de-energized ac motors is considered to be cost-effective and non-intrusive.

## 9.5 Experimental Validation

### 9.5.1 Experimental Setup

To validate the proposed technique, experimental testing has been conducted on a 7.5-hp ODP induction motor. A cutler-hammer S811 soft-starter rated at 10-30 hp and 200-575 volts are used to inject the dc signals. The nameplate information of the induction motor and the soft-starter is listed in Table 9.1. A dSpace DS1104 control system is used to control the switching of the thyristors. An analog circuit is designed as the gate drive of the thyristors, as shown in Figure 9.7. Nine K-type thermal couples are installed in the stator of each induction motor at different locations to measure the average stator temperature for validation purposes. A 10-hp dc generator supplying a resistor bank is used as the dynamometer. The motor's terminal voltage and phase

current are measured using Hall-effect sensors. The data are then acquired and stored using a *NI/LabView* data acquisition system with 16-bit A/D conversion at 50 kHz sampling frequency. The overall experimental setup is the same as shown in Figure 5.10.

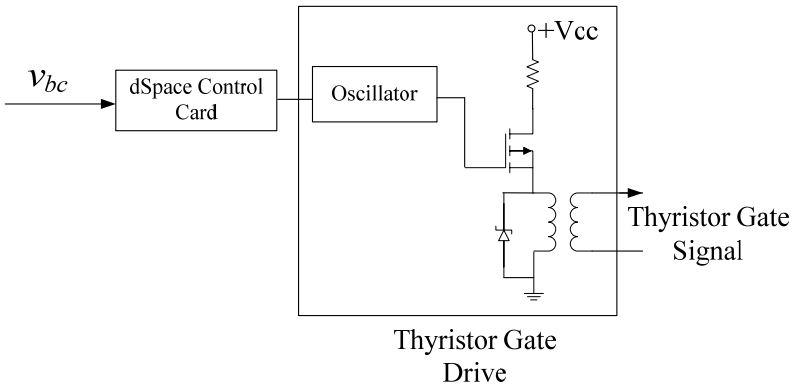


Figure 9.7: Control circuit of thyristors.

Table 9.1: Nameplate Information of Experiment Setup.

| Induction Motor | | | | | | | | |
|---|---|---|---|---|---|---|---|---|
| HP | Brand | CAT. NO. | RPM | Volts | SF | ENCL. | Nom. Eff. | F.L. AMPS |
| 7.5 | Leeson | G140417 | 1760 | 230/460 | 1.15 | ODP | 88.5 | 20/10 |
| Soft-Starter for Experimental Testing | | | | | | | | |
| Brand | | CAT. NO. | Volts | | HP | | Max. AMPS | Working Freq. Hz |
| Cutler-Hammer | | IT.S811N | 200/230/460/ 575 | | 10/10/25/30 | | 37 | 47-63 |

### 9.5.2 Stator Current and Voltage during DC Signal Injection

The typical waveforms of a motor's terminal voltage and current during dc signal injection are shown in Figure 9.8. The firing angle is about 20°. The determination of the firing angle, α, is a tradeoff between heat dissipation in the soft-starter and ac motor, and the accuracy of stator temperature estimation. It can be observed from Figure 9.8

that a dc signal is successfully injected into the motor for stator winding temperature and resistance estimation.

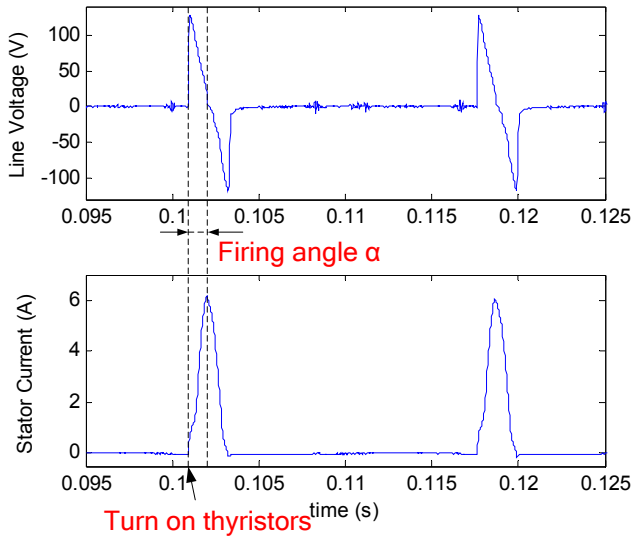


Figure 9.8: Motor terminal current and voltage during dc signal injection.

### 9.5.3 Stator Winding Temperature Estimation

With the periodic injection of dc signals, the stator winding resistance and average temperature can be estimated. To test the accuracy of the stator winding temperature estimation using proposed dc signal injection approach, the induction motor is first operated under full load condition to heat the motor. The motor is then de-energized, and dc signals are injected for 1 second every 1 minute to estimate the average stator winding temperature. The estimated stator winding temperature using the proposed dc signal injection technique and the measured average stator winding temperature from the embedded thermocouples are shown in Figure 9.9. The stator winding temperature estimation error is within 5°C, which is mainly caused by the limited resolution of the data acquisition system [12]. However, since it is known that the variation of stator

winding temperature when the motor is de-energized follows an exponential pattern, as shown in (9.1), least-square curve fitting is applied to further reduce the error in the stator winding temperature estimation using (9.1). It can be shown from Figure 9.9 that the estimated stator temperature after curve fitting is accurate compared to the measured average stator temperature, with an estimation error within 2°C. Therefore, based on the stator temperature estimation for de-energized ac motors, the thermal recovery time can be minimized to improve the overall usage of motors operated with intermittent duty type.

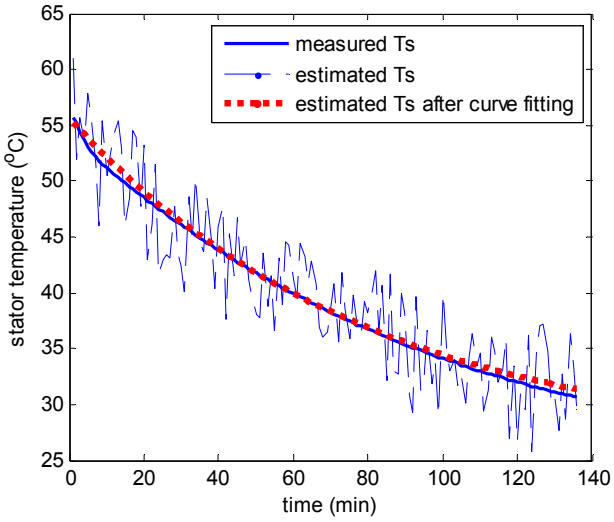


Figure 9.9: Comparison of measured and estimated stator temperature.

### 9.5.4 Reducing Thermal Recovery Time for AC Motors operated with S3 Duty Type

Since first-order thermal model-based stator winding temperature estimation is the most widely used technique in thermal relays, to evaluate the effectiveness of the proposed technique on reducing thermal recovery time and improve the overall usage of ac motors operated with intermittent operation duty type, the induction motor is operated

with S3 duty type, with stator temperature estimated using the proposed dc signal injection technique and the first-order thermal model-based techniques, respectively. It is assumed that the motor is operated for 16 minutes every cycle, with the estimated motor temperature below 35°C before each startup.

The motor is first operated under the aforementioned intermittent operating conditions with the motor's temperature estimated using first-order thermal model, with the thermal parameters calculated from the Service Factor and Trip Class [8], as commonly used in thermal relays. The cooling time constant is set to be 96 minutes, which is calculated using the measured average stator temperature from the testing, assuming that the accurate cooling time constant is provided by the manufacturer. As shown in Figure 9.10, the first-order thermal model-based approach largely overestimates the stator winding temperature during operation, with a stator temperature estimation error as large as 40°C. This is due to the conservative nature when thermal parameters are calculated from Service Factor and Trip Class. The thermal recovery time, $\Delta t_R$', is 170 minutes based on the estimated stator temperature using first-order thermal model. It should be noted that if the cooling time constant is not accurately known, a longer thermal recovery time may be required. It can be observed from Figure 9.10 that even with the accurate cooling time constant provided, the first-order thermal model-based approach still overestimate the stator temperature when the motor is de-energized. The motor's actual temperature is much lower than the required 35°C before each startup.

For comparison, the same motor operation is repeated with the motor's stator temperature estimated using the proposed dc signal injection-based technique, as shown in Figure 9.11. Least-square curve fitting is again applied to reduce the stator

temperature estimation error. Once the motor is de-energized in each operating cycle, the stator temperature is estimated using the proposed dc signal injection technique. Each time the estimated stator temperature reaches 35°C, the motor is re-started. The thermal recovery time with the stator temperature estimated using dc signal injection is 93 minutes, which is much shorter than the required thermal recovery time with stator temperature estimated using first-order thermal model.

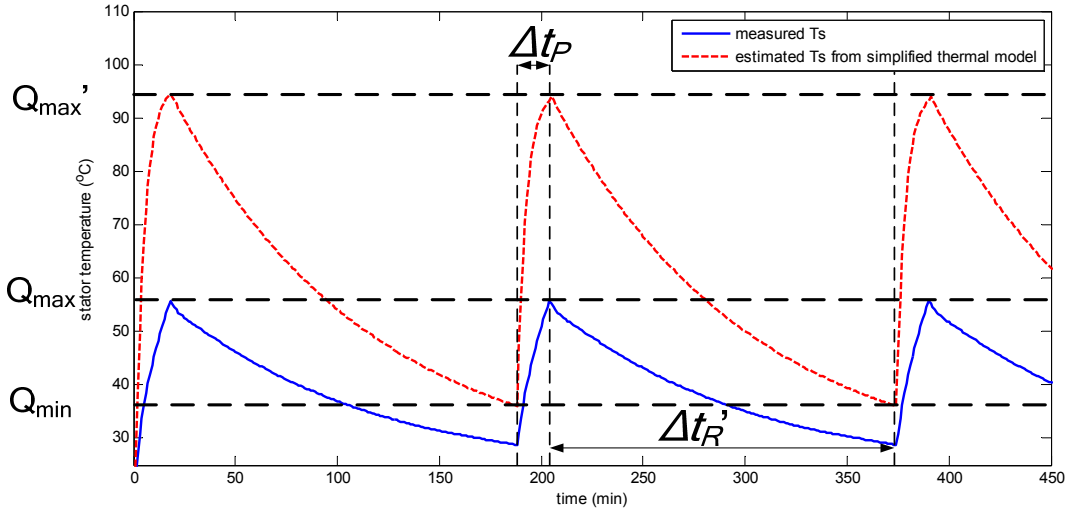


Figure 9.10: Intermittent operation with stator temperature estimated using first-order thermal model.

From the comparison between Figure 9.10 and Figure 9.11, it can be observed that with the stator temperature estimated using the proposed dc signal injection technique, the thermal recovery time can largely reduced, and therefore the overall usage of the industrial process can be improved. Under the testing conditions, the thermal recovery time can be reduced by 45%, and the overall usage of the intermittently operated motor system can be improved by 70%. Since the accurate cooling time constant is normally

not available from the manufacturers, in practical applications, the overall usage of the motor system may be even further improved.

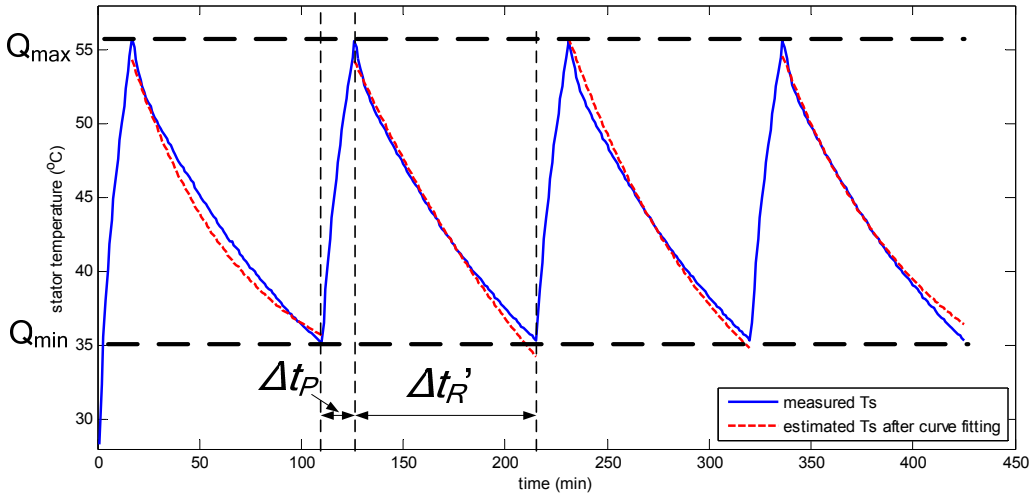


Figure 9.11: Intermittent operation with stator temperature estimated using dc signal injection.

## 9.6 Chapter Summary

The thermal characteristics of de-energized ac motors are largely different from the ones of operating motors. For ac motors operated with intermittent periodic duty type, conventional thermal protection techniques are not capable of providing accurate estimation of the stator temperature. The thermal recovery time, which allows the motor to cool down before the each startup, is normally conservatively estimated, which greatly decrease the usage of industrial processes.

This chapter has proposed a stator winding temperature estimation technique for de-energized ac motors connected with soft-starters. By modifying the operation of the

thyristors in soft-starters, dc signals can be intermittently injected into the motors, without inducing any output torque. Based on the dc model of ac motors, the stator winding resistance and temperature can be monitored using only voltage and current measurements. Via the monitoring of the stator temperature, the required thermal recovery time can be greatly reduced to improve the usage of the industrial process.

Experimental study on a 7.5-hp induction motor has been conducted for the validation of the proposed technique. The error in the stator winding temperautre estimation is within 5°C while the motor is de-energized. Using the proposed dc signal injection-based stator temperature estimation technique, the thermal recovery time can be reduced by 45%, with the overall usage of the motor system increased by 70%.

# CHAPTER 10 A Non-intrusive Motor Heating Technique of Preventing Moisture Condensation

## 10.1 Overview

Aside from thermal degradation during a motor's normal operation, the degradation of a motor's key components may also happen when a motor is at standstill. Moisture condensation is one of the major causes to the degradation of key motor components when a motor is de-energized. To prevent moisture condensation, a motor's temperature must be maintained above the ambient temperature when de-energized. This chapter proposes a non-intrusive motor heating technique using soft-starters. By controlling the operation of the solid-state switches in soft-starters, an adjustable ac current can be injected into the three phases of the stator windings without inducing any output torque. The motor temperature can therefore be maintained at a desired temperature based on the heat dissipation caused by current injection.

## 10.2 Introduction

When de-energized, severe degradation of motor components can be caused by moisture condensation [49]. Moisture condensation is very common for motors operating in high moisture environment, such as in petroleum and chemical processing, water and waste water treatment , on off-shore transportation, and offshore wind farms, etc [50-52]. To prevent moisture condensation, it is suggested to maintain a motor stator temperature at least 5° C above the ambient temperature [50-52].

Currently, the most commonly used techniques to heat de-energized motor are to implement additional heating windings in ac motors, , or to use additional low-voltage power supply to heat the stator winding [51-53] as soon as a motor is de-energized.

However, such motor heating techniques are intrusive and costly, since additional hardware is required to heat motor windings.

In this chapter, a non-intrusive winding heating method is proposed for de-energized induction motors using soft-starters to prevent moisture condensation. By controlling the operation of solid-state switches in soft-starters, each two of the three phases of ac motor's stator windings are alternately and periodically connected to the main power supply so that a current can be injected to *evenly* heat the motor windings. During the entire operation, no rotating torque is induced, so that the motor's operating condition is not interrupted. The approaches to control the motor temperature so that the energy consumption is minimized while heating the motor are also discussed. Experimental results are shown to validate the proposed technique.

## 10.3 A Non-intrusive Motor Heating Technique

A dc signal injection technique is proposed in CHAPTER 9. Since the injected dc signal can be controlled by adjusting the firing angle, as shown in Section 9.4.1, a motor can be heated by injecting sufficient magnitude of current into the stator windings using the same technique, given that a sufficiently large firing angle can result in the injection of a sufficient heating current. By applying such techniques, a motor can be heated without the needs of either additional heating winding or additional power supply. In addition, since no output torque is induced during the current injection, a motor's operating conditions are not interrupted by the current injection.

In order to evenly heat all three phases of the stator windings, such current injection can be alternately and periodically applied to each two of the three phases. The typical waveforms of the input voltages, current, and the gate drive signals for the six thyristors

in each cycle are shown in Figure 10.1. The six thyristors in the soft-starter are numbered as depicted in Figure 9.3. $v_{ab}$, $v_{bc}$, $v_{ca}$ are the line-line voltages of the main power supply; $v_{AB}$, $v_{BC}$, $v_{CA}$ are the line-line voltages at the motor terminals; $i_a$ is the phase current of phase ***a***. Similar to the dc signal injection approach in Section 9.4.1, before the zero-crossing of each line-line voltage, two thyristors are fired to allow current flow. By alternately injecting current into each two of the three phases, as shown in Figure 10.1, three phase ac currents can be evenly injected to the three phases of the stator windings so that the stator can be evenly heated. In addition, the magnitude of the injected current and the resulting heat dissipation can be controlled by adjusting the firing angle ***α***. However, it important to limit the firing angle ***α*** less than 60° so that the three phases of the stator windings are *never* simultaneously connected to the line voltage, which ensures that no output torque is induced to start the motor.

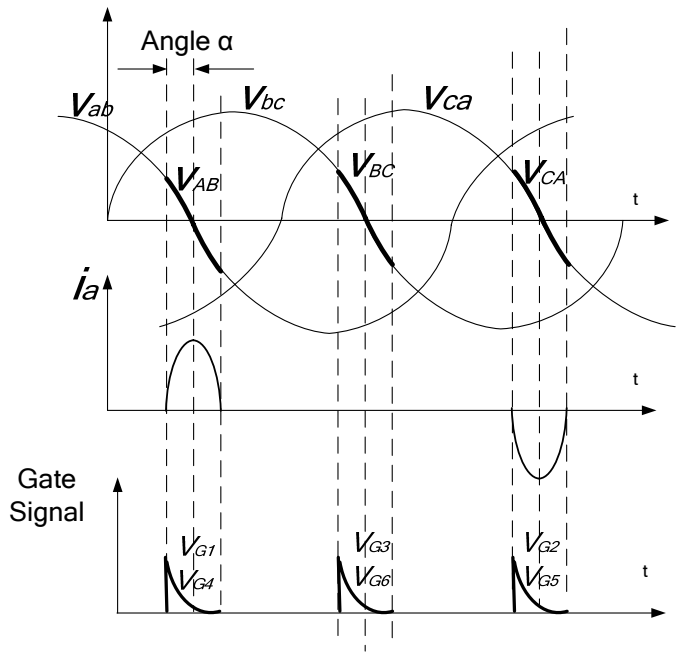


Figure 10.1: Typical waveform of the input voltage, current and the gate drive signal for thyristors during current injection.

It has been proven in Section 9.4.3 that no output torque is induced during the signal injection.

With reference to (9.9), neglecting the losses, the peak of the injected signal can be calculated as,

$$I_b = \frac{1}{2\omega(L_{ls} + L_{lr})} V_p[1 - \cos\alpha]. \tag{10.1}$$

Therefore, the magnitudes of the phase current are highly dependent on the value of the firing angle $\boldsymbol{\alpha}$. A larger phase current yields a higher motor temperature, which influences the effectiveness of moisture condensation prevention; meanwhile, the higher losses in the motor also require more energy consumption. Therefore, the determination of the firing angle α and the magnitude of the injected current signal is a tradeoff between the effectiveness of preventing moisture condensation and energy consumption. Typically, a stator temperature rise of 5° C above the ambient temperature is sufficient to prevent moisture condensation [49]. The proposed non-intrusive motor heating technique is totally based on the existing hardware of soft-starters, which guarantees its cost-efficient nature.

## 10.4 Control of Heat Dissipation and Motor Temperature

### 10.4.1 Heat Dissipation in AC Motors

However, it should be noted that equation (10.1) is derived without considering the losses during signal injection. Therefore, it is inaccurate to control the motor current or losses based on such equations. In addition, for different types of ac motors with different sizes, the actual losses may vary largely, depending on their different resistance values, different magnetic characteristics, etc., which makes it difficult to calculate the

losses during current injection. However, it is still understandable that by adjusting the firing angle, the magnitude of the injected current can be controlled, and thus the total heat dissipation in a motor.

The heat dissipation during current injection is caused by many different losses: stator copper losses due to the current flow; stator and rotor core losses due to the stator current and flux vibration. Since no output torque is induced, the total losses in the motor can be calculated using the measured motor terminal voltage and phase current, as,

$$P_{loss} = \frac{3}{2T}\int_{t=0}^{T} v_{ab}(t) \bullet i_a(t)\,. \tag{10.2}$$

Since the motor is always at standstill during the current injection, the motor's thermal characteristics remain unchanged. Therefore, the motor temperature and the heat dissipation can be controlled simply via adjusting the firing angle $\boldsymbol{\alpha}$.

### 10.4.2 Motor Temperature Control using a Simplified Thermal Model

When the motor is at standstill, the motor can be considered as a single object in the thermal model. Therefore, the first-order thermal model can be used to estimate the motor's temperature, as shown in Figure 2.3. Based on the simplified thermal model, the motor temperature can be represented as,

$$T(t) = P_{loss} \cdot R_{th}(1 - e^{-\frac{t}{\tau}}) + T_0 e^{-\frac{t}{\tau}} + T_A\,, \tag{10.3}$$

where $T_0$ is the initial motor temperature; $\tau$ is the thermal time constant ($R_{th}$ $C_{th}$). Considering that the motor heater needs to continuously work when the motor is de-energized, neglecting the time variation, the required heat dissipation can be estimated as,

$$P_{loss} = T_{rise} / R_{th}\,, \tag{10.4}$$

where $T_{rise}$ is the pre-defined motor temperature rise for preventing moisture condensation.

Therefore, based on this simplified thermal model, the motor temperature can be maintained at the desired value by controlling the total heat dissipation of the motor using (10.4). In many cases, the thermal parameters representing the motor's thermal characteristics at standstill are provided by the motor manufacturers. However, when the parameters are not provided, such thermal parameters are difficult to obtain without embedded thermal sensors, given the fact that the motor's thermal behavior at standstill is very different from that during normal operation. Therefore, an alternative technique to control the motor's temperature for the motor heater is highly desired.

### 10.4.3 Online Closed-loop Control of the Motor Temperature

A motor's average stator winding temperature can be non-intrusively estimated by dc signal injection when a motor is de-energized, as proposed in Chapter 9. Since the dc signal injection is only operated for 0.5 second every 3-5 minutes, such technique can be combined with the proposed motor heating approach to achieve the closed-loop control of the motor's temperature. The soft-starter can periodically work in the temperature estimation mode and motor heating mode when motor is de-energized, as shown in Figure 10.2. After each temperature estimation period, the total heat dissipation in a motor can be adjusted by tuning the firing angle, so that the desired motor temperature can be achieved. It should be noted that this closed-loop operation is still considered non-intrusive, since only voltage and current measurements are required; no output torque is induced either in the temperature estimation mode or motor heating mode, which ensures that the motor's operating condition is not interrupted.

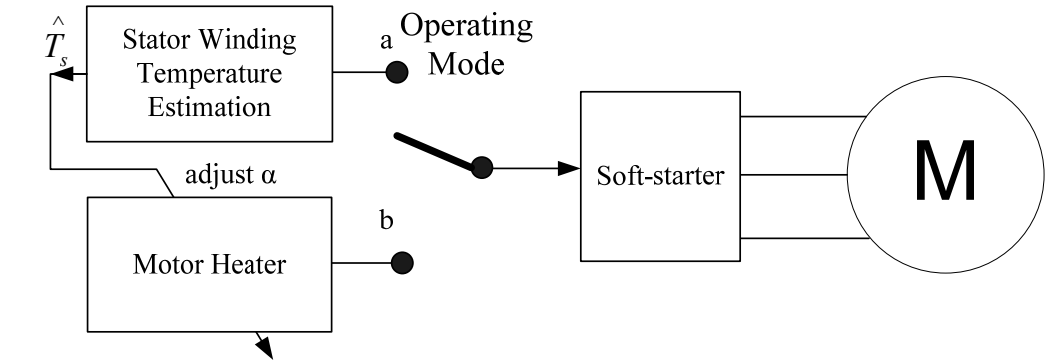


(a)

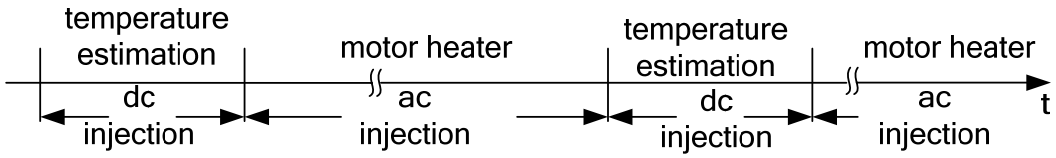


(b)

Figure 10.2: Close-loop temperature control for de-energized motor

## 10.5 Experimental Validation

### 10.5.1 Experimental Setup

To validate the proposed technique, experimental testing has been conducted on a 7.5-hp ODP induction motor. A cutler-hammer S811soft-starter rated at 10-30 hp and 200-575 volts are used to inject the dc signal as proposed in the previous Sections. The nameplate information of the induction motor and the soft-starter is listed in Table 9.1. A dSpace DS1104 control system is used to control the switching of the thyristors. An analog circuit is designed as the gate drive of the thyristors, as shown in Figure 9.7. 9 K-type thermal couples are installed in the stator of each induction motor at different locations to measure the stator temperature rise for validation purposes. The motor's terminal voltage and phase current are measured using Hall-effect sensors. The data are

then acquired and stored using a *NI/LabView* data acquisition system with 16-bit A/D conversion at 50 kHz sampling frequency. The overall experimental setup is shown in Figure 10.3.

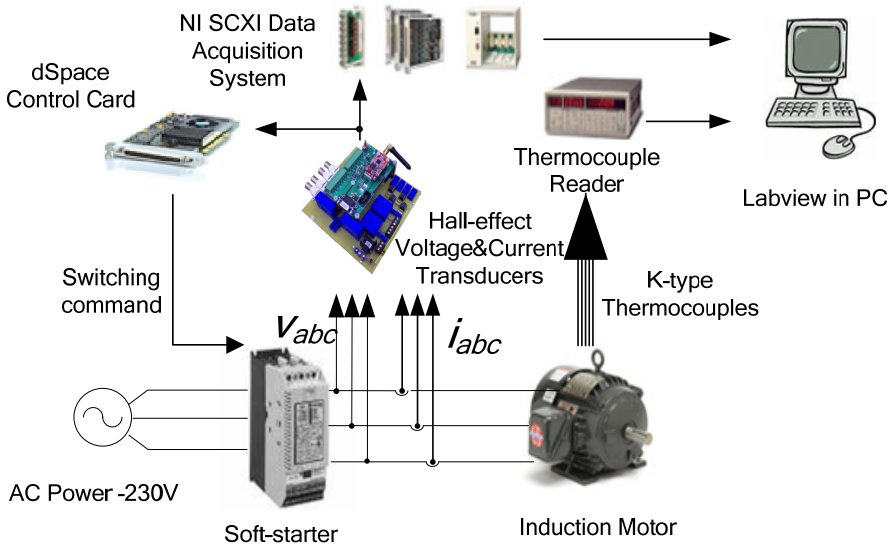


Figure 10.3: Overall Experimental Setup.

### 10.5.2 Motor Current, Voltage and Temperature during Current Injection

To test the effectiveness of the proposed motor heating technique, experiments are conducted by injecting a small ac current in a 7.5-hp induction motor with a firing angle of 27° . The motor line-line voltage $v_{ab}$ and phase current $i_a$ during the current injection are shown in Figure 10.4. It can be observed that currents are successfully injected. To show the effectiveness of the proposed motor heating technique, the stator winding temperature rise measured from the 9 thermocouples are shown in Figure 10.5. It can be observed that the stator winding temperature rise reaches 8° C -10° C above the ambient temperature, with a current peak value of 8 amps. The total heat dissipation in

the motor is measured to be 33.5 Watt. Because of the even injection of current, the temperatures of all three phases of the stator windings are balanced.

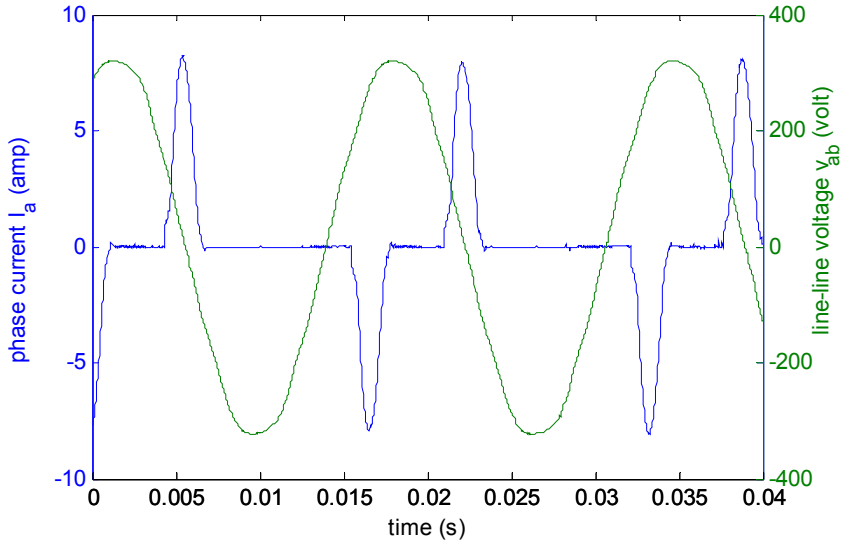


Figure 10.4: Motor line-line voltage and phase current during current injection.

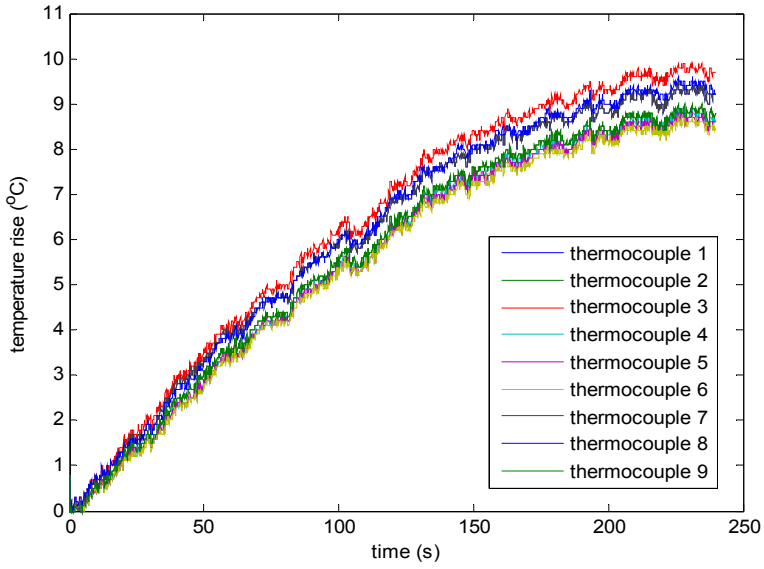


Figure 10.5: Stator winding temperature measurements from thermocouples during current injection.

Again, it is important to limit the firing angle $\alpha$ within 60°, so that the three phases of the stator windings are never connected to the power source simultaneously. Otherwise, output torque can be induced, which may lead to a motor startup.

### 10.5.3 Heat Dissipation and Motor Temperature with Different Firing Angles

To test the effectiveness of the motor heating technique with different firing angle $\alpha$, similar experimental tests with different firing angle values are conducted. The heat dissipation, the peak current and the average stator temperature rise with different firing angle values are compared in Table 10.1. The results clearly show that the motor temperature rise can be controlled via adjusting the firing angle $\alpha$, which accordingly adjusts the magnitudes of the currents injected.

Table 10.1: Heat Dissipation, Peak Current and Average Stator Temperature Rise with Different Firing Angles.

| Firing Angle $\alpha$ (°) | Heat Dissipation (W) | Peak Current (Amp) | Average Stator Temperature Rise (° C) |
|---|---|---|---|
| 18 | 12.9 | 1.6 | 3.5 |
| 20 | 14.8 | 2.6 | 4.0 |
| 22 | 17.5 | 3.7 | 4.7 |
| 24 | 22.5 | 5.2 | 6.1 |
| 26 | 30.9 | 7.0 | 8.3 |
| 28 | 40.8 | 8.5 | 10.9 |

## 10.6 Chapter Summary

Moisture condensation may cause degradation of a motor's key components while the motor is de-energized. This chapter has proposed a non-intrusive motor heating technique using soft-starters to prevent moisture condensation for motors at standstill.

The solid-state power switches in soft-starters are controlled so that currents are periodically injected into the three phases of the stator windings without inducing any output torque, which results in the evenly heating of the stator windings.

The proposed technique has been experimentally validated on a 7.5-hp ODP induction motor. It is shown that the average stator temperature can reach 9° C above the ambient temperature with acceptable magnitudes of the injected current. In addition, the motor temperature can be controlled by adjusting the firing angle in the proposed current injection technique. The proposed motor heating technique does not require any additional hardware, which makes it easy to implement for practical applications.

# CHAPTER 11 Conclusions, Contributions and Recommendations for Future Works

## 11.1 Summary

This dissertation has proposed non-intrusive, sensorless thermal protection techniques for the induction motors fed by motor control devices under both operating and de-energized conditions, using only motor terminal quantities.

Chapter 1 has introduced the background information related to the thermal protection of induction motors and states the objective of this research.

Chapter 2 has presented a comprehensive survey of the previous work on stator winding temperature estimation for in-service induction motors. Recent progresses in two categories of stator winding temperature estimation methods, namely, thermal model-based and resistance-based methods, have been discussed. It has been concluded that dc signal injection-based stator winding resistance and temperature estimation methods are the ideal candidate for the thermal protection of in-service induction motors.

Chapter 3 summarizes the previous work on monitoring the cooling capabilities of induction motors. It is clearly shown that an accurate and reliable abnormal cooling detection scheme is highly desirable for the thermal protection of in-service induction motors.

In Chapter 4, a model reduction study for thermal model-based stator winding temperature estimation techniques has been presented. An accurate yet simple to implement thermal model for mains-fed induction motors has been proposed. Experimental validation shows that the proposed thermal model can achieve stator temperature estimates with rms error within 3° C. Regardless of its high accuracy and

simplicity, these thermal model-based techniques are naturally sensitive to the change of a motor's cooling capability, which makes it unreliable for thermal protection of in-service induction motors. In addition, the requirement of thermal parameter identification largely limits their practical applications.

Chapter 5 has proposed an active stator winding temperature estimation technique for soft-starter-connected in-service induction motors. DC signals can be injected into an operating induction motor by altering the operation of power switches in a soft-starter. The stator winding resistance and thus stator winding temperature can therefore be estimated based on a motor's dc model. As a result, the stator winding temperature can be continuously monitored using only voltage and current measurements. In addition, an adaptive Kalman filter-based technique has been proposed for improving the stator winding temperature estimation accuracy. The practical considerations, including cable resistances, data acquisition systems, etc. have been discussed for evaluating and improving the accuracy of the proposed technique in practical application environment. Experimental validation has been shown for the validation of the proposed approaches. It's been shown that the proposed active stator winding temperature estimation approach can achieve accurate estimates with an rms error within 2.5° C using only voltage and current measurements.

In Chapter 6, an active thermal stator winding temperature estimation technique for inverter-fed in-service induction motors has been presented. A novel space vector PWM approach has been proposed to inject dc signals into an inverter-fed induction motor. The stator winding temperature can be estimated using only current measurements. It should be noted that this proposed active thermal stator winding temperature estimation

technique can be applied to both open-loop and closed-loop motor drives. The compensation techniques for internal resistance of a motor drive and the cable resistance have been discussed. Experimental validation has been shown for validation of the proposed approaches. It's been shown that the proposed active stator winding temperature estimation approach can achieve accurate estimates with a maximum error within 8° C using only current measurements.

Chapter 7 has shown a study on the magnetic effects of dc signal injection on in-service induction motors. The effects of the magnetic saturation on the motor currents, the motor's thermal behavior and the estimation of stator resistance and temperature have been analyzed. Finite-element simulation results and experimental results have been presented to illustrate the analysis. It has been shown that although the magnetic saturation affects the waveforms of the stator currents, it does not have any impact on their dc components. Therefore, the accuracy of the stator resistance and temperature estimation can be guaranteed even in the presence of magnetic saturation under different conditions.

Chapter 8 has proposed a cooling capability monitoring scheme for in-service induction motors based on the stator temperature estimation techniques proposed in Chapter 5 and 6. Via continuously monitoring of the values of $R_s$, the stator winding temperature, $T_s$, can be estimated, as proposed in Chapter 5 and Chapter 6. The cooling capability of the motor can be monitored based on the estimated $T_s$. An extended Kalman filtering approach has been proposed to identify the thermal parameters of a simplified thermal model for induction motors, which are used as indicators of motor cooling capability. The feasibility of the proposed cooling capability monitoring system has been

validated from experimental results under variable load conditions and different cooling capabilities. From the comparison of experimental results between normal cooling capability and the impaired cooling capabilities, it has been validated that the proposed cooling capability monitoring scheme is capable of providing accurate indication of the motor cooling capability.

With both the stator winding temperature and the motor cooling capability monitored, the overall thermal protection scheme for induction motors fed by motor control devices can trip the motor in the case of stator winding overheat, and warn the user for proactive inspections or maintenance in the case of cooling capability deterioration. Therefore, the proposed overall thermal protection scheme can provide complete, reliable thermal protection for in-service induction motors.

Chapter 9 has proposed a stator winding temperature estimation technique for de-energized ac motors connected with soft-starters. By modifying the operation of the thyristors in soft-starters, dc signals can be intermittently injected into the motors, without inducing any output torque. Based on the dc model of ac motors, the stator winding resistance and temperature can be monitored using only voltage and current measurements. Via the monitoring of the stator temperature, the required thermal recovery time can be greatly reduced for intermittently operated induction motors to improve the usage of the industrial process. Experimental study on a 7.5-hp induction motor has been conducted for the validation of the proposed technique. The error in the stator winding temperautre estimation is within 5°C while the motor is de-energized. Using the proposed dc signal injection-based stator temperature estimation technique, the

thermal recovery time can be reduced by 45%, with the overall usage of the motor system increased by 70%.

In Chapter 10, a non-intrusive motor heating technique using soft-starters to prevent moisture condensation for motors at standstill has been proposed. The solid-state power switches in soft-starters are controlled so that currents are periodically injected into the three phases of the stator windings without inducing any output torque, which results in the evenly heating of the stator windings. The proposed technique has been experimentally validated on a 7.5-hp ODP induction motor. It is shown that the average stator temperature can reach 9° C above the ambient temperature with acceptable current magnitudes. In addition, the motor temperature can be controlled by adjusting the firing angle in the proposed current injection technique. The proposed motor heating technique can non-intrusively protect induction motors from possible damage due to moisture condensation, and a motor's lifetime can be prolonged.

The importance of the proposed techniques lies in their non-intrusiveness: the motor protection methods only use the existing hardware in soft-starters or motor drive; the motor's operating condition is not interrupted.

## 11.2 Contributions

The research work presented in this dissertation has resulted in three patent applications:

"System and Method for Determining Stator Winding Resistance in an AC Motor," U.S. patent pending.

"System And Method For Monitoring And Controlling Stator Winding Temperature in a De-Energized AC Motor," U.S. patent pending.

"System and Method for Determining Stator Winding Resistance in an AC Motor using Motor Drives," U.S. patent pending.

In addition, the literature review and research work presented in this dissertation has resulted in several publications in both international conferences and journals.

Journal papers:

**P. Zhang**, B. Lu, and T. G. Habetler, "A Remote and Sensorless Stator Winding Resistance Estimation Method for Thermal Protection of Soft-Starter-connected Induction Machines," *IEEE Trans. on Industrial Electronics*, Vol. 55, no.10, pp.3611 – 3618, Oct. 2008.

**P. Zhang**, Y. Du, B. Lu, and T. G. Habetler, "A DC Signal Injection based Thermal Protection Scheme for Soft-starter connected Induction Motors," *IEEE Trans. on Industrial Applications*, vol. 45, pp. 1351-1358, 2009.

**P. Zhang**, Y. Du, J. Dai, T. G. Habetler, and B. Lu, "Impaired Cooling Condition Detection Using Dc Signal Injection For Soft-Starter-Connected Induction Motors," *IEEE Trans. on Industrial Electronics*, vol.56, no.11, pp.4642-4650, Nov. 2009.

**P. Zhang**, B. Lu, and T. G. Habetler, "An active stator temperature estimation technique for thermal protection of inverter-fed induction motors with considerations of impaired cooling detection," *IEEE Trans. on Industrial Applications*, Accepted for publication, Dec. 2009.

**P. Zhang**, Y. Du, and T. G. Habetler, "A transfer function-based thermal model reduction study for induction machine thermal overload protective relays," *IEEE Trans. on Industrial Applications*, Accepted for publication, Jan. 2009.

**P. Zhang**, Y. Du, T. G. Habetler, and B. Lu, "Improving thermal recovery time for soft-starter-connected AC motors with intermittent periodic duty cycles," *IEEE Trans. on Industrial Applications*, Accepted for publication, Jan. 2009.

**P. Zhang**, Y. Du, T. G. Habetler, and B. Lu, "A survey of condition monitoring and protection methods for medium voltage induction motors," *IEEE Trans. on Industrial Applications*, Accepted for publication, Mar. 2009.

Conference Papers

**P. Zhang**, Y. Du, T. G. Habetler, and B. Lu, "A survey of condition monitoring and protection methods for medium voltage induction motors," in *Energy Conversion Congress and Exposition, 2009. ECCE 2009. IEEE*, 2009, pp. 3165-3174.

**P. Zhang**, Y. Du, and T. G. Habetler, "A transfer function-based thermal model reduction study for induction machine thermal overload protective relays," in *Energy Conversion Congress and Exposition, 2009. ECCE 2009. IEEE*, 2009, pp. 2313-2320.

**P. Zhang**, Y. Duan, T. G. Habetler, and B. Lu, "An analysis of magnetic saturation in induction motors during dc signal injection," in *Diagnostics for Electric Machines, Power Electronics and Drives, 2009. SDEMPED 2009. IEEE International Symposium on*, 2009, pp. 1-8.

**P. Zhang**, Y. Du, T. G. Habetler, and B. Lu, "Improving thermal recovery time for soft-starter-connected AC motors with intermittent periodic duty cycles," in *Diagnostics*

*for Electric Machines, Power Electronics and Drives, 2009. SDEMPED 2009. IEEE International Symposium on*, 2009, pp. 1-9.

**P. Zhang**, B. Lu, and T. G. Habetler, "An active stator temperature estimation technique for thermal protection of inverter-fed induction motors with considerations of impaired cooling detection," in *Electric Machines and Drives Conference, 2009. IEMDC '09. IEEE International*, 2009, pp. 1326-1332.

**P. Zhang**, B. Lu, and T. G. Habetler, "Active stator winding thermal protection for AC motors," in *Pulp and Paper Industry Technical Conference, 2009. PPIC '09. Conference Record of 2009 Annual*, 2009, pp. 11-19.

**P. Zhang**, B. Lu, and T. G. Habetler, "Compensation for supply and motor unbalances and line resistance for a DC signal injection-based thermal protection method," in *Power Electronics and Motion Control Conference, 2009. IPEMC '09. IEEE 6th International*, 2009, pp. 855-859.

**P. Zhang**, Y. Du, B. Lu, and T. G. Habetler, "A Remote and Sensorless Thermal Protection Scheme for Soft-Starter-Connected Induction Motors," in *Industry Applications Society Annual Meeting, 2008. IAS '08. IEEE*, 2008, pp. 1-7.

**P. Zhang**, B. Lu, and T. G. Habetler, "Practical implementation of a remote and sensorless stator resistance-based thermal protection method," in *Proc. the International Conference on Condition Monitoring and Diagnosis (CMD'08)*, Apr. 2008, pp.159 – 162.

**P. Zhang**, B. Lu, and T. G. Habetler, "A Nonintrusive Induction Motor Stator Resistance Estimation Method using a Soft-Starter," *Proc. the 6th IEEE International Symposium on Diagnostics for Electric Machines, Power Electronics and Drives, (SDEMPED'07)*, Sep. 2007, pp. 197-202.

The main contributions of this research are summarized as following:

1. A comprehensive survey of the state of the art thermal protection techniques is presented. The thermal model-based and parameter-based stator temperature estimation approaches and cooling capability monitoring techniques for in-service motors are reviewed and compared in terms of accuracy, implementation complexity and practical feasibility.
2. A novel simplified thermal model for mains-fed induction motors is proposed. The proposed thermal model is simple to implement, has low requirement on computational effort, and has high accuracy in stator temperature estimation.
3. Non-intrusive, sensorless and online stator temperature estimation techniques are proposed via dc signal injection for induction motors fed by motor control devices. The stator temperature can be continuously monitored based on stator resistance estimation using motor's dc model. The proposed techniques are validated from experimental results. The non-intrusive nature of these techniques guarantees their feasibility for practical implementation. Using the proposed stator temperature monitoring techniques, the reliability of thermal protection for induction motors can be largely improved.
4. A study on the magnetic effects of dc signal injection is conducted. The impact of dc signal injection on induction motors' performances is discussed in detail. Simulation and experimental studies are conducted to validate such analysis.
5. A non-intrusive cooling capability monitoring scheme is proposed for detecting impaired cooling capability based on the stator temperature estimation. The proposed thermal protection scheme, including the stator temperature estimation

techniques and the cooling capability monitoring technique, can provide *complete* thermal protection for in-service induction motors fed by motor control devices. This thermal protection scheme allows the user to turn off the motor before stator winding overheating, and also to inspect and repair the motor in the case of cooling capability deterioration when necessary.

6. A non-intrusive stator winding temperature estimation technique is proposed for de-energized induction motors. For intermittently operated induction motors, the stator winding temperature estimation approach can minimize the thermal recovery time and optimize the usage of the motor system.
7. A non-intrusive motor heating technique is proposed for de-energized induction motors for preventing moisture condensation using soft-starters. Based on this proposed motor heating technique, a motor's temperature can be controlled and kept above the ambient temperature to prevent moisture condensation and its resultant damage to a motor's components.

## 11.3 Recommendations for Future Work

Although this work has presented contributions to various areas of thermal protection of induction motors, there are several directions in which further research could build on the results presented in this work.

The primary target of this research is to develop thermal protection schemes for induction motors fed by motor control devices. However, the thermal protection of mains-fed induction motors is still essential. Similar studies to the work presented in Chapter 4 need to be continued for the thermal protection of mains-fed induction motors when dc signal injection can not be achieved.

The active thermal protection scheme proposed in this work is primarily targeting small- to medium- size induction motors. This is due to the fact that embedded thermal sensors are commonly used on larger induction motors for thermal protection, since they are considered cost-efficient compared to the cost of the motor itself. Another reason is that since dc signal injection is applied for stator temperature estimation, oscillating output torque is induced during the signal injection. For larger induction motors, the mechanical strength of the rotor shaft is relatively weaker than that of a small motor. Therefore, the induced torque pulsation may cause damage to a large induction motor in some applications. In addition, for some applications of small- to medium- size induction motors, output torque oscillation may not be acceptable to a specific practical application. Therefore, alternative techniques for the online thermal protection of induction motors when dc signal injection is impractical are highly desirable.

In addition, the thermal behaviors of medium-voltage induction motors are largely different from those of small induction motors. The medium-voltage induction motors are commonly essential components in industrial processes. Embedded thermal sensors are commonly implemented in the stator of such motors for thermal protection. However, for induction motors, the thermal protection of not only the stator but also the rotor is important.

As a result of the aforementioned discussion, future research based on this work can generally develop in three directions: stator temperature estimation for mains-fed induction motors; thermal model studies for inverter-fed induction motors; thermal protection of medium-voltage motors.

### 11.3.1 Thermal Protection for Mains-fed Induction Motors

For mains-fed induction motors, no power switches are available to inject dc signals so that the motor's dc model can be used for stator resistance and temperature estimation. As a result, the application of dc signal injection techniques is limited for such motors. Therefore, thermal model-based stator temperature estimation techniques are preferred over dc signal injection-based techniques for their non-intrusiveness on mains-fed motors.

The novel simplified thermal model proposed in Chapter Four is an important start to such studies. The thermal model for mains-fed induction motors must has high accuracy while maintaining low requirement for implementation and computational effort. Such simplified thermal model still needs to be verified on more induction motors with different sized and configurations, so that it can be widely adopted for practical thermal protection.

Upon the validation of the proposed simplified thermal model, instead of two thermal parameters (service factor and trip class), which are currently provided by the motor manufacturers, three thermal parameters (as shown in Chapter Four in the proposed thermal model) can be provided for the thermal protection of mains-fed induction motors. This slightly increased request can largely improve the thermal protection reliability.

### 11.3.2 Thermal Model Study on Inverter-fed Induction Motors

When the torque oscillation caused by dc signal injection is not tolerable for a specific application, accurate thermal model-based stator temperature estimation is still highly desirable for induction motors fed by motor control devices. Considering that

soft-starter-connected induction motors are the same as mains-fed induction motors during operation, the thermal model study of inverter-fed induction motors is essential.

The thermal behaviors of inverter-fed induction motors are very different from those of the mains-fed ones. The loss distribution is very different due to the variation of input frequency. Similar to the mains-fed cases, thermal models that are accurate yet simple to implement are highly desirable. Such studies can be conducted based on the analysis presented in Chapter Four with analysis on the impact of input frequency variation on each type of losses.

### 11.3.3 Thermal Protection of Medium-Voltage Induction Motors

For medium-voltage (MV) large motors, embedded thermal sensors are broadly used to monitor the temperature of the stator winding to avoid thermal overload. However, MV motors are commonly thermally "rotor limited", considering the difficulty in the cooling of the rotor, thermal protection for the rotors of these motors are necessary for reducing bearing and rotor cage failures.

Medium voltage motors typically have lower starting torque (40%-50% normal torque [55-56]), and longer starting time. Most of the MV motors are started with reduced voltage due to the high starting current and torque pulsations. During the prolonged starting, both the stator current and rotor current are much higher than the rated current, which leads to extremely high thermal stresses on both the stator and the rotor. Therefore, for MV motors, the temperature peak typically appears during starting, instead of during an overload condition, as in small motors. Figure 11.1 shows the typical stating winding and rotor cage temperature during starting and after-starting. For some types of motors, the rotor cage temperature can rise to even 600°C [57]. These

extremely high thermal stresses not only greatly reduce the mechanical performance of the rotor cage, but also lead to thermal expansion of the rotor cage and thus mechanical stresses on the rotor cage, which eventually leads to rotor cage failure. Therefore, MV motors can typically be started fewer times than low voltage motors [58].

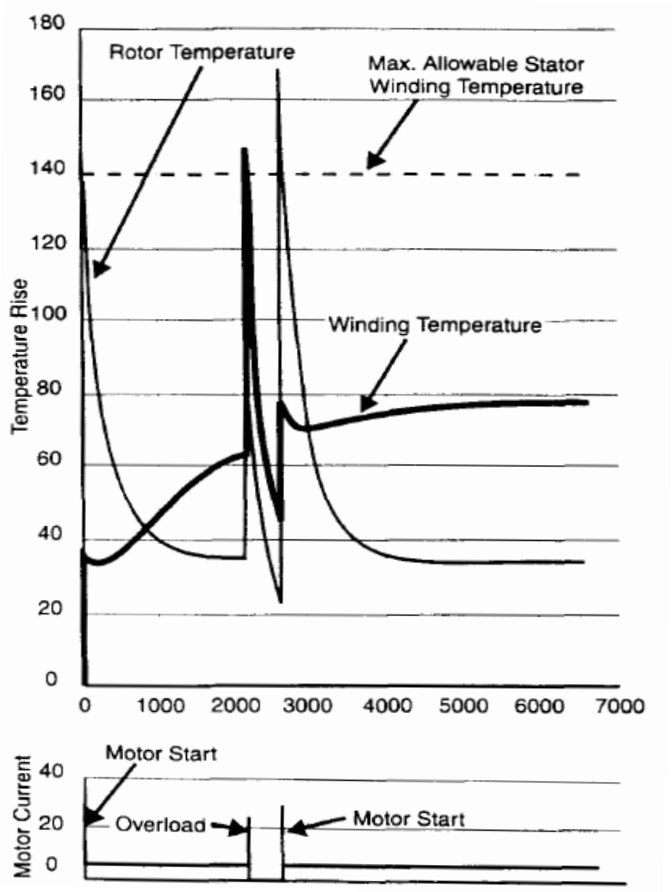


Figure 11.1: 400 Hp TEFC MV motor thermal signature [6].

As a result, the thermal protection for the rotor of the MV motors, during both the transient and the steady state, are essential for reducing catastrophic motor failures. Although many motor parameter-based rotor temperature estimation methods have been proposed, most of them can only be used during steady state or slow transient state. Therefore, non-intrusive rotor temperature estimation methods for fast transients, such as

starting, are highly desirable for MV motors, since the rotor temperature peaks during starting.

# BIBLIOGRAPHY


[1] "Report of Large Motor Reliability Survey of Industrial and Commercial Installations, Part I," *Industry Applications, IEEE Transactions on,* vol. IA-21, pp. 853-864, 1985.

[2] "Report of Large Motor Reliability Survey of Industrial and Commercial Installations, Part II," *Industry Applications, IEEE Transactions on,* vol. IA-21, pp. 865-872, 1985.

[3] "Report of Large Motor Reliability Survey of Industrial and Commercial Installations: Part 3," *Industry Applications, IEEE Transactions on,* vol. IA-23, pp. 153-158, 1987.

[4] G. C. Stone*, et al.*, "Stator insulation problems associated with low voltage and medium voltage PWM drives," in *Cement Industry Technical Conference Record, 2007. IEEE*, 2007, pp. 187-192.

[5] "Information Guide for General Purpose Industrial AC Small and Medium Squirrel-Cage Induction Motor Standards," *NEMA Standard MG1-2003,* August 2003.

[6] S. F. Farag*, et al.*, "An integrated on-line motor protection system," *Industry Applications Magazine, IEEE,* vol. 2, pp. 21-26, 1996.

[7] D. A. Paice, "Motor Thermal Protection by Continuous Monitoring of Winding Resistance," *Industrial Electronics and Control Instrumentation, IEEE Transactions on,* vol. IECI-27, pp. 137-141, 1980.

[8] S.-B. Lee and T. G. Habetler, "A remote and sensorless thermal protection scheme for small line-connected ac machines," *Industry Applications, IEEE Transactions on,* vol. 39, pp. 1323-1332, 2003.

[9] S.-B. Lee and T. G. Habetler, "An online stator winding resistance estimation technique for temperature monitoring of line-connected induction machines," *Industry Applications, IEEE Transactions on,* vol. 39, pp. 685-694, 2003.

[10] "Rotating Electrical Machines - Part 1: Rating and Performance," *IEC Standard 60034-1,* Apr 2004.

[11] "IEEE Standard Test Procedure for Polyphase Induction Motors and Generators," *IEEE Standard 112-2004,* 2004.

[12] B. Lu*, et al.*, "A Nonintrusive and In-Service Motor-Efficiency Estimation Method Using Air-Gap Torque With Considerations of Condition Monitoring," *Industry Applications, IEEE Transactions on,* vol. 44, pp. 1666-1674, 2008.

[13] "IEEE guide for the presentation of thermal limit curves for squirrel cage induction machines," *IEEE Standard 620-1996,* August 1996.

[14] M. S. Abou-El-Ela*, et al.*, "Thermal model based digital relaying algorithm for induction motor protection," in *Electrical and Computer Engineering, 1996. Canadian Conference on*, 1996, pp. 1016-1019 vol.2.

[15] Z. Gao*, et al.*, "A Sensorless Adaptive Stator Winding Temperature Estimator for Mains-Fed Induction Machines With Continuous-Operation Periodic Duty Cycles," *Industry Applications, IEEE Transactions on,* vol. 44, pp. 1533-1542, 2008.

[16] K. D. Hurst and T. G. Habetler, "A thermal monitoring and parameter tuning scheme for induction machines," in *proc. 32nd IAS Annual Meeting, IAS '97*, 1997, pp. 136-142 vol.1.

[17] J. F. Moreno*, et al.*, "Realisation of tests to determine the parameters of the thermal model of an induction machine," *Electric Power Applications, IEE Proceedings -,* vol. 148, pp. 393-397, 2001.

[18] Z. Gao*, et al.*, "A Complex Space Vector Approach to Rotor Temperature Estimation for Line-Connected Induction Machines With Impaired Cooling," *Industrial Electronics, IEEE Transactions on,* vol. 56, pp. 239-247, 2009.

[19] Z. Gao*, et al.*, "A Sensorless Rotor Temperature Estimator for Induction Machines Based on a Current Harmonic Spectral Estimation Scheme," *Industrial Electronics, IEEE Transactions on,* vol. 55, pp. 407-416, 2008.

[20] P. H. Mellor*, et al.*, "Lumped parameter thermal model for electrical machines of TEFC design," *Electric Power Applications, IEE Proceedings B [see also IEE Proceedings-Electric Power Applications],* vol. 138, pp. 205-218, 1991.

[21] A. Boglietti*, et al.*, "A simplified thermal model for variable speed self cooled industrial induction motor," in *proc. 37th IAS Annual Meeting, 2002.* , 2002, pp. 723-730 vol.2.

[22] A. Bousbaine*, et al.*, "In-situ determination of thermal coefficients for electrical machines," *Energy Conversion, IEEE Transaction on,* vol. 10, pp. 385-391, 1995.

[23] D. R. G. Champenois and D. S. Zhu, "Electrical and thermal performance predictions in inverter-fed squirrel-cage induction motor dirves," *Electric Machines and Power Systems,* vol. 22, pp. 355-369, May/June 1994.

[24] P. S. H. Nestler, "On-Line estimation of temperatures in electrical machines by an observer," *Electric Machines and Power Systems,* vol. 21, pp. 39-50, 1993.

[25] D. Staton*, et al.*, "Solving the More Difficult Aspects of Electric Motor Thermal Analysis in Small and Medium Size Industrial Induction Motors," *Energy conversion, ieee transactions on,* vol. 20, pp. 620-628, 2005.

[26] "IEEE Standard Test Code for Resistance Measurement," *IEEE Standard118-1978,* Mar. 1992.

[27] L. Umanand and S. R. Bhat, "Online estimation of stator resistance of an induction motor for speed control applications," *Electric Power Applications, IEE Proceedings -,* vol. 142, pp. 97-103, 1995.

[28] L. A. Cabrera*, et al.*, "Tuning the stator resistance of induction motors using artificial neural network," *Power Electronics, IEEE Transactions on,* vol. 12, pp. 779-787, 1997.

[29] B. K. Bose and N. R. Patel, "Quasi-fuzzy estimation of stator resistance of induction motor," *Power Electronics, IEEE Transactions on,* vol. 13, pp. 401-409, 1998.

[30] T. G. Habetler, *et al.*, "Stator resistance tuning in a stator-flux field-oriented drive using an instantaneous hybrid flux estimator," *Power Electronics, IEEE Transactions on,* vol. 13, pp. 125-133, 1998.

[31] G. Guidi and H. Umida, "A novel stator resistance estimation method for speed-sensorless induction motor drives," *Industry Applications, IEEE Transactions on,* vol. 36, pp. 1619-1627, 2000.

[32] C. B. Jacobina, *et al.*, "On-line estimation of the stator resistance of induction machines based on zero-sequence model," *Power Electronics, IEEE Transactions on,* vol. 15, pp. 346-353, 2000.

[33] E. D. Mitronikas, *et al.*, "A new stator resistance tuning method for stator-flux-oriented vector-controlled induction motor drive," *Industrial Electronics, IEEE Transactions on,* vol. 48, pp. 1148-1157, 2001.

[34] M. Tsuji, *et al.*, "A sensorless vector control system for induction motors using q-axis flux with stator resistance identification," *Industrial Electronics, IEEE Transactions on,* vol. 48, pp. 185-194, 2001.

[35] V. Vasic, *et al.*, "A stator resistance estimation scheme for speed sensorless rotor flux oriented induction motor drives," *Energy Conversion, IEEE Transaction on,* vol. 18, pp. 476-483, 2003.

[36] C. B. Jacobina, *et al.*, "Online estimation of the stator resistance and leakage inductance of a four-phase induction machine drive," *Power Electronics, IEEE Transactions on,* vol. 19, pp. 10-15, 2004.

[37] T. Bhattacharya and L. Umanand, "Improved flux estimation and stator-resistance adaptation scheme for sensorless control of induction motor," *Electric Power Applications, IEE Proceedings -,* vol. 153, pp. 911-920, 2006.

[38] S. Mir, *et al.*, "PI and fuzzy estimators for tuning the stator resistance in direct torque control of induction machines," in *Power Electronics Specialists Conference, PESC '94 Record., 25th Annual IEEE*, 1994, pp. 744-751 vol.1.

[39] K. Minami, *et al.*, "Multi-stage speed and parameter estimation for induction machines," in *Power Electronics Specialists Conference, 1991. PESC '91 Record., 22nd Annual IEEE*, 1991, pp. 596-604.

[40] L. Zhen and L. Xu, "Sensorless field orientation control of induction machines based on a mutual MRAS scheme," *Industrial Electronics, IEEE Transactions on,* vol. 45, pp. 824-831, 1998.

[41] S.-B. Lee*, et al.*, "An evaluation of model-based stator resistance estimation for induction motor stator winding temperature monitoring," *Energy Conversion, IEEE Transaction on,* vol. 17, pp. 7-15, 2002.

[42] P. Milanfar and J. H. Lang, "Monitoring the thermal condition of permanent-magnet synchronous motors," *Aerospace and Electronic Systems, IEEE Transactions on,* vol. 32, pp. 1421-1429, 1996.

[43] Z. Gao*, et al.*, "A Model Reduction Perspective on Thermal Models for Induction Machine Overload Relays," *Industrial Electronics, IEEE Transactions on,* vol. 55, pp. 3525-3534, 2008.

[44] M. Bemiaddadi*, et al.*, "Iron core losses impact in induction motor vector control: an overview," in *Electrical and Computer Engineering, 1998. IEEE Canadian Conference on*, 1998, pp. 782-785 vol.2.

[45] P. Zhang*, et al.*, "A Remote and Sensorless Stator Winding Resistance Estimation Method for Thermal Protection of Soft-Starter-Connected Induction Machines," *Industrial Electronics, IEEE Transactions on,* vol. 55, pp. 3611-3618, 2008.

[46] J. Plotkin*, et al.*, "A novel method for online stator resistance estimation of inverter-fed ac-machines without temperature sensors," in *Optimization of Electrical and Electronic Equipment, 2008. OPTIM 2008. 11th International Conference on*, 2008, pp. 155-161.

[47] M. A. Valenzuela*, et al.*, "Thermal evaluation for applying TEFC induction motors on short-time and intermittent duty cycles," *Industry Applications, IEEE Transactions on,* vol. 39, pp. 45-52, 2003.

[48] P. Zhang*, et al.*, "A Remote and Sensorless Thermal Protection Scheme for Soft-Starter-Connected Induction Motors," in *Industry Applications Society Annual Meeting, 2008. IAS '08. IEEE*, 2008, pp. 1-7.

[49] W. R. Finley, et al., "Storage of electric motors," in Pulp and Paper Industry Technical Conference, 1995., Conference Record of 1995 Annual, 1995, pp. 74-81.

[50] H. P. Walker and R. J. Flaherty, "Severe Moisture Conditioning Uncovers Weaknesses in Conventional Motor Insulation Systems for Naval Shipboard Use," *Power Apparatus and Systems, Part III. Transactions of the American Institute of Electrical Engineers,* vol. 80, pp. 23-31, 1961.

[51] D. V. Dikinis and M. H. Yuen, "Solid-State Control-Low Voltage Heating of Motors," *Industry Applications, IEEE Transactions on,* vol. IA-11, pp. 287-290, 1975.

[52] W. R. Keithly and S. P. Axe, "A Unique Solution to Improving Motor Winding Life in Medium-Voltage Motors," *Industry Applications, IEEE Transactions on,* vol. IA-20, pp. 514-518, 1984.

[53] J. Malinowski and J. McCormick, "AC induction motor specifications: an update on currently available procedures and options," *Industry Applications Magazine, IEEE,* vol. 9, pp. 50-56, 2003.

[54] P. Zhang*, et al.*, "Improving thermal recovery time for soft-starter-connected AC motors with intermittent periodic duty cycles," in *Diagnostics for Electric Machines, Power Electronics and Drives, 2009. SDEMPED 2009. IEEE International Symposium on*, 2009, pp. 1-9.

[55] J. Bredthauer and N. Struck, "Starting of large medium voltage motors: design, protection, and safety aspects," *Industry Applications, IEEE Transactions on,* vol. 31, pp. 1167-1176, 1995.

[56] L. B. Farr and T. A. Farr, "Considerations in Medium Voltage Reduced Voltage Motor Starting the Good, the Bad and the Ugly," in *Petroleum and Chemical Industry Technical Conference, 2007. PCIC '07. IEEE*, 2007, pp. 1-7.

[57] T. Albers and A. H. Bonnett, "Motor temperature considerations for pulp and paper mill applications," *Industry Applications, IEEE Transactions on,* vol. 38, pp. 1701-1713, 2002.

[58] G. J. Paoletti and A. Rose, "Improving existing motor protection for medium voltage motors," *Industry Applications, IEEE Transactions on,* vol. 25, pp. 456-464, 1989.

# VITA

Pinjia Zhang was born in China in 1984. He received a Bachelor of Engineering degree from Tsinghua University, Beijing, China, in 2006 and a Master of Engineering degree from Georgia Institute of Technology at Atlanta, Georgia, in 2009, both in Electrical Engineering.

Since July 2006, he has been working on the condition monitoring and protection of electric machines in collaboration with Eaton Corporation, as a graduate Research Assistant in the electric power group of the Georgia Institute of Technology. In 2009 summer, he worked at the Electric Machines and Drives Laboratory, General Electric (GE) Global Research Center, Schenectady, NY, as a graduate intern.

His research interests include electric machine protection and diagnostics, motor drives, power electronics, artificial intelligence and its applications in power system.

Mr. Zhang is the recipient of the second prize in the student paper and poster contest of the IEEE Power Energy Society General Meeting, Pittsburg, PA, USA, July 2008. He is also the recipient of the GE Student Intern/Co-op Contribution Award (SICCA) in 2009. He has published over 20 papers in refereed journals and international conference proceedings and has 3 patent applications in these areas.